Architecture of the Oman - UAE Ophiolite: evidence for a multi-phase magmatic history

Goodenough, K M[1], Styles M T[2], Schofield D[2], Thomas R J[2], Crowley Q C[3,*], Lilly R M[4, #], McKervey, J[2], Stephenson, D[1], Carney, J N[2]

1: British Geological Survey, West Mains Road, Edinburgh, EH9 3LA, UK.

2: British Geological Survey, Keyworth, Nottingham, NG12 5GG, UK

3: NERC Isotope Geoscience Laboratories, Keyworth, Nottingham, NG12 5GG, UK

4: School of Earth and Ocean Sciences, Cardiff University, Main Building, Park Place, Cardiff, CF10 3YE, UK

* Current address: School of Natural Sciences, Department of Geology, Trinity College, Dublin 2, Ireland

Current address: Xstrata Copper, Mount Isa, Queensland 4825, Australia

ABSTRACT

The Oman – UAE ophiolite is the world's largest ophiolite. It is divided into twelve separate fault-bounded blocks, of which the northern three lie wholly or partly in the United Arab Emirates (UAE). Extensive mapping has shown that the UAE blocks contain mantle and crustal sections which correspond to the classic 'Penrose conference' ophiolite definition, but which are cut by a voluminous later magmatic sequence including ultramafic, mafic and felsic components. Samples from the later magmatic sequence are dated at 96.4 ± 0.3 Ma, 95.74 ± 0.3 Ma, and 95.2 ± 0.3 Ma; the early crustal section, which has not been dated directly, is thus constrained to be older than c.96.4 Ma. Petrological evidence shows that the early crustal section formed at a spreading ridge, but the later magmatic sequence was formed from hydrous magmas that produced different mineral crystallisation sequences to normal MORB. Mineral and whole-rock geochemical analyses show that the early crustal rocks are chemically similar to MORB, but the later

magmatic sequence has chemical features typically found in supra-subduction zone (SSZ) settings. The ophiolite in the UAE thus preserves clear evidence for two stages of magmatism, an early episode formed at a spreading centre, and a later episode associated with the onset of subduction. Similar two-stage magmatism has been recognised in the Oman sector, but the UAE contains the most voluminous SSZ magmatism yet described from this ophiolite.

KEYWORDS

Oman-UAE ophiolite; Supra-Subduction Zone; Moho Transition Zone; Gabbro; Wehrlite

INTRODUCTION AND PREVIOUS WORK

The Oman – UAE Ophiolite (also known as the Semail Ophiolite) is the largest ophiolite complex in the world, and one of the most widely studied. Most of the ophiolite lies in Oman, where it has been mapped and described in great detail; this work has been summarised in a number of special volumes (Glennie et al. 1974; Coleman 1981; Lippard et al. 1986; Robertson et al. 1990; Boudier and Juteau 2000). However, the northern parts of the ophiolite are in the United Arab Emirates (UAE), and have been the subject of a relatively small number of papers (e.g. Peters and Kamber 1994; Reuber 1988; Cox et al. 1999; Searle and Cox 1999; Nicolas et al. 2000a,b). This paper presents results from a detailed field and geochemical study of the ophiolite in the UAE, carried out by the British Geological Survey (BGS) under contract to the Ministry of Energy of the UAE (Styles et al. 2006).

The Oman – UAE Ophiolite has traditionally been interpreted in terms of the classic ‘Penrose conference’ ophiolite definition (Anonymous 1972), with an ultramafic mantle section, and an overlying oceanic crustal section composed of gabbros, sheeted dykes, and pillow lavas (Lippard et al. 1986). However, many recent studies have recognised the existence of numerous later intrusions into the ophiolite sequence, formed during a later phase of magmatism (Ernewein et al. 1988; Juteau et al. 1988; Shervais 2001; Dilek and Flower 2003; Adachi and Miyashita 2003; Yamasaki et al. 2006; Python et al. 2008;

Rollinson 2009). This paper describes the composite nature of the ophiolite in the UAE, and draws upon field, geochronological and geochemical data to propose a model for the development of the ophiolite and the tectonic processes that operated during its formation and accretion.

The Oman – UAE Ophiolite was formed during the Cretaceous Period, at around 95 Ma (Tilton et al. 1981; Warren et al. 2005) as part of the Neo-Tethyan ocean floor. Dates on a range of minerals from the metamorphic sole to the ophiolite show that obduction began around a million years after the formation of the youngest magmatic rocks of the ophiolite (Hacker et al. 1996; Warren et al. 2005). The ophiolite belt extends for approximately 600 km and comprises twelve blocks, separated by faults (Glennie et al. 1974; Lippard et al. 1986). Of these blocks, the northernmost two - Khor Fakkan and Aswad – lie almost entirely within the UAE (Fig. 1). The northern tip of the Fizh block also extends into the south of the UAE.

Many advances have been made in understanding of the Oman – UAE Ophiolite over the last twenty-five years. In the context of our work in the UAE, two particular areas of research are crucial: the Moho Transition Zone (MTZ); and the younger magmatic phases.

The Moho Transition Zone lies between harzburgite of the mantle section and the overlying crustal layered gabbros. It includes dunites, wehrlites, pyroxenites and gabbros, with extremely complicated interrelationships. Broadly speaking, dunite is more common at the base of the MTZ, whereas gabbro is more common toward the top. It has previously been suggested that the ultramafic rocks of this zone simply represent part of the cumulate pile at the base of the crust (e.g. Coleman 1977; Lippard et al. 1986). However, a massive dunite band that forms the upper part of the mantle sequence has been interpreted as having a residual origin, formed by extraction of orthopyroxenes through melting, and this theory was extended to encompass all the dunites of the MTZ by Nicolas and Prinzhofer (1983). Benn et al. (1988) supported this view, and suggested that the transition zone is a composite of residual material, largely dunites that have been ‘impregnated’ by interstitial melt, and gabbroic to ultramafic intrusions. This model for the MTZ has largely been accepted, and developed via detailed field and geochemical studies (Boudier and Nicolas 1995; Korenaga and Kelemen 1997; Jousselin and Nicolas 2000; Koga et al. 2001).

The tectonic environment in which the Oman – UAE Ophiolite was formed has also been the subject of considerable debate. At first, it was considered to have formed at a fast-spreading mid-ocean ridge (Coleman 1981). However, field mapping has identified a number of different lava units in Oman, associated with late intrusions (Lippard et al. 1986). The lavas show a geochemical transition up-sequence, from MORB-like to more island-arc like chemistry, and thus a transition from a spreading-ridge environment to a supra-subduction zone environment has been suggested (Pearce et al. 1981; Alabaster et al. 1982). This model has broadly been accepted by many researchers, and is supported by mineral chemistry data from both gabbros and ultramafic rocks (Umino et al. 1990; Searle and Cox 1999; Shervais 2001; Ishikawa et al. 2002; Dilek and Flower 2003; Arai et al. 2006; Yamasaki et al. 2006; Python et al. 2008; Dare et al. 2009). However, some authors contend that the entire magmatic sequence may have formed at a mid-ocean ridge, with the later magmas being derived from a source that had been contaminated with seawater (Boudier et al. 1988; Boudier et al. 2000; Nicolas and Boudier 2003) or by second-stage melting of a previously-depleted mantle source (Ernewein et al. 1988; Godard et al. 2006). It has been suggested that evidence for a supra-subduction zone environment is stronger in the north-west of the ophiolite (Python et al. 2008), in which case the UAE represents the best place to test this evidence. This paper describes the evidence for voluminous SSZ-type magmatism in the UAE.

GEOLOGICAL SETTING

The two most northerly blocks of the Oman – UAE Ophiolite (the Khor Fakkan and Aswad blocks) occur wholly within the UAE, together with the northern tip of the Fizh block (Glennie et al. 1974; Fig. 1). Each of the two northern blocks is divided into two tectonic slices by a major ductile dislocation zone around 1 km below the Moho: the Bani Hamid Shear Zone in the Khor Fakkan block, and the Siji Shear Zone in the Aswad Block (Fig. 2).

The most northerly part of the ophiolite is the Khor Fakkan block, which is some 60 km in length and extends from the town of Dibba in the north to Fujairah in the south. Along its north side, it is separated from deformed sedimentary rocks of the Dibba Zone by the Wadi Sidir Fault Zone. To the west, the Khor Fakkan block is in tectonic contact with the metamorphic rocks of the Masafi-Ismah window, which have typically been interpreted as the metamorphic sole to the ophiolite (Searle and Cox 2002). To the east, the ophiolite continues offshore and can be recognised from aeromagnetic data to extend about 10 km beyond the coastline, where it is either terminated or downfaulted and buried beneath thick sediments. On its southern side, the Khor Fakkan block is bounded by the major NW-SE Wadi Ham Fault Zone.

The Khor Fakkan block also encloses the high-grade metamorphic rocks of the Bani Hamid Group, which occur in a tectonic window, bounded by thrusts which continue north-west as a major intra-ophiolite shear zone, the Bani Hamid Shear Zone. To the north and west of this shear zone, the block is made up exclusively of mantle harzburgite with subordinate dunite veins (Fig. 2). To the south and east of the shear zone, the Khor Fakkan block encompasses much of the typical ophiolite sequence, from a relatively thin horizon of mantle harzburgite up through the MTZ, into layered gabbro and high-level gabbro. Progressively higher parts of the sequence are encountered toward the east, suggesting that the whole block is gently inclined eastwards. The uppermost parts of the crustal section (sheeted dyke complex and pillow lavas) are not present in the Khor Fakkan block.

To the south, the Aswad block is one of the largest blocks in the Oman – UAE Ophiolite (Fig. 2). It extends approximately 70 km from north to south, and approaches 40 km in exposed east – west width. It is separated from the Khor Fakkan block to the north-east by the Wadi Ham Fault Zone and the Masafi-Ismah Metamorphic Window, and from the Fizh block to the south by the Hatta Zone. To the west, the Aswad block extends beneath the desert sands of the UAE, whereas to the east it continues for several kilometres beneath the Indian Ocean. A ductile thrust (the Siji Shear Zone) close to the base of the crustal section separates the northern part of the Aswad block, which is entirely composed of ultramafic mantle rocks, from the larger southern part. The latter consists chiefly of rocks of the crustal section (up to and including pillow lavas), together with the upper part of the mantle. The high-level gabbro, sheeted dykes and pillow lavas occur on the eastern side of the block, passing westwards into layered gabbro and then into ultramafic rocks, indicating that the Aswad block also has an overall dip to the east. However, in the central part of the block dips appear to be gentle to flat (as described by Nicolas et al. 2000b), and as a result the hills commonly have rocks of the MTZ exposed at their bases, capped by layered gabbro. The transition from the layered to the high-level gabbro is obscured in many areas by voluminous bodies of younger gabbro, as discussed below.

The Fizh block lies almost entirely within Oman, and only its northernmost tip extends into the UAE. This block is separated from the Aswad block to the north by the deformed sedimentary and metamorphic rocks of the Hatta Zone. The Fizh block in the UAE chiefly consists of mantle harzburgite, with only a small area of gabbro.

OPHIOLITE UNITS IN THE UAE

Our mapping has shown that the rocks of the ophiolite in the UAE can be divided into three broad groups, namely: the mantle section; the early crustal section, and the later magmatic sequence. The mantle and early crustal sections together represent the classic 'Penrose conference' ophiolite succession; they are separated by a gradational boundary zone (the MTZ). The later intrusive magmatic sequence encompasses a range of compositions, from ultramafic to felsic, and a range of forms, from large plutons to dykes and sheets, which cross-cut the earlier parts of the ophiolite.

Harzburgite and dunite of the mantle section

The mantle rocks of the Oman – UAE Ophiolite have been described in detail elsewhere (e.g. Lippard et al. 1986; Styles et al. 2006). In the UAE, they form the greater part of the Khor Fakkan block and the northern part of the Aswad and Fizh blocks. They also occur along the western fringe of, and in a small fault-bounded horst in the centre of, the Aswad block. They consist of coarse-grained harzburgite with subordinate dunite bands. The harzburgite is crudely foliated and lineated, as described by Nicolas et al. (2000b). Across much of the mantle section, the dunite forms networks of anastomosing veins that vary in width from about 10 cm to 1 m, and have gradational (over about 1 cm) contacts with the harzburgite. These dunite veins are considered to represent channels through which melt migrated towards the crust (Kelemen et al. 1995). In some areas, larger, irregular masses of dunite up to tens of metres across are seen.

Close to the major bounding thrusts and shear zones of the ophiolite, the dunite occurs as tabular, parallel bands in the harzburgite, which define a distinct layering. This ‘banded unit’ has also been described in Oman (Boudier et al. 1988) and is considered to have formed through emplacement-related deformation. The shear zones that separate the tectonic slices within the blocks are characterised by intense recrystallisation, producing ‘recrystallised harzburgite’ with a grain size of less than 1 mm. The shear zones also contain rocks with a higher clinopyroxene content than typical harzburgite, possibly indicating some infiltration of magmas. The top of the mantle section is marked by a discontinuous zone of massive dunite, which represents the base of the MTZ.

The Moho Transition Zone

The MTZ constitutes the zone of transition between the mantle harzburgite and the layered gabbro at the base of the crustal section. It is well exposed along the eastern side of the high mountains of the Khor Fakkan block, and also in the western and central parts of the Aswad block.

Most authors have described the MTZ of the ophiolite in Oman as largely composed of dunite, with an increasing amount of gabbroic sills up-section, and locally containing wehrlite, pyroxenite and troctolite bodies of various dimensions and geometries (Nicolas and Prinzhofer, 1983; Benn et al. 1988; Boudier and Nicolas 1995; Korenaga and Kelemen, 1997; Jousselin and Nicolas, 2000; Nicolas and Boudier 2000). In the UAE, we have delimited two separate components of the MTZ: a massive dunite unit, at the top of the mantle section; and an overlying layer that we have termed the Mixed Unit, which comprises varying quantities of dunite, wehrlite, pyroxenite, troctolite and gabbro (Fig. 3). Both layers are of very variable thickness, and in some areas one or the other layer may be almost entirely absent.

The massive dunite layer is a discontinuous zone that locally attains a thickness of several hundreds of metres, although large lateral variations occur over distances of a few kilometres. The base of the massive dunite unit is defined as the point at which dunite consists of >90% of the outcrop; above this point, harzburgite only occurs as relict patches. Chromite-rich zones are common, and locally layered.

The massive dunite unit is overlain by the Mixed Unit, which varies in thickness from a few metres up to around 1000 metres. Although it is laterally variable, a general stratigraphy can be recognised (Fig. 3). The base of the Mixed Unit is taken where patches rich in coarse grains of clinopyroxene and/or plagioclase feldspar begin to appear at the top of the massive dunite. These areas are known as 'impregnated dunite' (Benn et al. 1988). Continuing up-section, the proportion of plagioclase and/or clinopyroxene in the dunite increases, grading upwards into wehrlite and, less commonly, troctolite. In many areas the orange-brown dunite and impregnated dunite are cross-cut by coarse-grained, irregular intrusions of green clinopyroxenite and olivine clinopyroxenite, and dark brown wehrlite.

Higher in the Mixed Unit, wehrlite and pyroxenite dominate. These are associated with scattered tabular sheets and enclaves of gabbro, which vary from a few tens of centimetres up to tens of metres in size (Fig. 4). The gabbro is typically coarse-grained and shows modal layering, similar to that seen in the crustal layered gabbros. The layering is most commonly parallel to that in the overlying layered gabbros, but in many enclaves the layering is randomly orientated. Wehrlite and pyroxenite intrusions locally transgress the gabbro layering, clearly indicating that they were intruded into already-layered gabbro. The margins of the gabbro sheets and xenoliths vary from sharp to diffuse; in the latter case, there is a gradation over a few centimetres, from layered gabbro, through troctolite or melagabbro with 'ghost' layering, into wehrlite. This gradation indicates partial assimilation of the gabbroic rocks by the intruding wehrlite and pyroxenite.

The volume of gabbro increases higher up the succession, with a concomitant decrease in intrusive wehrlite. Pyroxenite becomes less common, and the feldspar content of the wehrlite increases, grading into melagabbro (> 10% plagioclase; Koga et al. 2001). The contact between the Mixed Unit and the overlying layered gabbro unit is generally very difficult to define, but is taken at the point where the gabbro appears as the dominant rock body, rather than as a stack of xenoliths within a wehrlite mass. This point roughly equates to layered gabbro being more than 50% of the outcrop. Above this, abundant sills and irregular intrusions of wehrlite occur within the gabbro.

The relationship between dunite and the layered gabbro in the Mixed Unit is not easy to determine, since they rarely occur in contact. Dunite is intruded by wehrlite and pyroxenite close to the base of the Mixed Unit; higher up, bodies of dunite locally appear to enclose gabbro xenoliths. The interlayering of dunite and gabbro that has been described in Oman (e.g. Boudier and Nicolas 1995; Korenaga and Kelemen 1997), is rarely if ever seen in the UAE.

Cross-cutting veins of coarse-grained to pegmatitic gabbro and clinopyroxenite occur throughout the Mixed Unit. These clearly post-date the main rock-types of the MTZ, and provide evidence for a further phase of magmatism. Similar late veins and dykes are seen cutting the mantle section of the ophiolite, and have also been described in Oman (Python and Ceuleneer 2003).

Nicolas and Prinzhofer (1983) and Benn et al. (1988) presented a model for the Oman ophiolite in which the massive dunite unit at the top of the mantle section was considered to be residual, and the gabbro, wehrlite and pyroxenite above were considered to be intrusive. The field relationships in the UAE accord well with the essential facts of this model. However, it is clear from the relationships seen in the Mixed Unit that formation of the layered gabbro pre-dated the intrusion of most, if not all of the wehrlite and pyroxenite bodies. The layered gabbro sheets and lenses seen within the Mixed Unit of the UAE represent xenoliths derived from the base of the crustal section. Although it is entirely possible that the lower units of layered gabbro formed as sills, intruding the upper part of the mantle section (Boudier et al. 1996; Korenaga and Kelemen 1997; Kelemen et al. 1997), evidence for this has been intensely disrupted by later magmatism in the MTZ of the UAE. Similar features have been described from Oman by Juteau et al. (1988), who recognised that a second magmatic event represents an important part of the history of the Oman ophiolite. The UAE blocks were identified as a part of the ophiolite with an unusually thick MTZ, and abundant wehrlite intrusions, by Nicolas and Boudier (2000), and were suggested to represent an area of mantle upwelling. The field relationships described here confirm the presence of abundant wehrlite and a generally thick MTZ, but show that this is indicative of a locus of later magmatism.

Gabbros of the early crustal section

The early crustal section of the ophiolite in the UAE contains good examples of both lower crustal layered gabbro and high-level gabbro. Both units occur along the eastern side of the Khor Fakkan block. The high-level gabbro occurs close to the eastern margin of the Aswad block, whereas the layered gabbro occupies a broad area of outcrop in the central part of the block. These units of the Oman – UAE Ophiolite have previously been described in detail from Oman (e.g. Lippard et al. 1986; Nicolas et al. 2000b).

The layered gabbro comprises coarse-grained olivine gabbro, and mostly preserves a clear rhythmic modal layering, generally on a scale of 1 – 20 cm. The layers are typically sharply bounded. Modally graded layering, which is common in Oman (e.g. Boudier et al. 1996), is very rarely seen in the UAE. Many layered gabbro outcrops also exhibit a mineral foliation, defined by aligned tabular plagioclase and clinopyroxene crystals. Layering is further emphasised by – and in places solely due to – sills of wehrlite and melagabbro which are mainly layer-parallel, although locally cross-cutting. These wehrlitic sills, which vary in thickness from 5 cm to several metres or more, are most common in the lower parts of the crustal section, decreasing in abundance upwards. In some areas, large masses of wehrlite and melagabbro, with some clinopyroxenite and dunite, have been intruded upwards from the Mixed Unit into the layered gabbro, and more rarely into the upper crustal rocks. These large masses can be up to a kilometre across, and their margins grade outwards into more typical layered gabbros with wehrlite sills.

Orientation of layering is variable; in the Khor Fakkan block it is typically moderately to steeply inclined toward the east, but is locally sub-vertical and is clearly not always parallel to the Moho. In the Aswad block, layering is typically shallowly to moderately inclined, giving the impression of an undulose geometry confined by a more or less flat-lying enveloping surface. However it is locally steeply inclined, particularly in the vicinity of fault zones or at the margins of steep sided bodies of younger gabbro.

Over much of the area, contacts between the layered and high-level gabbro are now largely obscured by bodies of younger gabbro (see below), or disrupted by faults. In the few places where the unmodified contact is exposed, the layered gabbro is observed to grade up-sequence, with gradual loss of layering, into the high-level gabbro. Bodies of high-level gabbro are typically medium- to coarse-grained, and very variable in texture, ranging from equigranular to extremely heterogeneous. The most 'varitextured' gabbro (Macleod and Yaouancq 2000) shows patchy gradation from medium-grained through to pegmatitic textures within a single outcrop. In some areas, the gabbro has a poorly penetrative foliation defined by aligned clinopyroxene crystals. However, there is no clear systematic variation in textural types across the outcrop.

The upper parts of the high-level gabbro are cut by abundant dykes of microgabbro, generally < 2 m in thickness and preserving sharp, chilled contacts against the host gabbros. In the Aswad block these dykes are most commonly north – south trending, although they cover a range of orientations round to NNW. In the Khor Fakkan block, the dykes typically have a NNW-SSE trend. Dyke density increases upwards in the high-level gabbro, and in the Aswad block this gives a transitional contact into the sheeted dyke complex (the dyke rooting zone), although in some places sharp contacts between sheeted dykes and gabbro indicate the emplacement of multiple pulses of magma. The transition into true sheeted dyke complex is not preserved in the Khor Fakkan block.

Sheeted dyke complex and pillow lavas

In the UAE, these upper parts of the early crustal section are only exposed on the eastern side of the Aswad block, south of Fujairah. The sheeted dyke complex is defined as being composed of more than 90% dykes, with up to 10% inter-dyke screens of gabbro or basalt. Individual dykes are up to 2 m wide, with 30 to 50 cm more typical. Some dykes preserve chilled margins on both sides, others have chills on only one side. The dyke trend varies from north to NNW, and the dykes are steeply dipping to vertical. Some distinct, later dykes cut across earlier chilled margins.

A transitional contact occurs between the sheeted dyke complex and the overlying pillow lavas. The pillow basalts occur as small, discontinuous outcrops, some of which have been heavily quarried in recent years. They are fine-grained, highly shattered (microjointed), and weathered to patchy green and purple colours. A few outcrops are vesicular, and pillow structures are present at some localities, although these are not always clearly recognisable due to the shattered nature of the outcrops. Small areas of basaltic microbreccia are also seen. Sedimentary layers are absent and interpillow sediment is rare. Only the lower part of the lava sequence (Lippard et al. 1986) is present in the UAE.

The later magmatic sequence in the UAE

One of the most distinctive features of the ophiolite in the UAE is the presence of abundant, cross-cutting, bodies of younger gabbro that intrude all levels of the crust, from the Mixed Unit up to the pillow lava, and locally also intrude down into the mantle harzburgite and dunite. These younger gabbros in the UAE have been fully described for the first time during the BGS mapping project, which has identified a number of different facies, and mapped out the extent and morphology of the gabbroic bodies in detail (Styles et al. 2006).

The younger gabbros are most abundant in the Aswad block, where they form an extensive network that makes up around half of all crustal exposure (Fig. 2). In the Khor Fakkan and Fizh blocks only small areas have been identified, the most extensive of which occurs in the southern part of the Khor Fakkan block. These younger gabbros are clearly similar to the late intrusive complexes that have been identified in Oman (Smewing 1980; Lippard et al. 1986; Adachi and Miyashita 2003), but they appear to be considerably more voluminous in the UAE.

The younger gabbros are highly heterogeneous, and it has proved possible to map out a number of different facies in the field. However, they have certain characteristic features that distinguish them from the gabbros of the main ophiolite succession: 1) although markedly heterogeneous they are, in general, finer-grained than the layered and high-level gabbros, and contain areas of microgabbro; 2) they are commonly associated with more-evolved, dioritic and tonalitic intrusions; 3) they are typically associated with ductile shear zones and faults; 4) evidence of polyphase intrusions is common.

The younger gabbros form a network of intrusions with a very complex geometry (Fig. 5). Large areas of younger gabbro (up to several km across) typically contain abundant xenoliths of the host rocks up to a kilometre in size. The margins of the intrusive bodies are intricate, with many sheets and veins of younger gabbro cutting the host rocks (Fig. 6). In the Khor Fakkan block most of the younger gabbro occurs as a relatively coherent, inclined sheet-like body with an elongate north-trending outcrop. Along much of its length this body intervenes between the Mixed Unit and the base of the layered gabbro, but toward the south and north, it transgresses the layered gabbro and intrudes the base of the high-level gabbro. In the Aswad block the younger gabbros preserve a complex morphology that includes flat-lying sheet-like elements, particularly in the western and southern parts of the block (Fig. 6a). Broad, composite dyke-like bodies and sheets (Fig. 6b) characterise the central part of the block, confined within or associated with north- to NW-trending zones of ductile shearing and brittle faulting. The former are characterised by intense zones of mylonitisation with small-scale isoclinal shear folds. In the east of the block, contacts with layered gabbro are generally steep and strongly discordant to the layering (Fig. 6c), and monoclinal drag-like folds tens of metres in amplitude have been recognised at some of these contacts. In the Aswad block, the younger gabbros most commonly occupy a structural position between the layered gabbro and higher units, but with many offshoots extending both upwards and downwards and transgressing the earlier ophiolite sequence (Fig. 5).

Although the younger gabbros are texturally heterogeneous, their most distinctive feature is the presence of large amounts of microgabbro. In some areas, particularly in the eastern part of the Aswad block, the younger gabbros are characterised by a groundmass of microgabbro, with irregular patches and veins of coarser-grained gabbroic and dioritic material. Locally, intense foliation can be seen. This type of younger gabbro has been mapped out as the ‘Fujairah facies’. In the western part of the Aswad block, a more varitextured groundmass is shot through with dyke-like intrusions of a brown-weathering, fine- to medium-grained microgabbro with a distinctive ‘splintery’ appearance, and has been mapped as the ‘Bithnah facies’.

The younger gabbros are commonly associated with intrusions of more-evolved magma; this is particularly clear in the Fujairah facies of the eastern part of the Aswad block, which is intimately associated with veins, sheets and larger irregular bodies of white-weathering tonalite up to 1 km^2 in outcrop area. The tonalites most commonly form sub-vertical sheets a few metres across, but also occur as larger bodies and as vein networks throughout the younger gabbros. Some tonalitic intrusions have a characteristic texture known as 'vinaigrette' (Styles et al. 2006), with blebs of microgabbro within the tonalite groundmass indicating mingling of two immiscible magmas (Fig. 6b).

The younger gabbros typically occupy rather different structural levels to the wehrlitic and pyroxenitic rocks of the Mixed Unit, and so the relationships of these units are not clear, although younger gabbros can be seen to cut across the Mixed Unit rocks in many places. At some localities it is clear that more than one phase of wehrlite intrusion is present, with phases pre- and post-dating younger gabbro. Both the younger gabbros and the wehrlite and pyroxenite, together with some microgabbro dykes as described below, clearly cross-cut the early crustal section of the ophiolite. Therefore, all these units can be grouped together as a later magmatic sequence.

Younger microgabbro dykes

Dykes of microgabbro occur throughout the ophiolite crustal section, and much less commonly in the mantle. They are typically 10 cm to 1 m in width, rarely up to a few metres, and most examples are chilled against the host rocks. A number of different dyke types can be identified on the basis of field relationships, although the relative age of an individual dyke may not always be clear in the field. Many of the dykes in the upper parts of the high-level gabbro are related to the sheeted dyke complex, and represent an integral part of the early crustal section. However, a number of younger dykes are also present; some of these are considered to be related to the younger gabbros, whilst others are clearly later still. In particular, some very young dykes cut across rocks of the mantle section.

Most of the microgabbro dykes are vertical to steeply dipping and have a WNW-ESE to NW-SE trend, although there are variations. They typically weather to a pale greenish-grey colour, and break into angular blocks that stand out against the more rounded weathering of the surrounding coarse-grained gabbro. Some dykes contain small phenocrysts of black clinopyroxene or white plagioclase.

PETROGRAPHY

The petrography of the main units of the Oman – UAE Ophiolite has been described in detail elsewhere (e.g. Lippard et al. 1986). In this section, therefore, we focus on those units that have been recognised as parts of the later phase of magmatism in the UAE, in particular the rocks of the Mixed Unit and the younger gabbros.

The Mixed Unit wehrlites are coarse-grained rocks, consisting of ~ 70 % forsteritic olivine (partially serpentinised), 20-30 % clinopyroxene (diopside – diopsidic augite), and up to 10 % plagioclase. These grade into olivine-clinopyroxenites, largely consisting of clinopyroxene with up to 20 % olivine. Textures are equigranular to poikilitic, with clinopyroxene forming large, poikilitic plates up to several centimetres across with rounded inclusions of olivine. Plagioclase, where present, is typically interstitial. Similar textures have been described in Oman wehrlite by Juteau et al. (1988) and Boudier and Nicolas (1995). These textures indicate a crystallisation sequence of olivine – clinopyroxene – plagioclase, which contrasts with the typical MORB crystallisation sequence of olivine – plagioclase – clinopyroxene (Koga et al. 2001; Koepke et al. 2009), and suggests that the wehrlites were derived from a non-MORB hydrous parental magma. The impregnated dunites also have poikilitic textures, being largely composed of equigranular olivine crystals (often highly serpentinised) with rare, large poikilitic clinopyroxene plates. Up to 5 % spinel is typically present in these rocks.

Wehrlite sills intrusive into the layered gabbro tend to be more feldspathic than Mixed Unit wehrlite, and grade into melagabbro. Overall, the wehrlite consists of 60 – 80 % olivine and 10 – 40 % clinopyroxene, with up to 15 % interstitial, highly altered plagioclase. Some samples contain large poikilitic clinopyroxenes enclosing smaller olivine crystals; other samples are fairly equigranular and are possibly recrystallised. The olivine is commonly serpentinised, although the amount of alteration varies from a few thin veins in olivine crystals to complete serpentinisation with no relict olivine.

The layered gabbro consists of 20 – 50 % clinopyroxene (diopside to diopsidic augite) and up to 15 % olivine, with the remainder of the rock being composed of plagioclase (bytownite). A few samples contain primary amphibole or orthopyroxene. Small amounts (< 1%) of spinel are present in most samples. In many layered gabbros, there is significant evidence of late alteration: the clinopyroxene has been replaced by amphibole and chlorite, the olivine is partly serpentinised, and the plagioclase is saussuritised. Texture is quite variable; some samples are granular, whereas others have a distinct lamination defined by the parallel alignment of elongate plagioclase laths. Clinopyroxene crystals are commonly poikilitic, enclosing grains of plagioclase and/or olivine, and indicating the typical MORB crystallisation sequence of olivine – plagioclase – clinopyroxene. Although layering can be seen in some thin sections, it is generally of a larger scale than can be easily studied in thin section. No systematic textural difference has been observed between the layered gabbro within the Mixed Unit and those within the main layered gabbro unit. The high-level gabbro has similar mineralogy to the layered gabbro, and poikilitic textures are common, with large clinopyroxene crystals enclosing plagioclase laths and olivine grains. Many of the high-level gabbros are finer-grained than the layered gabbro.

The younger gabbros show a wider variation in mineralogy and texture. They vary from medium- to coarse-grained, and from equigranular to sub-ophitic or moderately foliated. Many samples are essentially bimineralic, being composed of around 30-50 % clinopyroxene and 50-70 % plagioclase. The clinopyroxenes, which vary in composition from diopside to augite, typically have a dusky appearance due to fine exsolution textures. They are commonly partly altered to brown hornblende at the grain margins by late magmatic processes, and a few examples have large plates of poikilitic brown amphibole with little or no pyroxene present. Pervasive post-crystallisation hydrothermal alteration to pale green to colourless, fibrous (actinolitic) clinoamphibole is widespread. Plagioclase shows variable amounts of saussuritic and/or sericitic alteration.

Some 5 – 10 % interstitial quartz, commonly with feldspar in symplectic intergrowth, is a fairly common constituent of the younger gabbros, particularly in the north-eastern part of the Aswad block. Olivine is a very rare constituent of the younger gabbros, but a few samples contain up to 5 %. Most rocks contain very minor amounts of opaque mineral and apatite as accessory phases.

In the south of the Aswad block, a distinct orthopyroxene-bearing facies of the younger gabbros has been identified, and has a very characteristic appearance in thin section. The major component of the outcrops is a sub-ophitic to granular, reasonably fresh, two-pyroxene microgabbro. The mineralogy includes 40 – 60 % plagioclase, 20 – 40 % clinopyroxene, and 5 – 20 % orthopyroxene. Some samples also have poikilitic plates of brown-green amphibole. Both pyroxenes tend to occur as subhedral to euhedral crystals, and some examples have long bladed orthopyroxenes which formed early in the crystallisation process. Similar rocks have been described from the Fizh-South Complex in Oman, which is also considered to represent a younger intrusion (Adachi and Miyashito, 2003).

The tonalitic rocks associated with the younger gabbros are medium- to coarse-grained and generally consist of 30 – 50% quartz and 40 – 60% plagioclase, with smaller amounts of hornblende and biotite. Some samples contain concentrically zoned plagioclase phenocrysts. Zircon, apatite and titanite are relatively common accessories in these more evolved intrusions.

Most microgabbro dykes comprised ~ 30-70 % clinopyroxene and 30-70 % plagioclase when fresh, but in the majority of samples the clinopyroxene has been replaced by a green amphibole ± chlorite. A few dykes contain up to 15% quartz or orthopyroxene, and opaque oxides are common accessories. Textures are most commonly ophitic to sub-ophitic, typically with pyroxene crystal shapes preserved by the amphiboles that have replaced them.

GEOCHRONOLOGY OF THE OPHIOLITE UNITS

Sampling and analytical methods

Dating of ophiolites has always proved difficult because zircon is generally most abundant in evolved, felsic rock types and least abundant in primitive, mafic, MORB-like rock-types with low Zr contents. Previous U-Pb dates have thus only been obtained from trondhjemitic intrusions (Tilton et al. 1981; Warren et al. 2005). However, the likelihood of successfully finding zircon in mafic igneous rocks may increase with the degree of chemical evolution and grain size, and so we sampled both tonalites and a number of coarse-grained and pegmatitic gabbros. Large samples (15-20 kg) were taken to further improve chances of success and where possible duplicate samples were taken from the same area. Dating was carried out at the NERC Isotope Geoscience Laboratory, UK.

Zircons were separated and hand picked to obtain the best quality grains. Carefully selected zircon grains were then abraded using the air abrasion technique of Krogh (1982) or a modified chemical abrasion technique based on that developed by Mattinson (2005). U-Pb chemistry used either a $^{233}U/^{235}U/^{205}Pb/^{230}Th$ or $^{235}U/^{205}Pb$ mixed spike solution and followed the procedures of Krogh (1973), Parrish (1987) and Parrish and Noble (2003). Analyses were conducted on a VG 354 multi-collector Thermal Ionisation Mass Spectrometer (TIMS) equipped with a WARP filter, axial Daly photomultiplier and Ortec ion counting detection system, or using a Thermo-Electron Triton multi-collector TIMS instrument fitted with an axial secondary electron multiplier and multiple-ion counters. Data were processed using error propagation and data reduction methods of Parrish et al. (1987) and Roddick (1987). Concordia diagrams were plotted using the Isoplot 3 macro of Ludwig (2003).

Results

Several samples were collected from the early crustal section, but unfortunately none yielded sufficient zircon for analysis. However, dates were successfully obtained from three samples from the later magmatic sequence. Images of the zircons from these samples are shown in Fig. 7, and the data are shown in Table 1.

Sample UAE167 was taken from a sheet of pegmatitic gabbro intruding dunite and wehrlite of the Mixed Unit in the Khor Fakkan Block at grid reference [431488 2803498]. Four separate zircon fractions from this sample were analysed and give a concordia age of 96.40 ± 0.29 Ma (Fig. 8a). This date provides a younger limit for the age of the early crustal section.

Sample UAE163 was taken from a pegmatitic gabbro associated with the Bithnah facies of the younger gabbros at grid reference [413816 2786470]. Four separate zircon fractions from this sample gave concordant analyses with a Concordia age of 95.74 ± 0.32 Ma (Fig. 8b).

Sample UAE180 was taken from the felsic part of a mingled-magma (‘vinaigrette’) intrusion within the Fujairah facies of the younger gabbros at grid reference [423702 2781090]. This sample contained very low-U zircons and out of twelve separate multi-grain fractions, three gave reliable analyses, producing a Concordia age of 95.26 ± 0.31 Ma (Fig. 8c).

MINERAL CHEMISTRY OF THE OPHIOLITE UNITS

Major-element chemistry of minerals from a small subset of ophiolite rocks was obtained by electron microprobe analysis (EPMA) of carbon-coated polished thin sections, carried out at the British Geological Survey, Keyworth, UK. The EPMA analyses were obtained using a Cameca SX50 wavelength dispersive electron microprobe. The rocks were analysed using an accelerating potential of 15kV and a 20nA beam current. Elements were analysed using the PET, LiF and TAP diffracting crystals, calibrated using internal mineral and pure metal standards. All Fe was measured as FeO and mineral formulae were calculated by the Cameca software. For every sample clinopyroxene and plagioclase were analysed by selecting ~10 examples and analysing the core and rim of each crystal. Using these data, averages were calculated to characterise the mineral chemistry of the rocks; a summary of the data is presented in Table 2. Magnesium numbers (Mg#) were calculated as Mg# = atomic Mg/ (Mg+Fe^{2+})) x 100.

A total of 50 samples of the gabbroic rocks were analysed, as well as eight samples of wehrlite. The clinopyroxenes in all the different gabbros were found to have clinopyroxene Mg# between 70 and 95, whilst all analysed plagioclases have anorthite contents above 50%, and more commonly above 70%. The wehrlite samples have high clinopyroxene Mg#s, > 85, and anorthite contents > 80%, but they clearly fall within the same range as the layered gabbro. Closer study shows that, at any given feldspar An%, many of the younger gabbros have lower clinopyroxene Mg#s than the gabbros of the early crustal section, though complete separation of the two suites is not possible (Fig. 9). Mineral compositions of the wehrlites plot with those of the layered gabbro rather than the younger gabbros. This difference between the gabbros accords with the work of Yamasaki et al. (2006), who used major element chemistry to recognize two gabbroic suites (GB1 and GB2) in the Wadi Haymiliyah section of the ophiolite in Oman. The dividing line between their two suites does not fully discriminate the two gabbroic suites in the UAE (Fig. 9), but in general the UAE younger gabbros are more similar to the GB2 suite. Similar mineral chemistry features have been recognized in the Fizh-South intrusions (Adachi and Miyashito 2003). The clinopyroxenes of the UAE younger gabbros are also characterized by lower Al_2O_3 contents than those of the main crustal section (0.7 – 2.5% in the younger gabbros; 2.0 – 3.3% in the layered and high-level gabbros and in the wehrlites). The TiO_2 contents of clinopyroxene from all the gabbros and wehrlites overlap, lying between 0.1 and 0.7%; the orthopyroxene-bearing younger gabbros have TiO_2 contents < 0.3%, whereas those of the Bithnah facies gabbros range between 0.3 and 0.7%. In general, the clinopyroxenes of the younger gabbros have a lower Mg# at any given TiO_2 content than those in the gabbros of the early crustal section and the wehrlites.

GEOCHEMISTRY OF THE OPHIOLITE UNITS

Whole-rock samples representing all the rock-types of the ophiolite have been analysed for major, trace and rare-earth elements by ICP-OES and ICP-MS at Cardiff University, UK. Over 150 of these samples were from rocks of the crustal section and the intruding younger gabbros and wehrlites, and these data are presented in Table 3. Full analytical procedures are documented by Lilly (2006).

In Oman, most detailed geochemical studies have been carried out on the volcanic rocks, which provide the most direct way of studying the chemistry of the magmas (e.g Alabaster et al. 1982; Einaudi et al. 2000). However, in the UAE, outcrops of the volcanic section are limited, and so magmatic variations have to be deduced from dykes and from the plutonic rocks. Analysis shows that most of the gabbros are cumulate, as indicated by geochemical features such as positive Eu anomalies and depletion in incompatible elements and the LREE (Fig. 10). Their whole-rock geochemistry thus does not represent the original magma compositions, although ratios of elements that are similarly compatible may provide information about the magmas. Despite careful sample selection, the chemical compositions of the rocks may also have been affected by hydrothermal alteration. This alteration has chiefly affected some major elements and the Large Ion Lithophile Elements; other trace elements have remained relatively immobile (Lilly, 2006).

All the gabbros (layered, high-level and younger gabbros) have SiO_2 contents between 40 and 53 wt%, MgO between 5 and 15 wt%, and TiO_2 commonly <0.4 wt%. In general, the gabbros are difficult to distinguish on the basis of their whole-rock chemistry: an example is given by the TiO_2 – Mafic Index gabbro discrimination plot of Serri (1981), in which all the gabbro types overlap, the majority lying within the low Ti field which is considered to represent supra-subduction zone ophiolites (Fig. 11). Similar features are seen on a plot of Nb/Yb vs La/Nb (Fig. 12); the younger gabbros perhaps tend towards lower Nb/Yb ratios and higher La/Nb ratios than the layered and high-level gabbros, but there is much overlap. An interesting exception to the typical variation is the orthopyroxene-bearing younger gabbros, which can be easily distinguished on this plot by their high Nb/Yb and low La/Yb ratios. They are most clearly characterised as having a La/Nb ratio < 1, whereas all the other gabbros have La/Nb > 1. The association of high Nb contents with orthopyroxene in the gabbros might be interpreted to suggest that Nb is concentrated in the orthopyroxene, but in fact Nb is incompatible in orthopyroxene (Kelemen and Dunn 1992). The unusually high Nb contents thus appear to be a feature of the original magmas, but the origin of these magmas would require further study.

In contrast to the gabbros, the whole-rock chemistry of the microgabbro dykes typically represents magma compositions that have been unaffected by cumulus processes, and these provide a clearer picture of magma evolution with time in the UAE part of the ophiolite. All samples show wide variation in the mobile elements Rb, Sr, Ba and Th (Fig. 13), but the other trace elements are relatively immobile (Lilly, 2006).

Samples from the sheeted dyke complex and the dyke rooting zone vary from basaltic to andesitic, with SiO_2 from 48 to 62 wt% and MgO from 1.8 to 8 wt%. All these samples have relatively flat, MORB-like, trace element and REE patterns, some with a slight Nb, Ta and LREE depletion relative to MORB (Fig. 13). Samples of pillow basalts, from the few outcrops that occur in the UAE, have similar patterns. These compositions essentially match those of the Geotimes unit identified in the Oman volcanic rocks by Alabaster et al. (1982) and are the most similar in chemistry to MORB.

Many of the dykes found in both the Khor Fakkan and Aswad blocks represent part of the later magmatic suite. Many can be identified as later intrusions in the field because they cut, or are associated with, younger gabbro bodies; others are characterised by distinctive chemical features that differ from those of the sheeted dyke complex. These dykes are typically basalt or basaltic andesite in composition. Many of them have clear negative Nb, Ta, Zr and Hf anomalies on MORB-normalised spider diagrams (Fig. 13). The majority of these dykes are characterised by LREE depletion, although some samples have more ‘u-shaped’ boninitic patterns with depletion of the MREE (Fig. 13). They are geochemically similar to the Clinopyroxene-phyric and Lasail units identified by Alabaster et al. (1982) in Oman.

The youngest dykes found in the UAE are a group of basaltic dykes, chiefly occurring in the Khor Fakkan block, some of which cut rocks of the mantle section. These dykes have strongly LREE-enriched compositions (Fig. 13), and compare to the lavas of the Salahi Unit of Oman (Alabaster et al. 1982).

The three different groups of dykes found in the UAE can be clearly identified by a number of common discrimination plots (Fig. 14). On a plot of Ti versus V (Fig. 14a), the pillow lavas and sheeted dykes can be seen to have Ti/V ratios > 20, which is a feature of MORB (Shervais 1982). Most of the later dykes have Ti/V ratios < 20 (and many < 10), placing them in the field of island arc basalts. The youngest, enriched dykes have higher Ti/V ratios, approaching the values expected for alkaline rocks. On a Zr versus Zr/Y diagram (Fig. 14b; Alabaster et al. 1982), the pillow lavas and sheeted dykes plot within the MORB field, whereas the younger dykes plot in or below the field of island-arc basalts. Again, the later, enriched, Salahi-type dykes are distinguished by this plot. On a Cr/Y plot (Fig. 14c; Pearce 1982) the sheeted dykes and pillow lavas, and the late enriched dykes plot in or close to the MORB field, whereas the other dykes plot in the island arc basalt field. On the Th/Yb – Nb/Yb plot of Pearce (2008) (Fig. 14d), most of the pillow lavas and sheeted dykes fall in the MORB end of the oceanic basalt array, although some are displaced towards the volcanic arc field; the majority of the dykes associated with the later magmatic sequence fall above the oceanic basalt array, indicating an arc component. The later enriched dykes are displaced to the higher Nb/Yb area that is typically associated with alkaline, OIB-like volcanics.

DISCUSSION

Detailed field data from the BGS mapping project in the UAE have clearly indicated the presence of voluminous younger magmatism within the Oman – UAE Ophiolite. This later magmatic sequence includes wehrlite and pyroxenite that intrude the Moho Transition Zone and the lower part of the early crustal section, as well as larger gabbro bodies with dioritic and tonalitic to trondhjemitic components, and microgabbro dykes, all of which intrude the higher parts of the early crustal section. Although components of a similar younger magmatic sequence have been identified in Oman (Ernewein et al. 1988; Juteau et al. 1988; Shervais 2001; Dilek and Flower 2003; Adachi and Miyashita 2003; Yamasaki et al. 2006), they have typically been described as distinct intrusive complexes. This contrasts with the pervasive later magmatic sequence that has been mapped out in detail across much of the ophiolite outcrop in the UAE.

New geochronological data indicate that the later magmatic sequence in the UAE formed over a period of around 1.2 million years, between c. 96.40 and 95.26 Ma. The magmatism in the early crustal section is constrained to before 96.40 ± 0.29 Ma, but its exact age and duration are not known; it is likely to have formed during the preceding 1-2 million years (Rollinson 2009). The date of 95.26 ± 0.31 Ma obtained in this study for a tonalitic sample is essentially identical to the age given by Warren et al. (2005) for a trondhjemite intrusion from the ophiolite in Oman, indicating that emplacement of the later magmatic sequence was occurring along the length of the ophiolite at broadly the same time. Obduction of the ophiolite began around 94.5 Ma (Warren et al. 2005), less than one million years after the later sequence of magmatism had ceased, indicating that it is likely to have formed in a marginal, supra-subduction zone environment rather than at a mid-ocean ridge (Warren et al. 2005; Styles et al. 2006).

The early crustal section of the Oman – UAE Ophiolite has commonly been considered to have formed from MORB-like magmas at a constructive plate margin (Lippard et al. 1986; Boudier and Juteau 2000), although some authors have suggested formation in a back-arc basin environment (Pearce et al. 1981) or a zone of spreading above a nascent subduction zone (Shervais 2001). In the UAE, the crystallisation sequences of early crustal gabbros are those that would be expected from MORB magmas. The geochemistry of pillow lavas and sheeted dykes is broadly similar to that of MORB, but some aspects appear transitional towards island arc-type magmas. Similarly, some gabbro samples from the early crustal section show geochemical features more characteristic of island arc settings. In general, then, evidence from the UAE fits with the theory that the early crustal section was formed from MORB-like magmas at a spreading centre that was in close proximity to a zone of subduction initiation (Dilek and Furnes, 2009).

The origin and internal relationships of the later magmatic sequence in the UAE are rather more complicated, due to the presence of a number of different components. These are discussed in turn below.

The Moho Transition Zone in the UAE can be divided into a massive dunite unit and the upper Mixed Unit, as described above. The massive dunite unit is considered to be residual, as described by Nicolas and Prinzhofer (1983), but the overlying Mixed Unit clearly represents multiple phases of intrusion. During the earliest of these, layered gabbros were formed at the base of the early crustal section. The mode of formation of these layered gabbros has been the source of some considerable debate, as summarised by Macleod and Yaouancq (2000). They may, at least in part, have been injected as sills as suggested by Kelemen et al. (1997); but in the UAE, the lower layered gabbros have been so much disrupted by later magmatism that it is difficult to draw definitive conclusions.

Following formation of the early crustal section, the Mixed Unit developed through the intrusion of large volumes of ultramafic, chiefly pyroxenitic and wehrlitic, magmas. These ponded close to the base of the crust, with offshoots rising up through the crust and spreading out to form wehrlite and melagabbro sills within the layered gabbro sequence. At the base of the crust, blocks and sheets of layered gabbro were stoped, surrounded and disrupted by intrusive ultramafic material, forming xenoliths. Locally, the margins of these xenoliths were partially assimilated by the intruding magmas, producing gradational contacts with ‘ghost’ layering.

Petrographical analysis shows that the wehrlites have a different mineral crystallisation sequence to that expected for MORB, with early crystallisation of pyroxenes which indicates more hydrous melts (Yamasaki et al. 2006; Koepke et al. 2009), typical of magmas formed above subduction zones. Some previous workers (e.g. Juteau et al. 1988) have interpreted this crystallisation sequence as indicating that the wehrlites were formed from a different parental magma to the layered gabbros. However, others have questioned this, suggesting that the majority of wehrlites record equilibration with parent melts that were similar to MORB (Koga et al. 2001). Adachi and Miyashito (2003) were able to recognise two groups of wehrlites in Oman, one of which was chemically similar to the layered gabbros, whilst the other (the Fizh-South complex) was distinctly different and considered to be later.

In the UAE, the mineral chemistry of the analysed wehrlites appears to overlap with that of the layered gabbro and to be distinct from that of the younger gabbros. However, field relationships clearly show that the large wehrlite bodies were intruded following crystallisation of the early crustal gabbros; and the crystallisation sequence indicates that there must have been some change in the parental magma, probably due to the addition of fluids. This in itself is enough to identify the wehrlites as part of a second magmatic phase, although the origin of the parental magma is not clear.

As with the wehrlitic intrusions, field relationships show that the younger gabbros clearly cross-cut the gabbros of the early crustal section. Relationships between the younger gabbros and wehrlites are less clear, although at the few localities where they are seen together, the younger gabbros appear to intrude the wehrlites.

Petrographical analysis shows that a phase of the younger gabbros crystallised orthopyroxene at an early stage. Earlier crystallisation of pyroxenes is considered to indicate more hydrous melts (Yamasaki et al. 2006), and thus is linked to magmas formed above subduction zones. Mineral analysis indicates generally lower Mg# in clinopyroxene (at given feldspar An contents) in the younger gabbros than in the gabbros of the early crustal section. This has also been recognised in Oman as a diagnostic feature for younger gabbros, which have been proposed to have formed in a supra-subduction zone setting (Yamasaki et al. 2006).

The whole-rock chemistry of the younger gabbros shows characteristics related to cumulate processes, so that it can be difficult to interpret these data in terms of magma compositions. However, in general, the younger gabbros have some geochemical features that are commonly ascribed to supra-subduction zone magmas, such as lower TiO_2 and lower Nb contents. An exception to this is the orthopyroxene-bearing facies, which shows unusually high whole-rock Nb contents; the origin of these unusual magmas is uncertain.

Associated with the later magmatic sequence are a number of microgabbro and basalt dykes. As discussed above, the dykes can be divided into three clear groups on the basis of their geochemistry. The first group, which has a MORB-like geochemistry, occurs as dykes in the sheeted dyke complex or in the high-level gabbros; these dykes are always <2 m thick and north- to NNW-trending. The second group has more variable field relationships, but includes dykes that are found within the rocks of the later magmatic sequence, and thus can clearly be shown to be part of this later set of intrusions. This group of dykes has many of the geochemical features that are associated with island arc magmatism. They include some dykes with boninitic chemistry, which is generally considered to be a good indicator of the onset of subduction (Pearce et al. 1984). The third group is a volumetrically minor phase of enriched magmatism; these dykes are found at a variety of structural levels, including the mantle section, and so are considered to be among the youngest intrusions in the UAE part of the Oman – UAE ophiolite.

This division into three magmatic phases, based on dyke geochemistry, fits with divisions recognised in the volcanic pile of the Oman section of the ophiolite (e.g. Alabaster et al. 1982, Lippard et al. 1986). The MORB-like intrusions belonging to the early crustal section correspond to the Geotimes unit of Alabaster et al. (1982); the dykes associated with the later magmatic sequence show more similarity to the Lasail unit; and the youngest, enriched dykes correspond to the Salahi unit. Many workers in Oman have similarly identified later phases of magmatism within the intrusive rocks, although these have typically been volumetrically restricted (examples include the Lasail Complex of Lippard et al. 1986; the Fizh-South Complex of Adachi and Miyashito, 2003; and the

DWGB2 suite of Yamasaki et al. 2006). Two stages of melt production have also been recognised from study of chromites in the mantle section (Python et al. 2008; Dare et al. 2008; Rollinson 2008). The newly mapped later magmatic sequence of the UAE represents the first time that these younger intrusions have been recognised on such a large scale.

The origin of the younger intrusions within the Oman – UAE Ophiolite has long been a matter for debate. Many authors have attributed them to the onset of subduction, citing their chemical resemblance to arc-type basalts (e.g. Alabaster et al. 1982; Umino et al. 1990; Searle and Cox 1999; Shervais 2001; Ishikawa et al. 2002; Dilek and Flower 2003; Arai et al. 2006; Yamasaki et al. 2006; Lilly 2006). However, others have suggested different mechanisms, such as melt/rock interaction between the shallow upper mantle and melts produced by high degrees of melting of previously depleted mantle (Godard et al. 2006).

Our work in the UAE provides several separate strands of evidence that indicate a supra-subduction zone setting for the later magmatic sequence: 1) widespread, heterogeneous intrusions that do not show the physical features expected of MORB magmatism, but instead cut across the early mantle and crustal ophiolite sections; 2) emplacement of the later magmatic sequence less than 1 Ma before the start of obduction; 3) petrological data consistent with the involvement of hydrous magmas; 4) mineral and whole-rock geochemical data that show features, such as low Ti and Nb, and high Th, associated with SSZ settings. A trend of increasing influence of SSZ processes towards the north-west of the ophiolite has been suggested on the basis of work in Oman (Python et al. 2008) and the later magmatic sequence of the UAE could represent the culmination of this trend. We suggest that subduction initiation may have occurred at an earlier stage in the north-west, thus allowing the generation of the voluminous later magmatic sequence of the UAE.

CONCLUSIONS

1. The northern end of the Oman – UAE Ophiolite, exposed in the UAE, is characterised by early, ‘classic’ ophiolite mantle and crustal sections cross-cut by

a voluminous later magmatic sequence which can constitute up to 50% of the total exposure.

2. The magmas of the early crustal section were formed before c. 96. 4 Ma, at a spreading centre, either on a mid-ocean ridge or in a marginal basin.
3. The magmas of the later magmatic sequence were formed between c. 96.4 and c. 95.2 Ma, above a newly initiated subduction zone. They show many features of SSZ-type magmas, including petrological evidence for hydrous magmas and geochemical evidence for depletion in Ti, Nb and LREE relative to MORB.
4. Emplacement of the later magmatic sequence ended with obduction of the ophiolite around two million years after the onset of subduction.

ACKNOWLEDGEMENTS

This work was funded by the Ministry of Energy in the UAE and their help and support is gratefully acknowledged. This paper is published by permission of the Executive Director of the British Geological Survey. Graham Leslie, Hugh Rollinson and an anonymous referee provided constructive comments on an earlier version of this paper, which were much appreciated by the authors.

REFERENCES

Adachi, Y, Miyashita, S (2003) Geology and petrology of the plutonic complexes in the Wadi Fizh area: Multiple magmatic events and segment structure in the northern Oman ophiolite. Geochemistry, Geophysics, Geosystems 4

Alabaster, T, Pearce, J A, Malpas, J (1982) The Volcanic Stratigraphy and Petrogenesis of the Oman Ophiolite Complex. Contributions to Mineralogy and Petrology 81: 168-183

Anonymous (1972) Penrose field conference on ophiolites. Geotimes 17: 24-25

Arai, S, Kadoshima, K, Morishita, T (2006) Widespread arc-related melting in the mantle section of the northern Oman ophiolite as inferred from detrital chromian spinels. Journal of the Geological Society of London 163: 869-879

Benn, K, Nicolas, A, Reuber, I (1988) Mantle-crust transition zone and origin of wehrlitic magmas: Evidence from the Oman ophiolite. Tectonophysics 151: 75-85

Boudier, F, Ceuleneer, G, Nicolas, A (1988) Shear zones, thrusts and related magmatism in the Oman ophiolite: initiation of thrusting on an oceanic ridge. Tectonophysics 151: 275-296

Boudier, F, Godard, M, Armbruster, C (2000) Significance of gabbronorite occurrence in the crustal section of the Semail ophiolite. Marine Geophysical Researches 21: 307-326

Boudier, F, Juteau, T (2000) The ophiolite of Oman and United Arab Emirates. Marine Geophysical Researches 21: 145-407

Boudier, F, Nicolas, A (1995) Nature of the Moho Transition Zone in the Oman Ophiolite. Journal of Petrology 36: 777-796

Boudier, F, Nicolas, A, Ildefonse, B (1996) Magma chambers in the Oman ophiolite: fed from the top and the bottom. Earth and Planetary Science Letters 144: 239-250

British Geological Survey (2006) Geological Map of the Northern Emirates, 1:250,000 scale. British Geological Survey, Keyworth, Nottingham

Coleman, R G (1977) Ophiolites. Springer-Verlag, Berlin-Heidelberg

Coleman, R G (1981) Tectonic setting of ophiolite obduction in Oman. Journal of Geophysical Research 86: 2497-2508

Cox, J, Searle, M P, Pedersen, R (1999) The petrogenesis of leucogranitic dykes intruding the northern Semail ophiolite, United Arab Emirates: field relationships, geochemistry and Sr/Nd isotope systematics. Contributions to Mineralogy and Petrology 137: 267-288

Dare, S A S, Pearce, J A, McDonald, I, Styles, M T (2009) Tectonic discrimination of peridotites using fO_2–Cr# and Ga–Ti–Fe^{III} systematics in chrome–spinel. Chemical Geology 261: 199-216

Dilek, Y, Flower, M F J (2003) Arc-trench rollback and forearc accretion: 2. A model template for ophiolites in Albania, Cyprus and Oman. In: Dilek, Y, Robinson P T (eds) Ophiolites in Earth History. Special Publication of the Geological Society No. 218. The

Geological Society, London. pp 43-68

Dilek, Y, Furnes, H (2009) Structure and geochemistry of Tethyan ophiolites and their petrogenesis in subduction rollback systems. Lithos 113: 1-20

Einaudi, F, Pezard, P A, Cocheme, J-J, Coulon, C, Laverne, C, Godard, M (2000) Petrography, Geochemistry and Physical Properties of a Continuous Extrusive Section from the Sarami Massif, Semail Ophiolite. Marine Geophysical Researches 21: 387-407

Ernewein, M, Pflumo, C, Whitechurch, H (1988) The death of an accretion zone as evidenced by the magmatic history of the Sumail ophiolite (Oman). Tectonophysics 151: 247-274

Glennie, K W, Boeuf, M G A, Hughes Clark, M W, Moody-Stewart, M, Pilaar, W H F, Reinhardt, B M (1974) Geology of the Oman Mountains. Verhandelingen van het Koninklijk Nederlands geologisch mijnbouwkundig Genootschap, Transactions 31 (1): 423

Godard, M, Bosch, D, Einaudi, F (2006) A MORB source for low-Ti magmatism in the Semail ophiolite. Chemical Geology 234: 58-78

Hacker, B R, Mosenfelder, J L, Gnos, E (1996) Rapid emplacement of the Oman ophiolite: thermal and geochronologic constraints. Tectonics 15: 1230-1247

Ishikawa, T, Nagaishi, K, Umino, S (2002) Boninitic volcanism in the Oman ophiolite: implications for thermal condition during transition from spreading ridge to arc. Geology 30: 899-902

Jousselin, D, Nicolas, A (2000) The Moho transition zone in the Oman ophiolite - relation with wehrlites in the crust and dunites in the mantle. Marine Geophysical Researches 21: 229-241

Juteau, T, Ernewein, M, Reuber, I, Whitechurch, H, Dahl, R (1988) Duality of magmatism in the plutonic sequence of the Sumail Nappe, Oman. Tectonophysics 151: 107-135

Kelemen, P B, Dunn, J T (1992) Depletion of Nb relative to other highly incompatible elements by melt/rock reaction in the upper mantle. Transactions of the American

Geophysical Union 73: 656-657

Kelemen, P B, Shimizu, N, Salters, V J N (1995) Extraction of mid-ocean-ridge basalt from the upwelling mantle by focused flow of melt in dunite channels. Nature 375: 747-753

Kelemen, P B, Koga, K, Shimizu, N (1997) Geochemistry of gabbro sills in the crust-mantle transition zone of the Oman ophiolite: implications for the origin of the oceanic lower crust. Earth and Planetary Science Letters 146: 475-488

Koepke, J, Schoenborn, S, Oelze, M, Wittmann, H, Feig, S T, Hellebrand, E, Boudier, F, Schoenberg, R (2009) Petrogenesis of crustal wehrlites in the Oman ophiolite: Experiments and natural rocks. Geochemistry, Geophysics, Geosystems 10

Koga, K T, Kelemen, P B, Shimizu, N (2001) Petrogenesis of the crust-mantle transition zone and the origin of lower crustal wehrlite in the Oman ophiolite. Geochemistry, Geophysics, Geosystems 2

Korenaga, J, Kelemen, P B (1997) Origin of gabbro sills in the Moho transition zone of the Oman ophiolite: Implications for magma transport in the oceanic lower crust. Journal of Geophysical Research 102: 27729-27749

Krogh, T E (1973) A low contamination method for the hydrothermal decomposition of zircon and extraction of U and Pb for isotopic age determinations. Geochimica et Cosmochimica Acta 46: 637-649

Lilly, R M (2006) The Magmatic Evolution and Crustal Accretion of the Northern Oman–United Arab Emirates Ophiolite. PhD Thesis, University of Cardiff.

Lippard, S J, Shelton, A W, Gass, I G (1986) The Ophiolite of Northern Oman. Blackwell Scientific Publications, Oxford

Ludwig, K R (2003) Isoplot 3, A Geochronological Toolkit for Microsoft Excel. Berkeley Geochronology Centre Special Publication 1a.

Macleod, C J, Yaouancq, G (2000) A fossil melt lens in the Oman ophiolite: Implications for magma chamber processes at fast spreading ridges. Earth and Planetary Science Letters 176: 357-373

Nicolas, A, Boudier, F (2003) Where ophiolites come from and what they tell us. In: Dilek, Y, Newcomb S (eds) Ophiolite concept and the evolution of geological thought. Geological Society of America Special Paper 373. Geological Society of America, Boulder, Colorado. pp 137-152

Nicolas, A, Boudier, F, Ildefonse, B, Ball, E (2000a) Accretion of Oman and United Arab Emirates ophiolite - discussion of a new structural map. Marine Geophysical Researches 21: 147-179

Nicolas, A, Boudier, F, Michibayashi, K, Gerbert-Gaillard, L (2000b) Aswad Massif (United Arab Emirates): Archetype of the Oman - UAE ophiolite belt. In: Dilek, Y, Moores E M, Elthon D, Nicolas A (eds) Ophiolites and Oceanic Crust: New Insights from Field Studies and the Ocean Drilling Program. Geological Society of America Special Paper 349, Boulder. pp 499-512

Nicolas, A, Boudier, F (2000) Large mantle upwellings and related variations in crustal thickness in the Oman ophiolite. In: Dilek, Y, Moores E M, Elthon D, Nicolas A (eds) Ophiolites and Oceanic Crust: New Insights from Field Studies and the Ocean Drilling Program. Geological Society of America Special Paper 349, Boulder. pp 67-73

Nicolas, A, Prinzhofer, A (1983) Cumulative or Residual Origin for the Transition Zone in Ophiolites: Structural Evidence. Journal of Petrology 24: 188-206

Parrish, R R (1987) An improved micro-capsule for zircon dissolution in U-Pb geochronology. Chemical Geology (Isotope Geoscience section) 66: 99-102

Parrish, R R, Noble, S R (2003) Zircon U-Th-Pb geochronology, by Isotope Dilution - Thermal Ionisation Mass Spectrometry (ID-TIMS). In: Zircon, reviews in mineralogy and geochemistry. Mineralogical Society of America Special Paper 53. pp 183-214

Parrish, R R, Roddick, J C, Loveridge, W D, Sillivan, R W (1987) Uranium-lead analytical techniques at the geochronology laboratory, Geological Survey of Canada. In: Radiogenic age and isotope studies, Report 1. Geological Survey of Canada Paper 87-2. pp 3-7

Pearce, J A (1982) Trace element characteristics of lavas from destructive plate boundaries. In: Thorpe, R S (ed) Andesites. John Wiley and Sons, pp 525-547

Pearce, J A (2008) Geochemical fingerprinting of oceanic basalts with applications to ophiolite classification and the search for Archaean oceanic crust. Lithos 100: 14-48

Pearce, J A, Alabaster, T, Shelton, A W, Searle, M P (1981) The Oman ophiolite as a Cretaceous arc-basin complex: evidence and implications. Phil. Trans. R. Soc. Lond. A 300: 299-317

Pearce, J A, Lippard, S J, Roberts, S (1984) Characteristics and tectonic significance of supra-subduction zone ophiolites. Journal of the Geological Society of London 16: 77-94

Peters, T, Kamber, B S (1994) Peraluminous, potassium-rich granitoids in the Semail Ophiolite. Contributions to Mineralogy and Petrology 118: 229-238

Python, M, Ceuleneer, G (2003) Nature and distribution of dykes and related melt migration structures in the mantle section of the Oman ophiolite. Geochemistry, Geophysics, Geosystems 4: 8612

Python, M, Ceuleneer, G, Arai, S (2008) Chromian spinels in mafic–ultramafic mantle dykes: Evidence for a two-stage melt production during the evolution of the Oman ophiolite. Lithos 106: 137-154

Reuber, I (1988) Complexity of the crustal sequence in the northern Oman ophiolite (Fizh and southern Aswad blocks): the effect of early slicing? Tectonophysics 151: 137-165

Robertson, A H F, Searle, M P, Ries, A C (1990) The Geology and Tectonics of the Oman Region. Geological Society of London Special Publication 49. London, the Geological Society.

Roddick, J C (1987) Generalized numerical error analysis with applications to geochronology and thermodynamics. Geochimica et Cosmochimica Acta 51: 123-138

Rollinson, H (2008) The geochemistry of mantle chromitites from the northern part of the Oman ophiolite: inferred parental melt compositions. Contributions to Mineralogy and Petrology 156: 273-288

Rollinson, H (2009) New models for the genesis of plagiogranites in the Oman ophiolite. Lithos 112: 603-614

Searle, M, Cox, J (1999) Tectonic setting, origin and obduction of the Oman ophiolite.

Geological Society of America Bulletin 111: 104-122

Searle, M P, Cox, J (2002) Subduction zone metamorphism during formation and emplacement of the Semail ophiolite in the Oman Mountains. Geological Magazine 139: 241-255

Serri, G (1981) The petrochemistry of ophiolite gabbroic complexes: a key for the classification of ophiolites into low-Ti and high-Ti types. Earth and Planetary Science Letters 52: 203-212

Shervais, J W (1982) Ti-V plots and the petrogenesis of modern and ophiolitic lavas. Earth and Planetary Science Letters 59: 101-118

Shervais, J W (2001) Birth, death and resurrection: the life cycle of suprasubduction zone ophiolites. Geochemistry, Geophysics, Geosystems 2

Smewing, J D (1980) Regional setting and petrological characteristics of the Oman ophiolite in North Oman. Ofioliti 2: 335-378

Stacey, J S, Kramers, J D (1975) Approximation of terrestrial lead isotope evolution by a two-stage model. Earth and Planetary Science Letters 26: 207-221.

Styles, M T, Ellison, R A, Arkley, S L B, Crowley, Q, Farrant, A, Goodenough, K M, McKervey, J A, Pharaoh, T C, Phillips, E R, Schofield, D, Thomas, R J (2006) The Geology and Geophysics of the United Arab Emirates. British Geological Survey, Keyworth, Nottingham

Sun, S-S, McDonough, W F (1989) Chemical and isotopic systematics of oceanic basalts: implications for mantle composition and processes. In: Saunders, A D, Norry M J (eds) Magmatism in the Ocean Basins. Geological Society Special Publication 42. The Geological Society, London. pp 313-346

Tilton, G R, Hopson, C A, Wright, G E (1981) Uranium-lead isotopic ages of the Semail Ophiolite, Oman, with applications to Tethyan Ridge Tectonics. Journal of Geophysical Research 86: 2763-2775

Umino, S, Yanai, S, Jaman, A R, Nakamura, Y, Iiyama, J T (1990) The transition from spreading to subduction: evidence from the Semail ophiolite, northern Oman mountains.

In: Malpas, J, Moores E M, Panayiotou A, Xenophontos C (eds) Ophiolites: Oceanic Crustal Analogues. Proceedings of the Symposium "Troodos 1987" Geological Survey Department, Cyprus, Nicosia. pp 375-395

Warren, C J, Parrish, R R, Waters, D J, Searle, M P (2005) Dating the geologic history of Oman's Semail ophiolite: insights from U-Pb geochronology. Contributions to Mineralogy and Petrology 150: 403-422

Yamasaki, T, Maeda, J, Mizuta, T (2006) Geochemical evidence in clinopyroxenes from gabbroic sequence for two distinct magmatisms in the Oman ophiolite. Earth and Planetary Science Letters 251: 52-65

Figure list

Figure 1: Overview map showing the location of the main blocks of the Oman-UAE ophiolite (ophiolite blocks shown in grey), after Lippard et al. (1986).

Figure 2: Simplified geological map showing the main features of the ophiolite in the UAE, after British Geological Survey (2006).

Figure 3: Cartoon of a hypothetical vertical section illustrating the main features of the Moho Transition Zone in the UAE. The vertical extent from the top of the harzburgite to the base of the layered gabbro varies from a few tens of metres to more than a kilometre.

Figure 4: Photographs of Mixed Unit outcrops, showing paler-coloured gabbro enclaves isolated within darker-coloured, intrusive wehrlites. Tabular shape of enclaves is controlled by layering. Hammer for scale, c. 30 cm long. Photographs © Ministry of Energy, UAE.

Figure 5: Cartoon illustrating the pervasively sheeted and cross-cutting nature of the younger gabbros.

Figure 6: Photographs showing the relationships of the later magmatic sequence: a) sheets of pale-coloured younger gabbro cut darker Mixed Unit lithologies across a hillside (view about 1 km across); b) “Vinaigrette” sheet associated with the later magmatic sequence truncates layering in layered gabbro in a new road cutting, figure for scale; c) Irregular sheet of younger gabbro cuts across layering in layered gabbro, figure for scale; d) Close-up of margin of younger gabbro dyke cutting layered gabbro. Pen c. 10 cm long for scale.

Figure 7: Transmitted light images of zircons from dated samples, indicating representative morphologies of dated zircons.

Figure 8: U-Pb concordia plots for the dated samples

Figure 9: Mg# in clinopyroxenes vs An % in plagioclase for gabbroic rocks. Both core and rim samples are plotted. Solid line shows the distinction between the GB1 and GB2 suites of Yamasaki et al. (2006).

Figure 10: N-MORB normalized trace element patterns for representative samples of layered gabbro (black), high-level gabbro (white) and younger gabbro (grey). Normalising factors from Sun and McDonough (1989).

Figure 11: TiO_2 versus Mafic Index plot for whole-rock gabbroic samples, after Serri (1981).

Figure 12: Nb/Yb vs La/Nb plot for whole-rock gabbroic samples.

Figure 13: N-MORB normalized trace element patterns for representative samples of pillow basalt and sheeted dyke complex (white), dykes associated with the later magmatic sequence (grey) and late, enriched dykes (asterisk). Normalising factors from Sun and McDonough (1989).

Figure 14: a) Ti versus V plot for lavas and dykes. Lines indicate constant Ti-V ratios; b) Zr versus Zr/Y plot for lavas and dykes. Fields after Alabaster et al. (1982): MORB – Mid-ocean Ridge Basalt, IAT – Island Arc Tholeiite; c) Cr vs Y plot for lavas and dykes. Fields after Pearce (1982), names as in c); Nb/Yb versus Th/Yb plot for lavas and dykes. MORB-OIB array after Pearce (2008).

Tables (could be online only)

Table 1: U-Pb isotopic analyses for the dated samples

Table 2: Summary mineral chemistry data

Table 3: Whole-rock major, trace element and REE data

Figure 1
Click here to download high resolution image

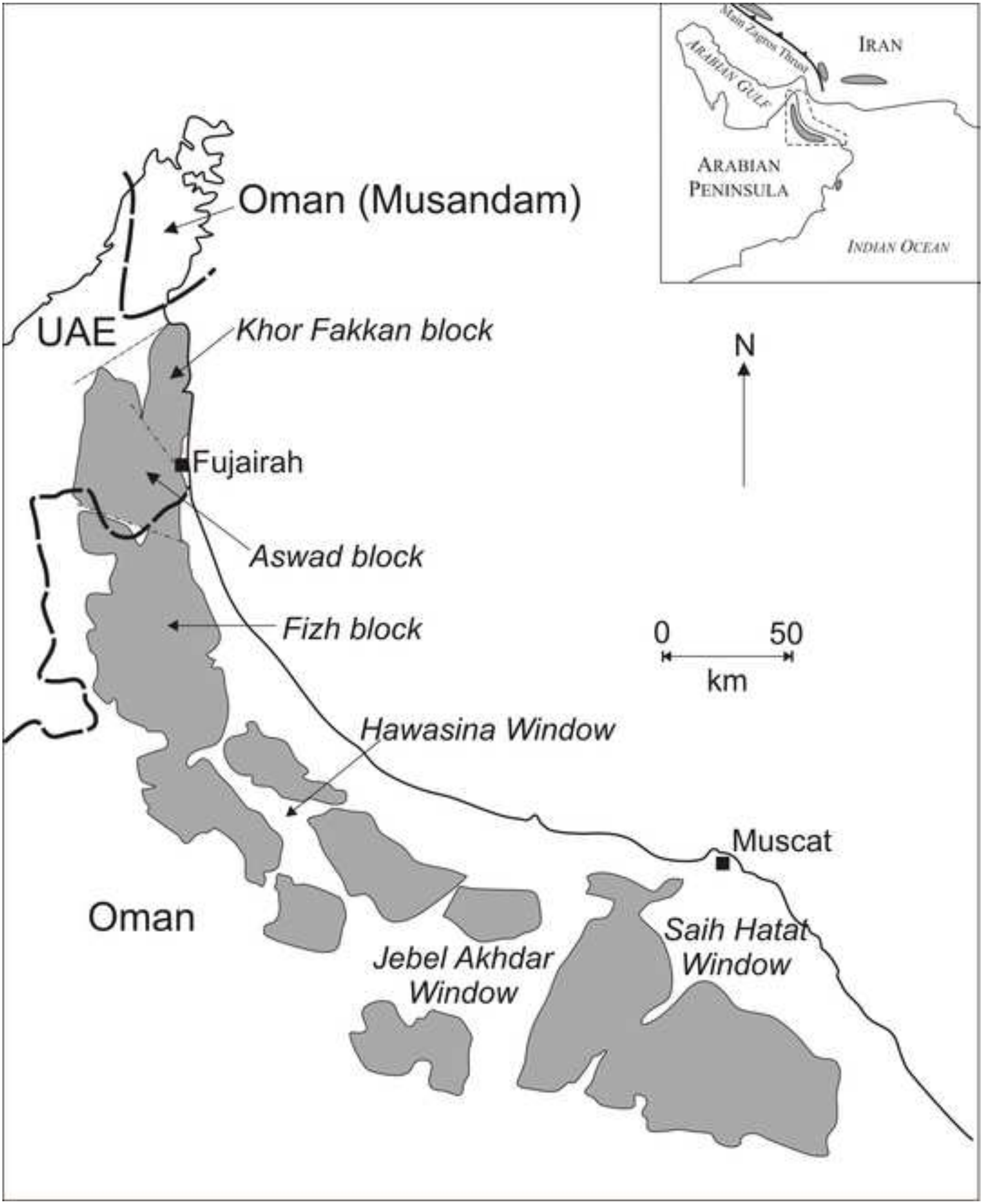

Figure 2_black&white

Click here to download high resolution image

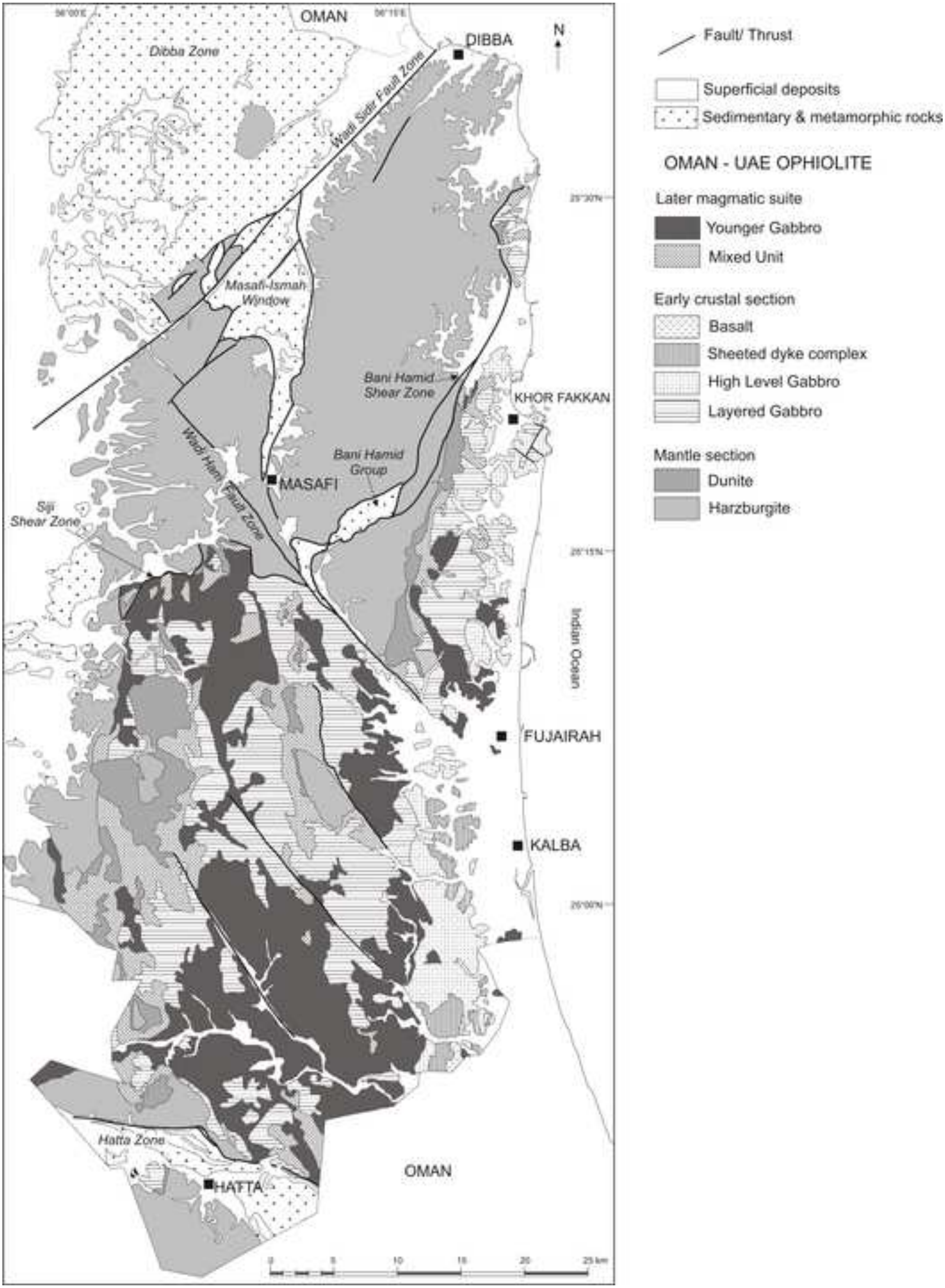

Figure 2_colour

Click here to download high resolution image

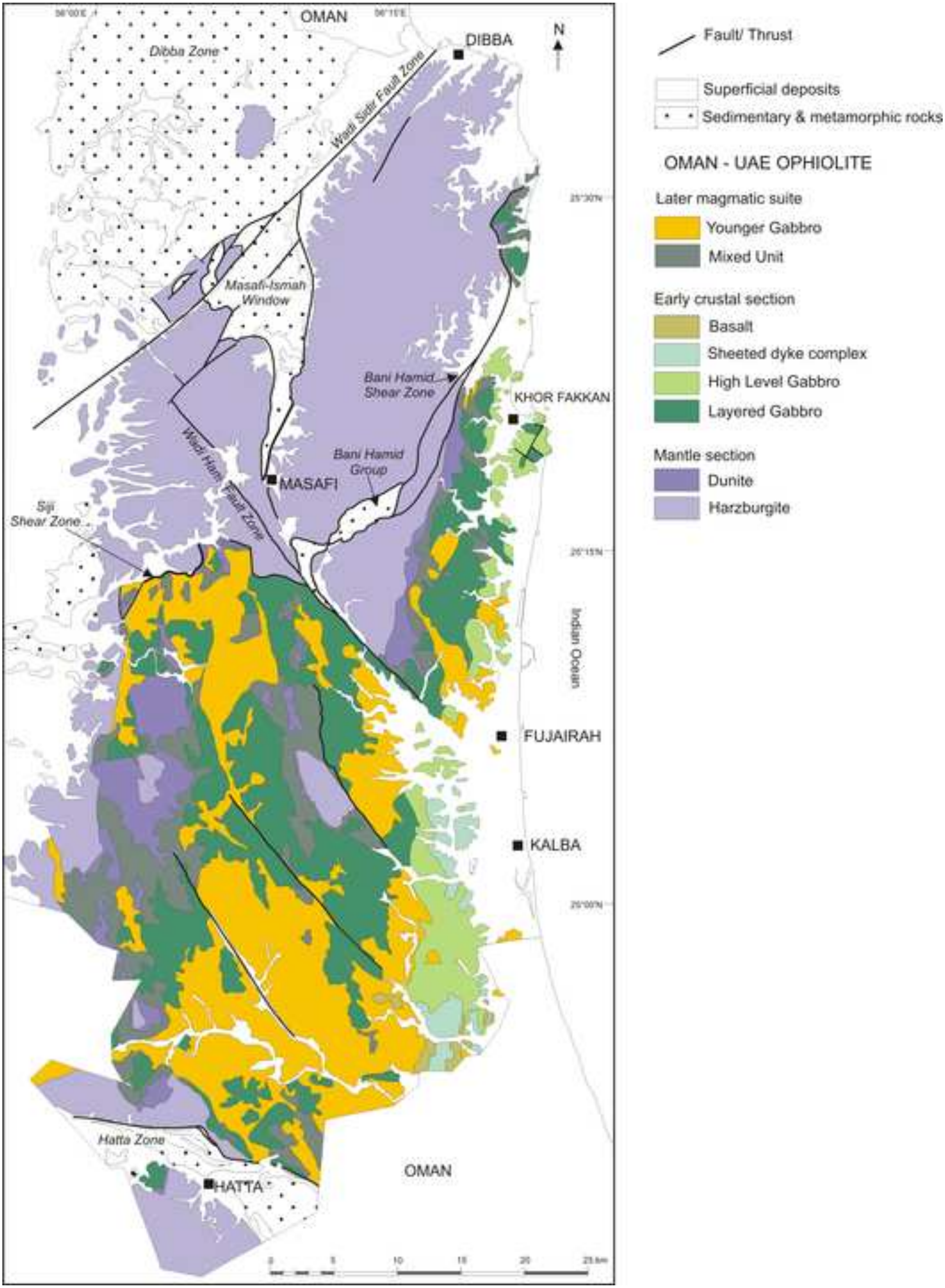

Figure 3

Click here to download high resolution image

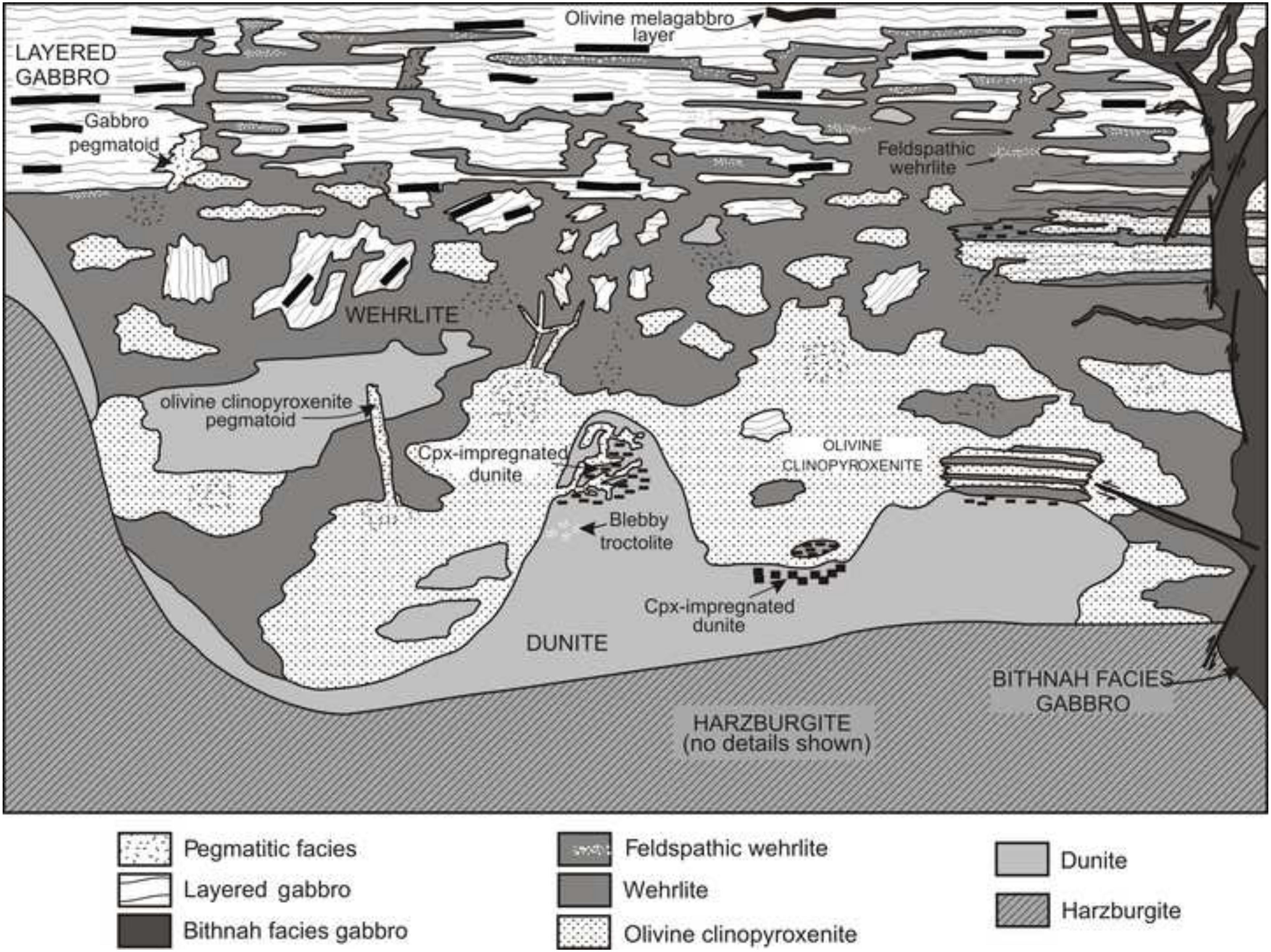

Figure 4_black&white
Click here to download high resolution image

Figure 4_colour
Click here to download high resolution image

Figure 5

Click here to download high resolution image

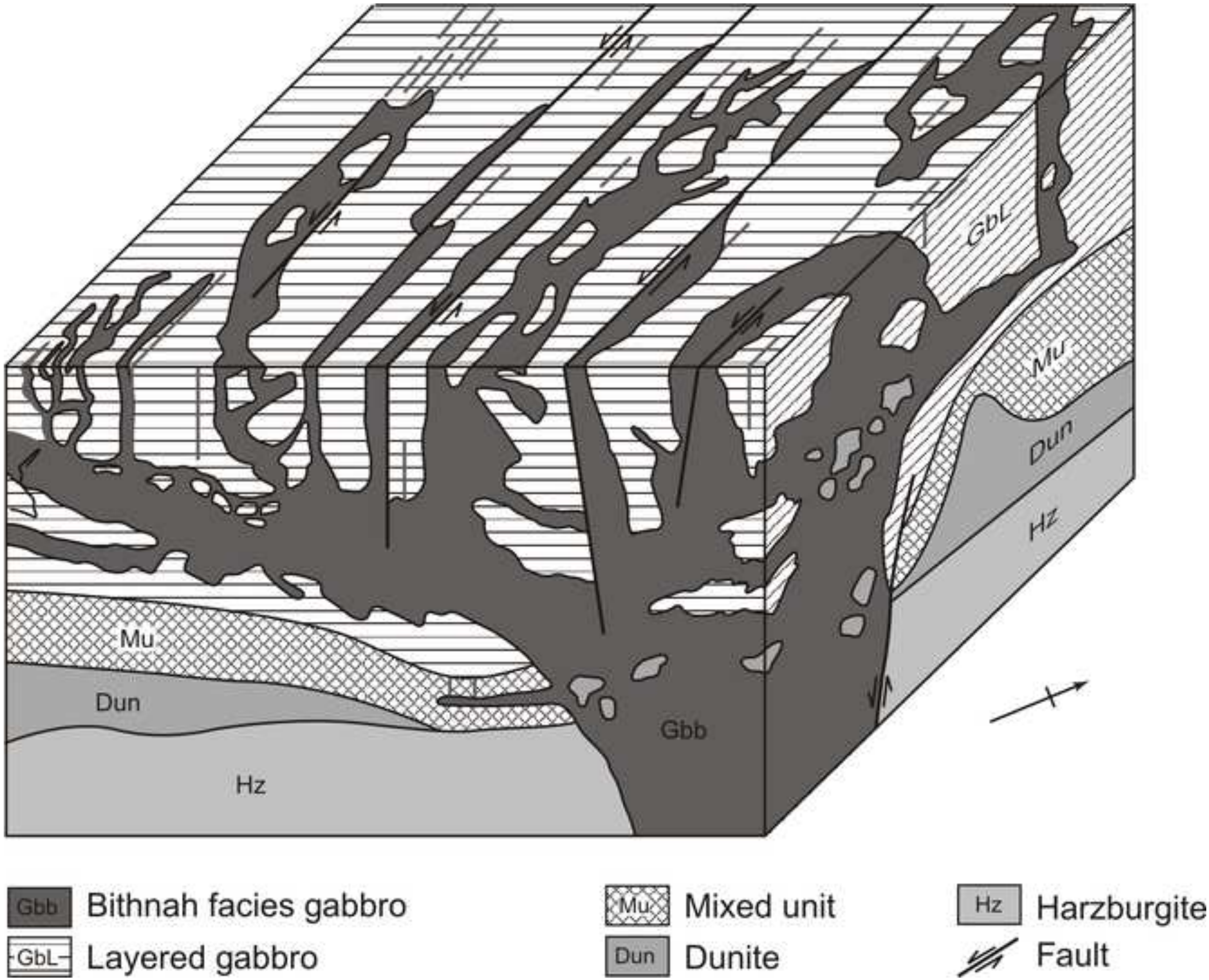

Figure 6_black&white
Click here to download high resolution image

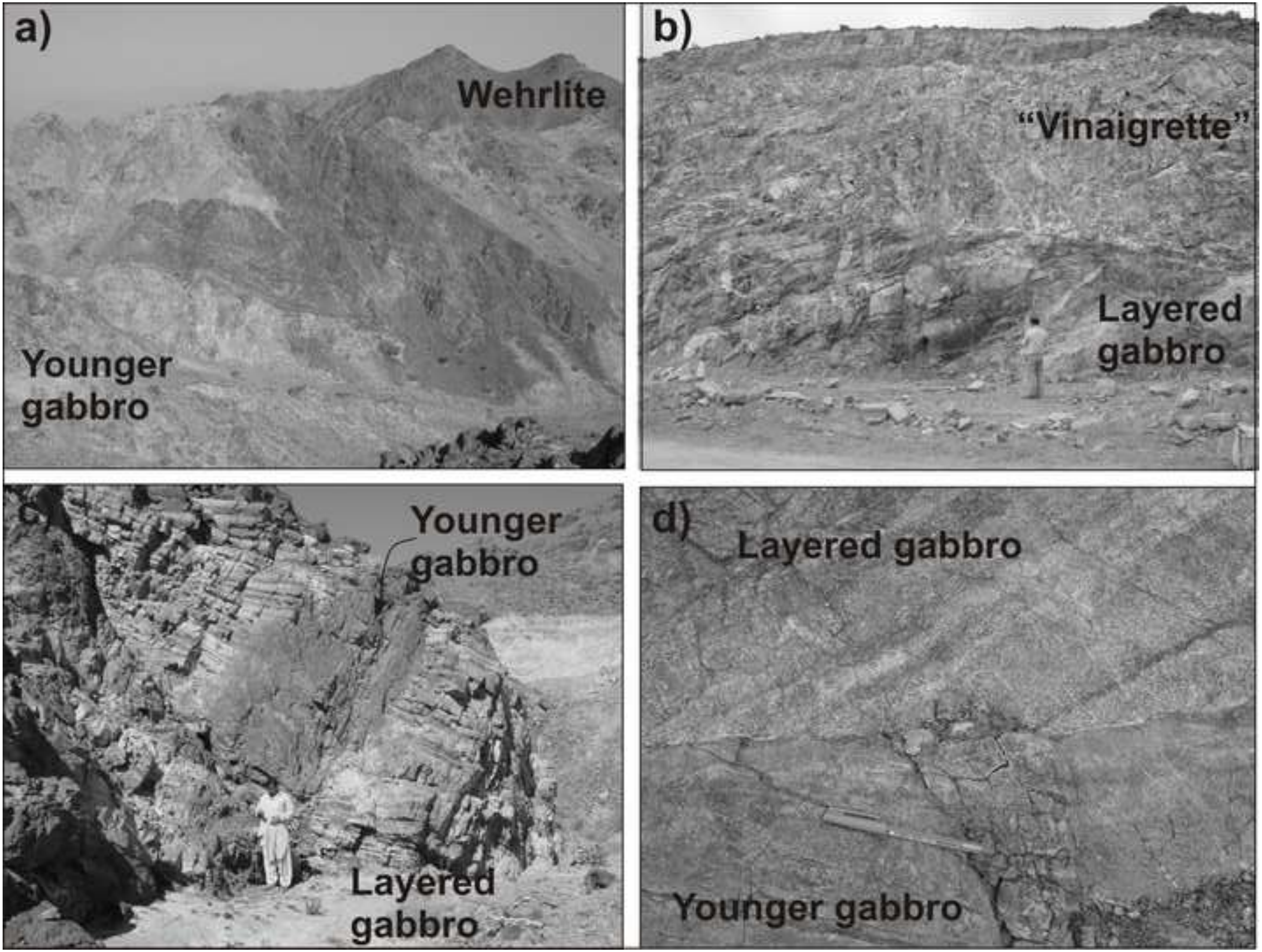

Figure 6_colour

Click here to download high resolution image

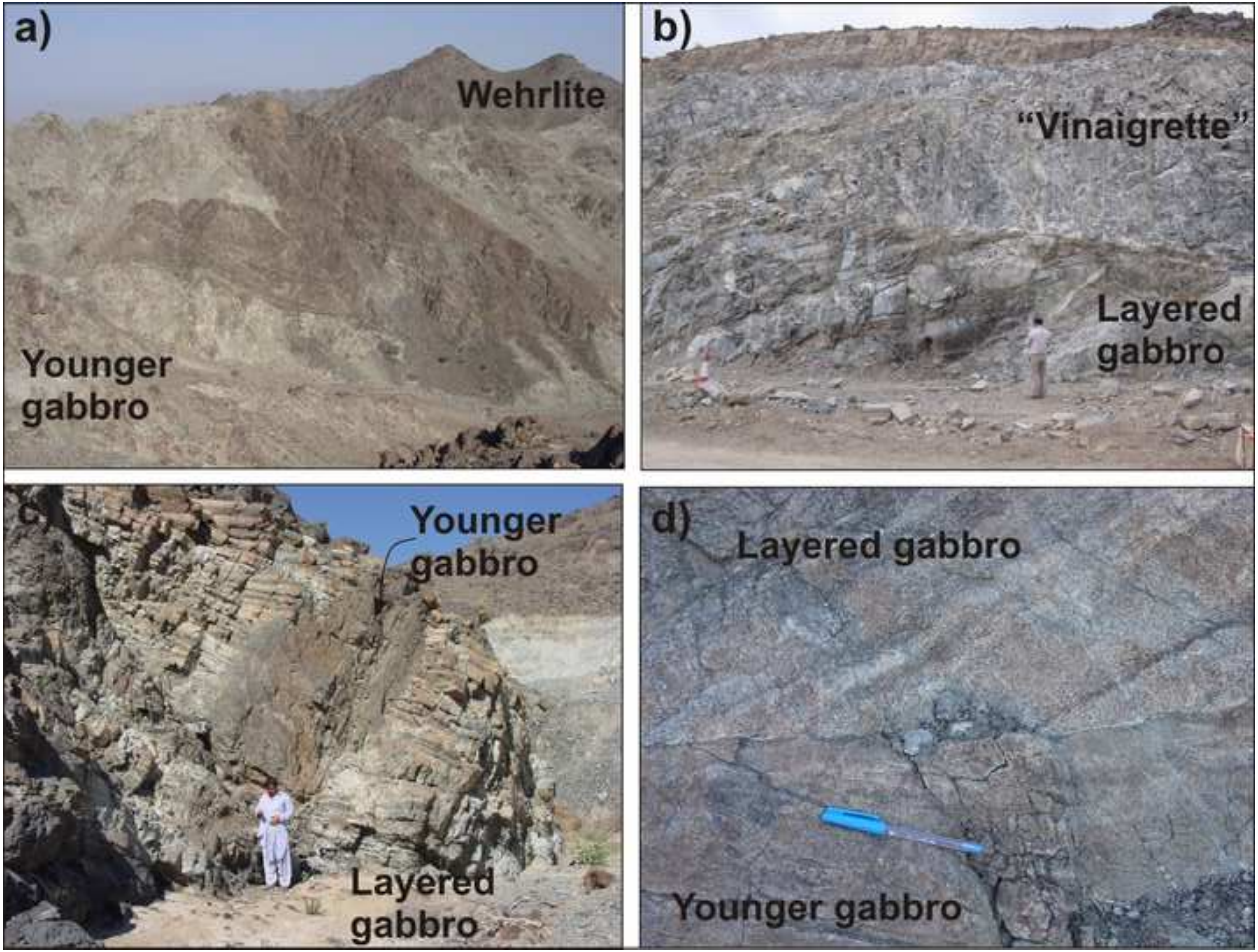

Figure 7

Click here to download high resolution image

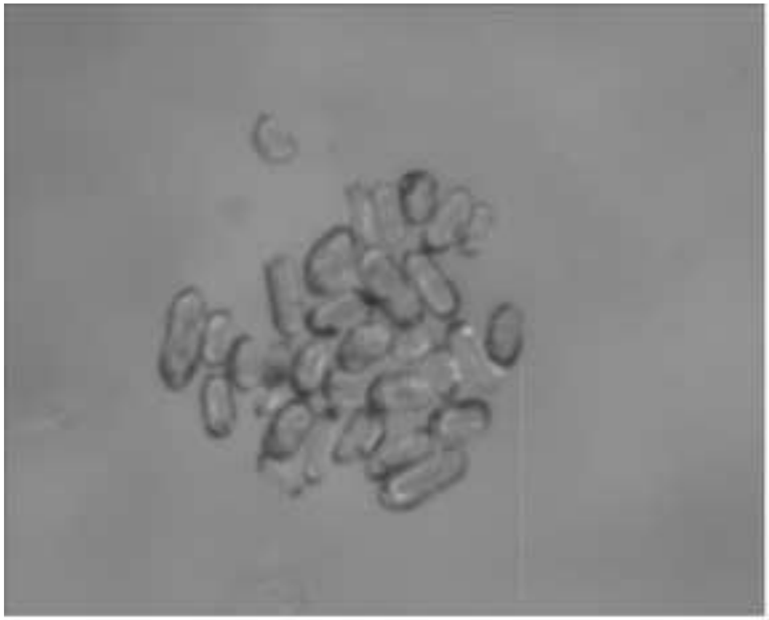

Sample UAE180

Sample UAE163

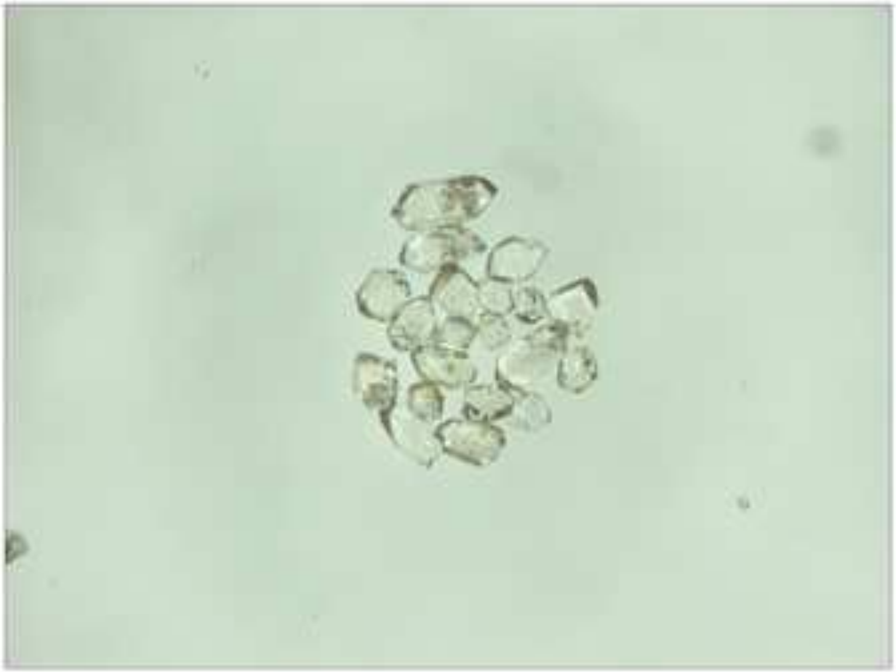

Sample UAE167

Figure 8

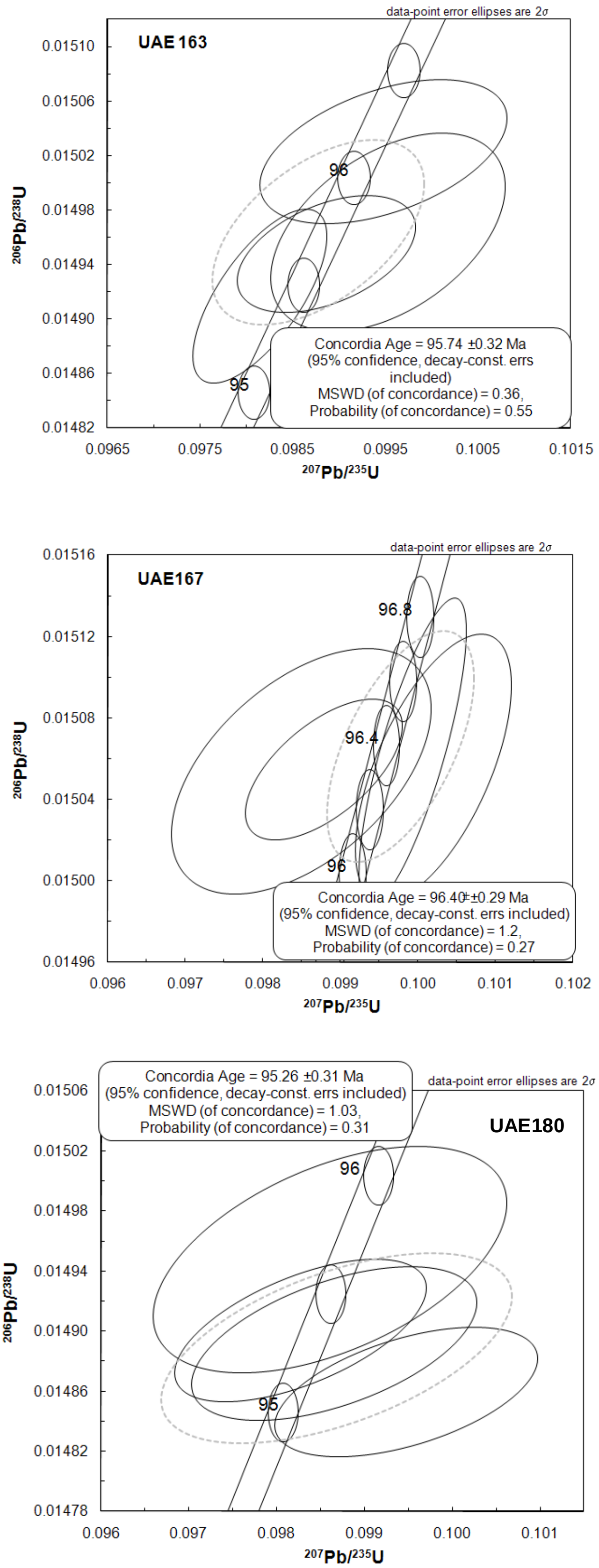
data-point error ellipses are 2σ
UAE 163
0.01510
0.01506
0.01502
0.01498
0.01494
0.01490
0.01486
0.01482
96
95
Concordia Age = 95.74 ±0.32 Ma
(95% confidence, decay-const. errs included)
MSWD (of concordance) = 0.36,
Probability (of concordance) = 0.55
0.0965
0.0975
0.0985
0.0995
0.1005
0.1015
207Pb/235U
206Pb/238U
data-point error ellipses are 2σ
UAE167
0.01516
0.01512
0.01508
0.01504
0.01500
0.01496
96.8
96.4
96
Concordia Age = 96.40 ±0.29 Ma
(95% confidence, decay-const. errs included)
MSWD (of concordance) = 1.2,
Probability (of concordance) = 0.27
0.096
0.097
0.098
0.099
0.100
0.101
0.102
207Pb/235U
206Pb/238U
Concordia Age = 95.26 ±0.31 Ma
(95% confidence, decay-const. errs included)
MSWD (of concordance) = 1.03,
Probability (of concordance) = 0.31
data-point error ellipses are 2σ
UAE180
0.01506
0.01502
0.01498
0.01494
0.01490
0.01486
0.01482
0.01478
96
95
0.096
0.097
0.098
0.099
0.100
0.101
207Pb/235U
206Pb/238U

Figure 9

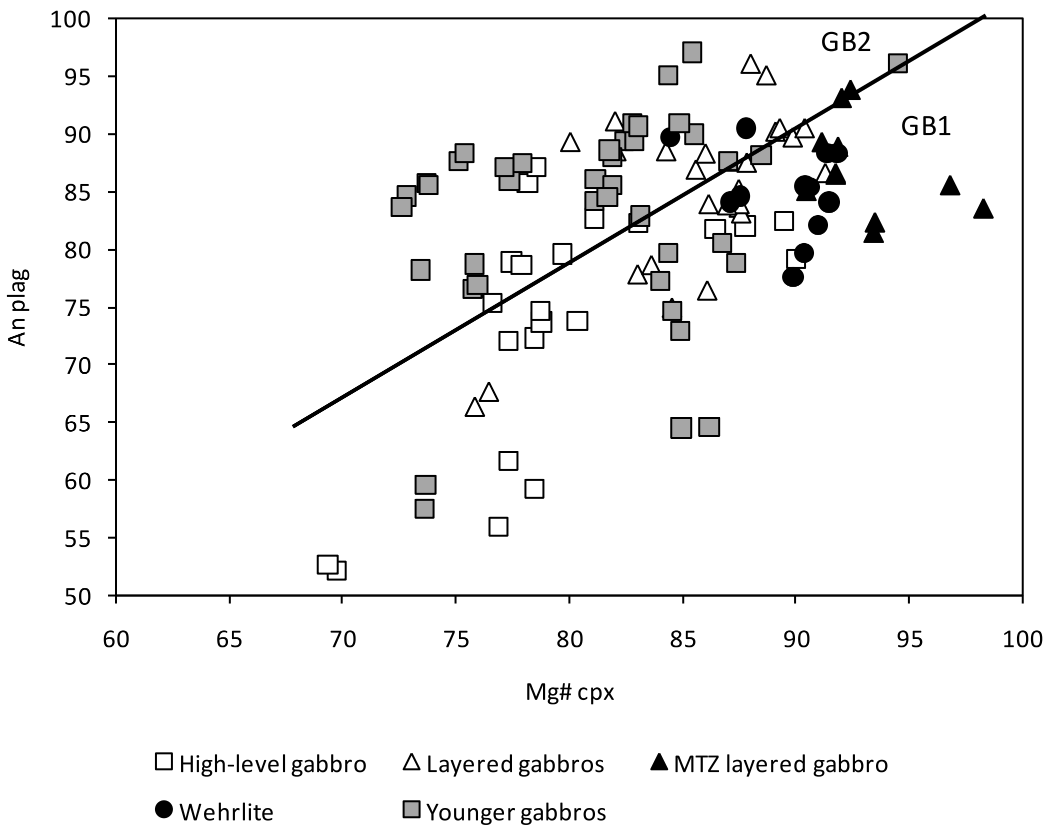
100
95
90
85
80
75
70
65
60
55
50
An plag
60
65
70
75
80
85
90
95
100
Mg# cpx
GB2
GB1
High-level gabbro
Layered gabbros
MTZ layered gabbro
Wehrlite
Younger gabbros

Figure 10

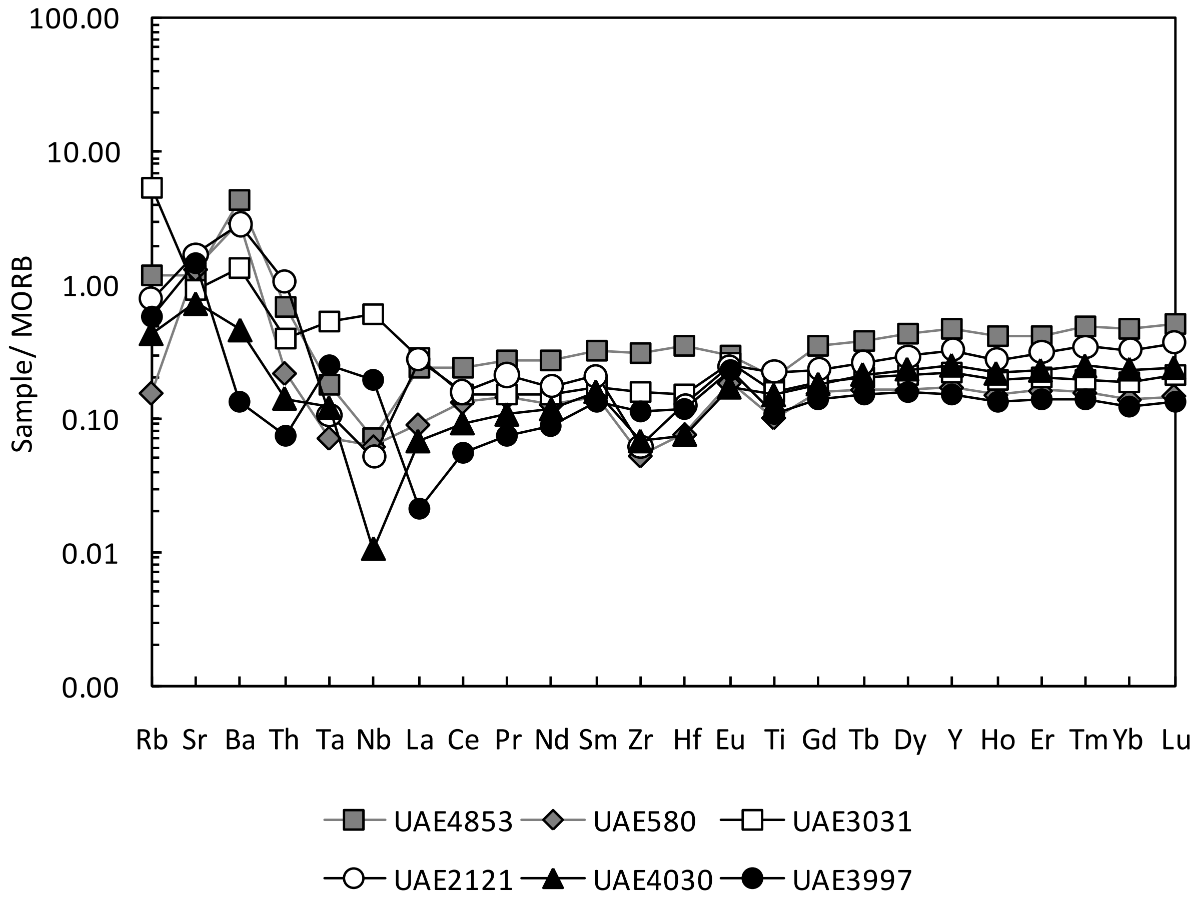
100.00
10.00
1.00
0.10
0.01
0.00
Sample/ MORB
Rb
Sr
Ba
Th
Ta
Nb
La
Ce
Pr
Nd
Sm
Zr
Hf
Eu
Ti
Gd
Tb
Dy
Y
Ho
Er
Tm
Yb
Lu
UAE4853
UAE580
UAE3031
UAE2121
UAE4030
UAE3997

Figure 11

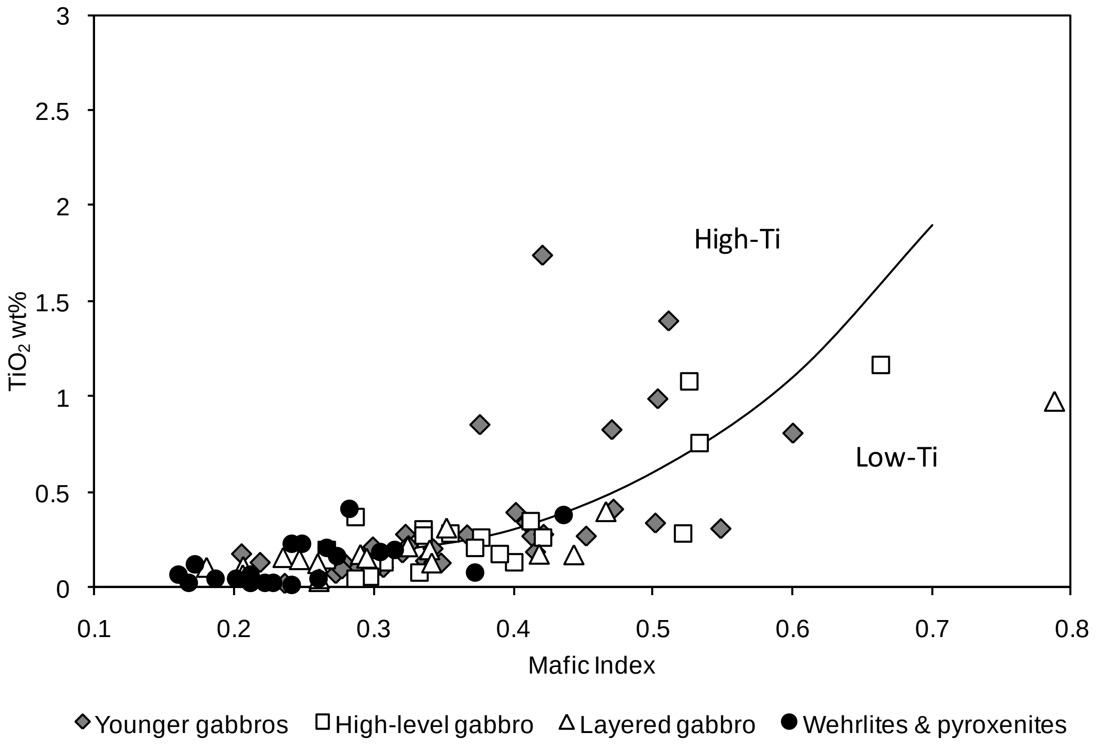
3
2.5
2
1.5
1
0.5
0
TiO_2 wt%
High-Ti
Low-Ti
0.1
0.2
0.3
0.4
0.5
0.6
0.7
0.8
Mafic Index
Younger gabbros
High-level gabbro
Layered gabbro
Wehrlites & pyroxenites

Figure 12

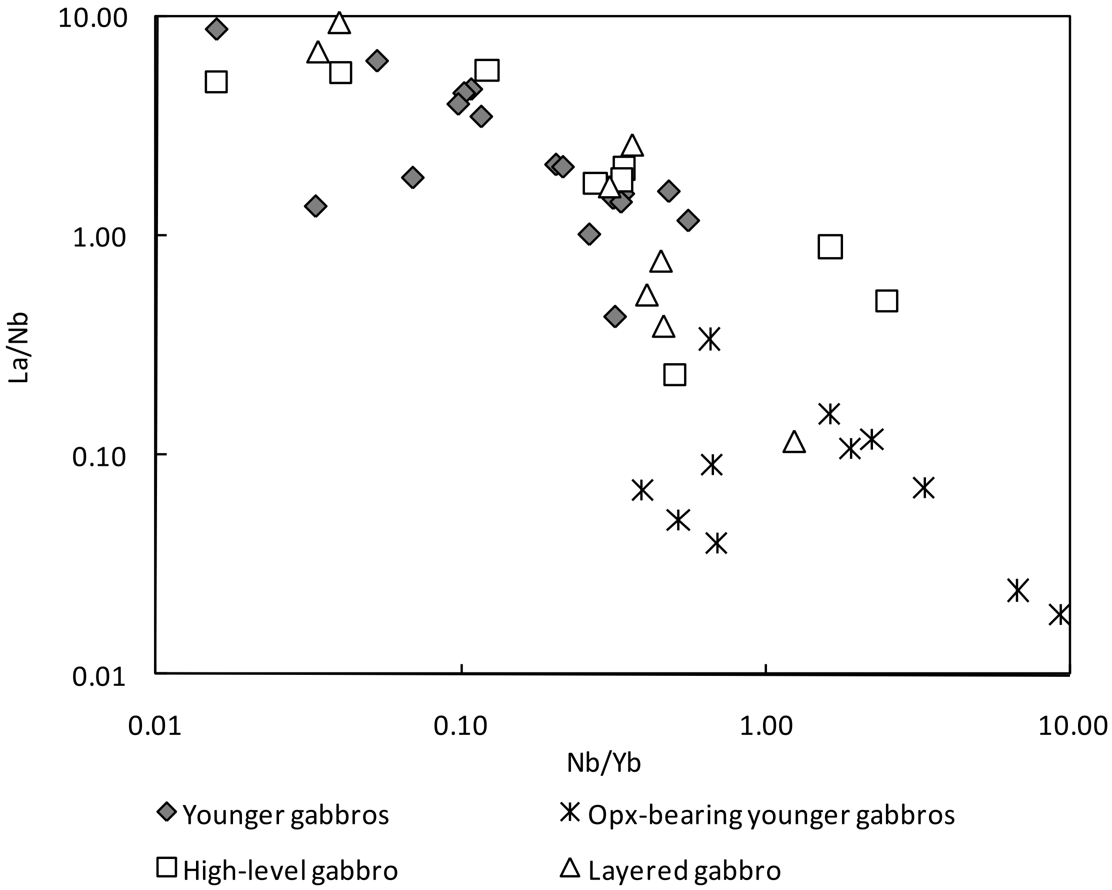
10.00
1.00
0.10
0.01
La/Nb
0.01
0.10
1.00
10.00
Nb/Yb
Younger gabbros
Opx-bearing younger gabbros
High-level gabbro
Layered gabbro

Figure 13

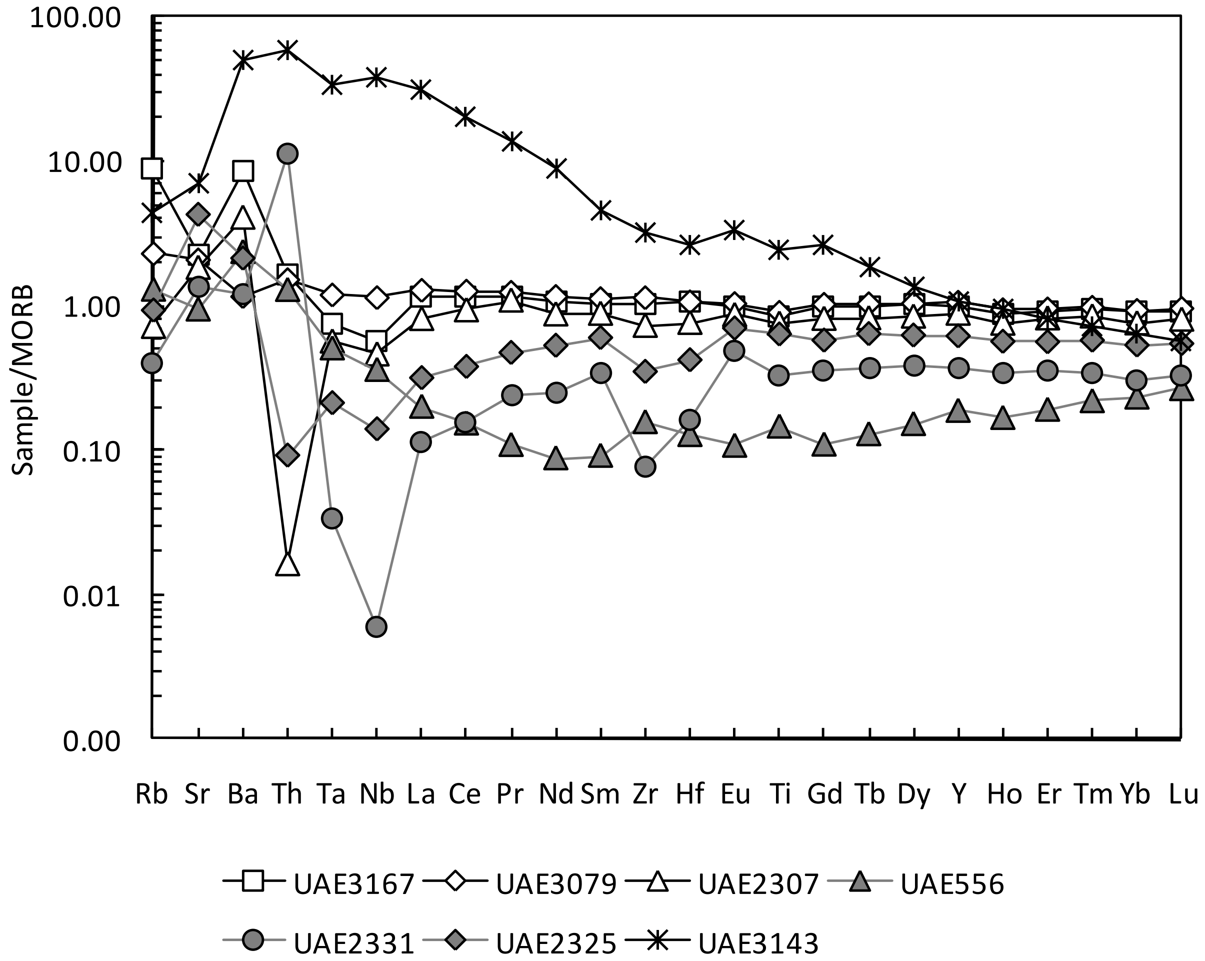

100.00
10.00
1.00
0.10
0.01
0.00
Sample/MORB
Rb
Sr
Ba
Th
Ta
Nb
La
Ce
Pr
Nd
Sm
Zr
Hf
Eu
Ti
Gd
Tb
Dy
Y
Ho
Er
Tm
Yb
Lu
UAE3167
UAE3079
UAE2307
UAE556
UAE2331
UAE2325
UAE3143

Figure 14

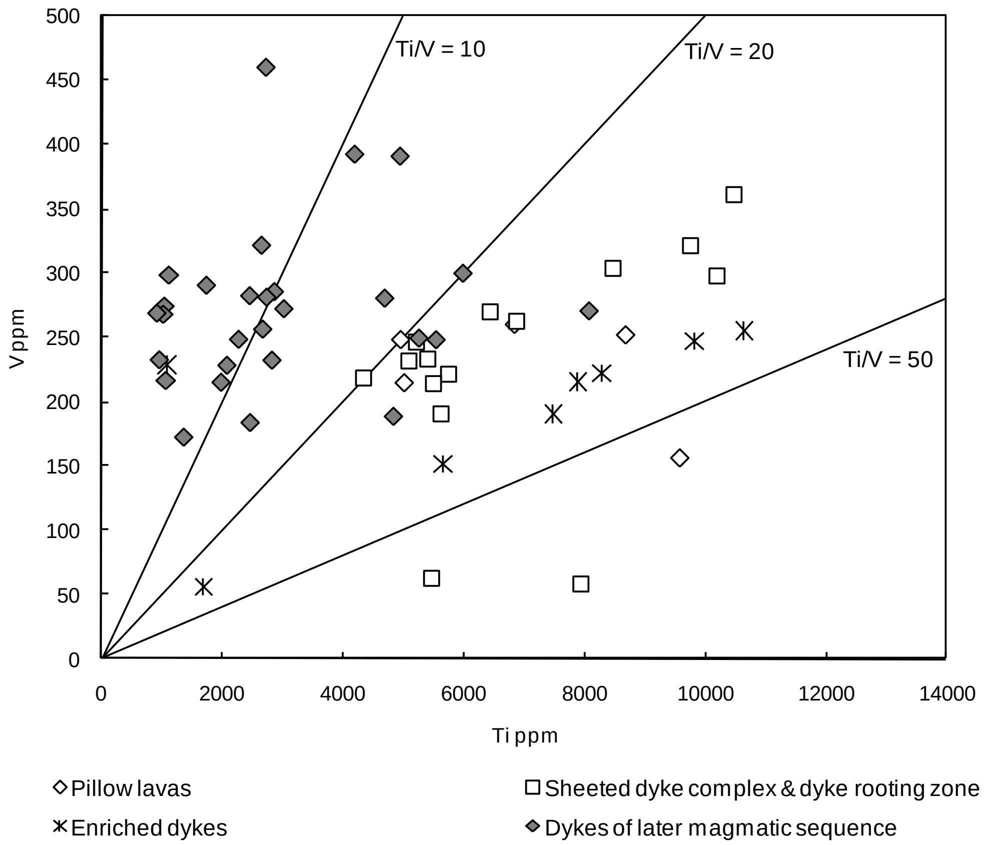

Ti/V = 10
Ti/V = 20
Ti/V = 50
V ppm
Ti ppm
0
50
100
150
200
250
300
350
400
450
500
0
2000
4000
6000
8000
10000
12000
14000
Pillow lavas
Sheeted dyke complex & dyke rooting zone
Enriched dykes
Dykes of later magmatic sequence

a)

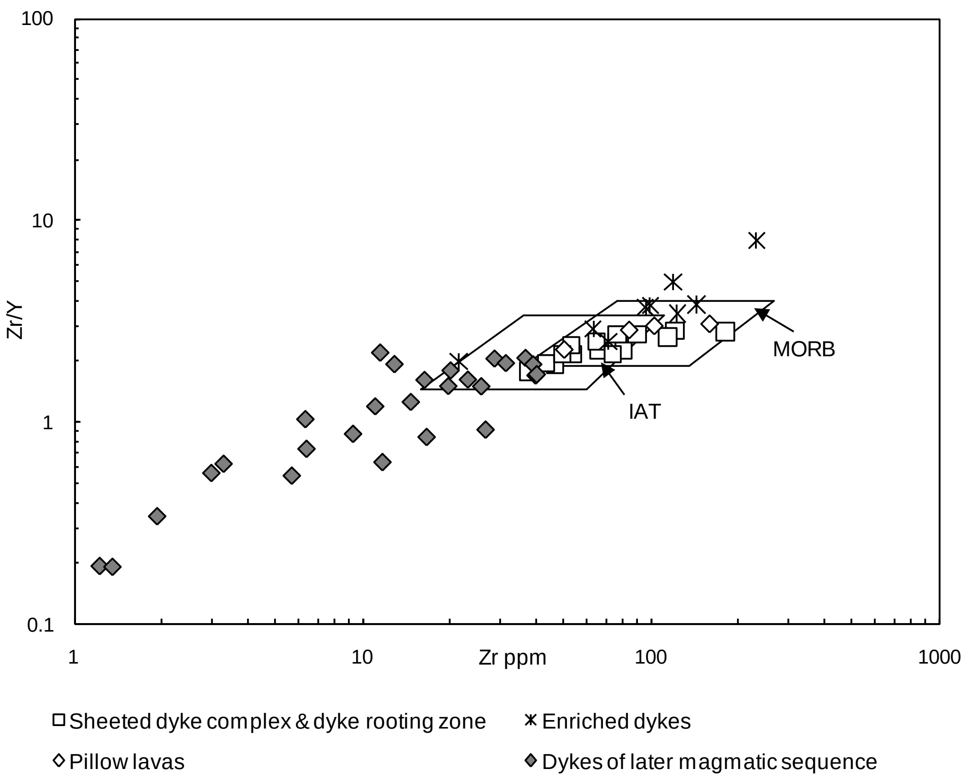

Zr/Y
Zr ppm
0.1
1
10
100
1
10
100
1000
MORB
IAT
Sheeted dyke complex & dyke rooting zone
Enriched dykes
Pillow lavas
Dykes of later magmatic sequence

b)

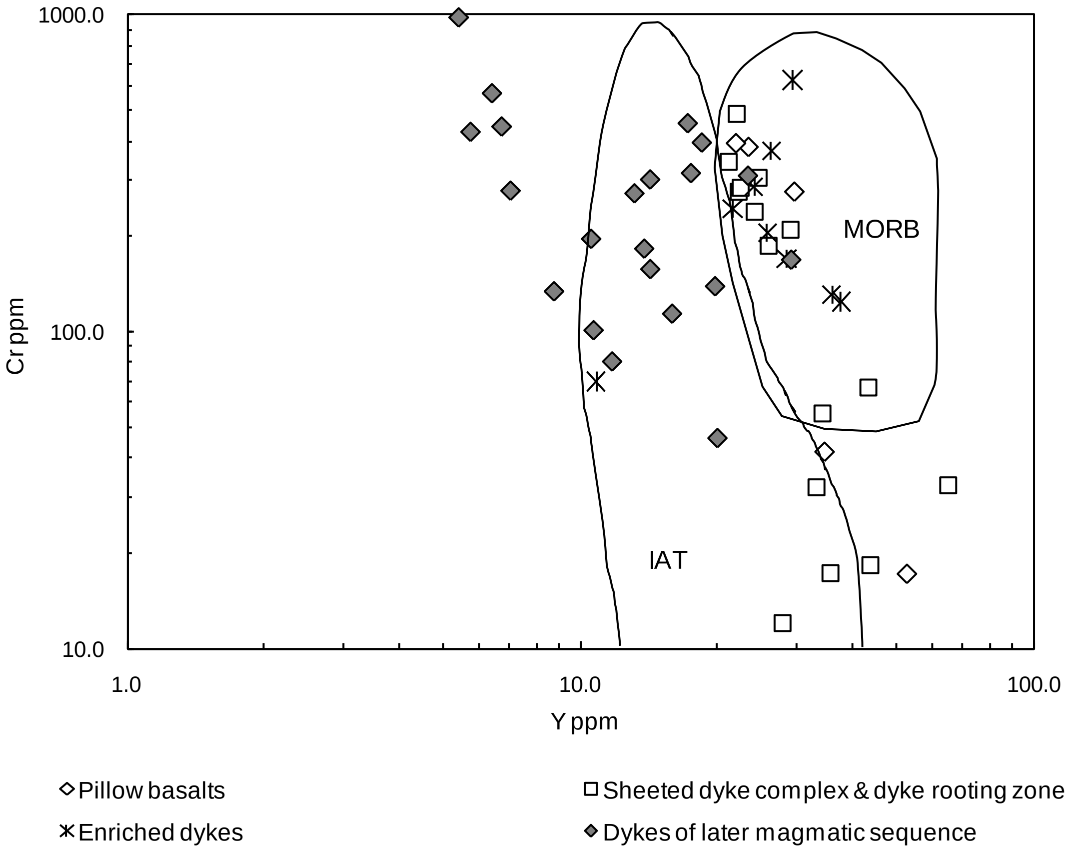

1000.0
100.0
10.0
Cr ppm
1.0
10.0
100.0
Y ppm
MORB
IAT
◇Pillow basalts
□Sheeted dyke complex & dyke rooting zone
✳Enriched dykes
◆Dykes of later magmatic sequence

c)

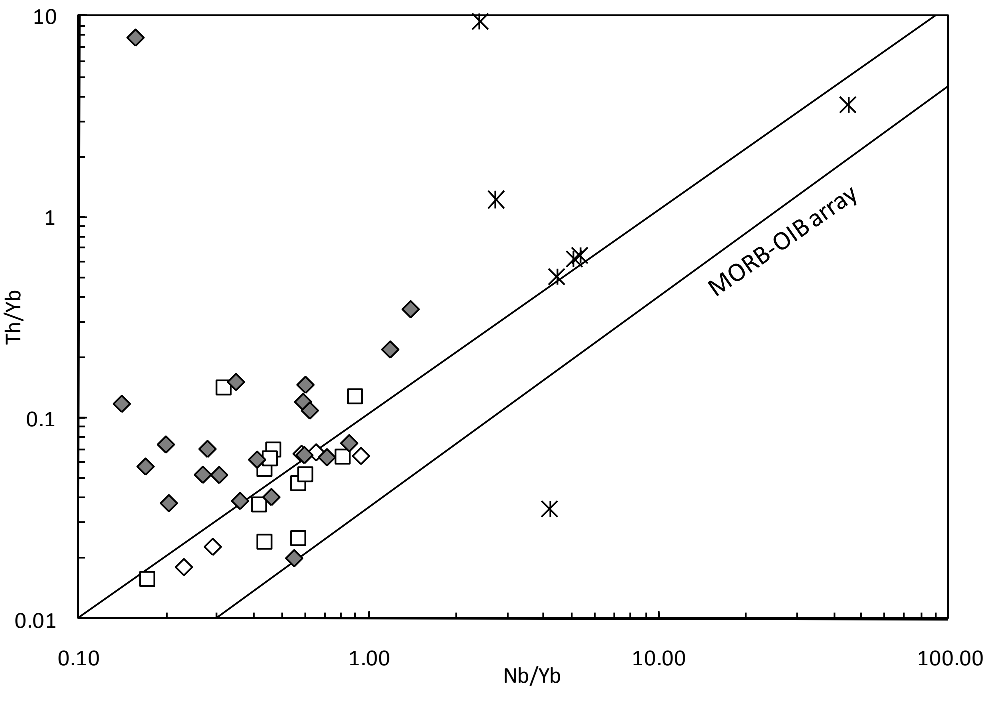

10
1
0.1
0.01
Th/Yb
0.10
1.00
10.00
100.00
Nb/Yb
MORB-OIB array
◇Pillow basalt
□Sheeted dyke complex & dyke rooting zone
◆Dykes of later magmatic sequence
✳Enriched dykes

d)

Table 1

Sample	Fraction	Weight (µg)	U (ppm)	Cm-Pb (ppm) ‡	Ratios								Ages (Ma)	
					$^{206}Pb/^{204}Pb$ †	$^{207}Pb/^{206}Pb$*	2σ%	$^{206}Pb/^{238}U$*	2σ%	$^{207}Pb/^{235}U$*	2σ%	Rho	$^{206}Pb/^{238}U$	2σ abs
UAE163	Z4	21.2	216.6	15.6	191.6	0.04905	2.35	0.01492	0.64	0.10090	2.50	0.358	95.47	0.61
	Z5	38.3	154.5	25.0	169.2	0.04870	3.02	0.01495	0.78	0.10037	3.21	0.353	95.66	0.74
	Z6	40.8	79.6	14.1	136.2	0.04890	5.27	0.01496	1.37	0.10086	5.59	0.352	95.72	1.31
	Z14	8.7	339.3	0.9	387.3	0.04783	1.26	0.01488	0.39	0.09814	1.36	0.372	95.22	0.37
UAE167	Z-2	42.3	77.6	0.5	451.1	0.04820	1.12	0.01494	0.35	0.09993	1.21	0.786	95.60	0.33
	Z-5	25.5	57.0	1.2	204.4	0.04847	2.51	0.01494	0.71	0.10020	2.68	0.615	95.60	0.68
	Z-16	27.9	71.2	2.8	230.3	0.04777	0.27	0.01497	0.50	0.09878	0.58	0.619	95.76	0.48
	Z-18	9.4	77.4	0.3	135.7	0.04796	5.09	0.01496	1.40	0.09850	5.42	0.511	95.70	1.34
UAE180	Z-12	10.8	213.4	7.7	217.8	0.05173	4.42	0.01502	1.28	0.10711	4.73	0.373	96.08	1.23
	Z-13	10.8	213.4	8.3	206.1	0.04742	4.81	0.01488	1.28	0.09731	5.11	0.352	95.25	1.22
	Z-14	17.8	108.9	8.4	161.3	0.04737	5.72	0.01488	1.51	0.09716	6.07	0.351	95.20	1.44
	Z-27	7.0	107.0	2.3	136.4	0.04965	4.25	0.01489	1.20	0.10196	4.54	0.364	95.30	1.14

All errors are 2σ (per cent for ratios, absolute for ages)
‡ Total common Pb in analysis, corrected for spike and fractionation (0.09%/amu)
† Measured ratio, corrected for spike and Pb fractionation
* Corrected for blank Pb, U and common Pb (Stacey and Kramers 1975)

Table 2 (may be supplementary)

Sample	Sample type	core/ rim	n=	Clinopyroxene averages wt%												
				SiO_2	TiO_2	Al_2O_3	Cr_2O_3	Fe_2O_3	MgO	CaO	MnO	FeO	Na_2O	Total	Mg# cpx	An plag
UAE103	High-level gabbro	c	10	51.2275	0.6092	2.7454	0.0225	2.1418	15.6365	19.2142	0.2212	7.6515	0.3112	99.781	78.47757	72.3
UAE103	High-level gabbro	r	10	50.9805	0.6178	2.7139	0.0005	1.9541	14.7754	21.0889	0.2095	6.4335	0.3274	99.1015	80.37265	73.8
UAE314	High-level gabbro	c	10	51.4434	0.5503	2.8329	0.0133	1.8144	14.5782	20.9396	0.214	6.997	0.4283	99.8114	78.77133	73.7
UAE314	High-level gabbro	r	10	51.587	0.5178	2.7367	0.0189	1.5223	14.5225	21.2377	0.2113	6.9987	0.3981	99.751	78.7076	74.6
UAE559	High-level gabbro	c	10	51.5838	0.6936	2.5937	0.3602	2.356	15.7176	22.9305	0.103	3.2959	0.3267	99.961	89.46768	82.4
UAE559	High-level gabbro	r	9	51.36256	0.792556	2.594222	0.297222	2.759444	15.70867	22.86933	0.129	3.114444	0.342556	99.97	90	79.2
UAE2201	High-level gabbro	c	10	51.7465	0.6175	3.0043	0.023	0.5971	14.1828	21.7615	0.2223	7.4145	0.3524	99.9219	77.32558	72
UAE2201	High-level gabbro	r	8	51.84363	0.499375	2.98475	0.023375	0.560875	14.1335	21.35338	0.19225	7.692125	0.41675	99.7	76.59782	75.3
UAE2181	High-level gabbro	c	11	50.76664	0.438	2.439	0.121818	0.512091	14.47664	20.76082	0.198455	7.215909	0.263	97.19236	78.1485	85.7
UAE2181	High-level gabbro	r	11	50.937	0.434091	2.345091	0.126455	0.904909	14.85945	20.49855	0.168091	7.225182	0.242727	97.74155	78.5696	87.1
UAE2184	High-level gabbro	c	8	50.6185	0.598625	2.5725	0.351	0.7345	14.38425	21.299	0.153625	6.538125	0.3115	97.56163	79.67679	79.6
UAE2184	High-level gabbro	r	6	50.73	0.600833	2.4095	0.266167	0.794333	14.43467	21.7935	0.139	5.983	0.3085	97.4595	81.1227	82.7
UAE2174	High-level gabbro	c	11	51.5919	0.5938	2.4675	0.0554	1.2641	14.8523	20.6176	0.1798	7.7122	0.3118	99.6464	77.45844	78.9
UAE2174	High-level gabbro	r	11	51.58927	0.595545	2.385909	0.058182	1.173727	14.47036	21.43027	0.209091	7.313364	0.313455	99.53918	77.90002	78.6
UAE2262	High-level gabbro	c	11	52.53155	0.192091	0.845727	0.043545	0.213182	13.14327	21.65273	0.217727	10.17509	0.26	99.27491	69.71047	52.1
UAE2262	High-level gabbro	r	11	52.48427	0.213364	0.905545	0.055818	0.06	13.29045	21.16409	0.192545	10.48009	0.272091	99.11827	69.33434	52.6
UAE2265	High-level gabbro	c	11	51.85491	0.377727	3.069364	1.131273	0.113636	16.43818	21.26945	0.076545	4.081818	0.265091	98.678	87.77846	82
UAE2265	High-level gabbro	r	11	51.50745	0.396273	3.498091	1.247364	0.328818	16.49627	20.72555	0.081273	3.944818	0.386091	98.612	88.18294	
UAE3114	High-level gabbro	c	9	50.101	1.059667	2.405	0.073778	1.674222	14.55356	19.88578	0.181222	7.592444	0.36	97.88667	77.33764	61.6
UAE3114	High-level gabbro	r	8	49.82888	1.088375	2.51875	0.07475	2.091	14.32325	20.36625	0.183375	7.02	0.37425	97.86888	78.44463	59.2
UAE3031	High-level gabbro	c	10	52.7821	0.2894	2.6288	0.6895	0.2505	16.75	21.3344	0.0722	4.6781	0.2723	99.7473	86.45991	81.8
UAE3031	High-level gabbro	r	7	52.72314	0.345143	2.556	0.656571	0	16.69743	20.03229	0.090857	6.073143	0.287429	99.462	83.06556	82.3
UAE3107	High-level gabbro	c	9	52.02978	0.646889	2.006889	0.047111	0.711667	15.69056	19.34211	0.203778	8.387222	0.305444	99.37144	76.90044	55.9
UAE3107	High-level gabbro	r	8	51.95013	0.668125	1.97425	0.039375	0.9445	15.6695	19.17025	0.185375	8.63775	0.303625	99.54288	76.35506	48.4
UAE235	Layered gabbro	c	8	52.53725	0.431625	3.01825	0.913375	0.134375	15.43088	22.6145	0.065125	3.938375	0.471875	99.55563	87.48382	83.7
UAE235	Layered gabbro	r	7	52.64786	0.405857	2.927429	0.772571	0	15.47914	22.67186	0.099143	3.95	0.435	99.38886	87.47975	85.3
UAE269	Layered gabbro	c	10	50.1395	0.4887	3.1256	0.2271	3.3779	15.6972	20.9255	0.1335	3.9651	0.3251	98.4052	87.58745	83.2
UAE269	Layered gabbro	r	8	50.65925	0.422625	3.069	0.1895	2.971125	15.59825	21.51538	0.15625	3.9675	0.315625	98.8645	87.51263	84
UAE290	Layered gabbro	c	10	51.8022	0.3736	3.0333	0.133	1.0555	15.6532	20.4384	0.1597	6.9504	0.2338	99.8331	80.0427	89.4
UAE290	Layered gabbro	r	10	51.9312	0.3395	2.8977	0.1188	1.0513	15.1026	22.1072	0.136	5.8992	0.2427	99.8262	82.0207	91.2
UAE305	Layered gabbro	c	8	52.68363	0.09	2.188625	0.287	1.1695	16.76138	22.35863	0.083125	3.801125	0.145375	99.56838	88.69817	95.2
UAE305	Layered gabbro	r	8	52.47688	0.072875	2.123875	0.268125	1.084375	16.90775	21.68638	0.11175	4.107875	0.145625	98.9855	88.0052	96.2
UAE419	Layered gabbro	c	10	51.6313	0.3924	2.6363	0.134	1.3289	15.6989	20.6383	0.1388	6.1176	0.3046	99.0211	82.07352	88.6
UAE419	Layered gabbro	r	9	51.39878	0.407444	2.466667	0.108111	2.038667	15.45244	21.52378	0.145222	5.137222	0.307778	98.98611	84.27543	88.6
UAE421	Layered gabbro	c	10	52.5515	0.2045	2.684	0.7084	0.964	17.1641	21.3379	0.0791	3.7392	0.2698	99.7025	89.10043	90.3
UAE421	Layered gabbro	r	10	52.7469	0.1927	2.4227	0.6443	0.5964	16.4538	22.65	0.0763	3.5113	0.2836	99.578	89.29032	90.6
UAE448	Layered gabbro	c	10	52.3386	0.37	2.3516	0.75	1.1588	16.4348	22.8762	0.0771	2.7864	0.3133	99.4568	91.29729	86.7
UAE448	Layered gabbro	r	9	52.387	0.359222	2.189222	0.648111	1.200778	16.652	22.60167	0.093444	2.664778	0.305	99.10122	91.75683	86.7
UAE517	Layered gabbro	c	9	52.32867	0.405222	2.028778	0.311111	1.034667	15.99389	22.32689	0.112667	4.275667	0.298444	99.116	86.96747	83.9
UAE517	Layered gabbro	r	10	52.6676	0.3444	1.8929	0.3196	0.6868	15.9532	22.6065	0.1166	4.5714	0.2582	99.4172	86.15173	84
UAE561	Layered gabbro	c	11	52.26673	0.518818	2.218909	0.226636	1.258273	15.73027	21.34982	0.150636	5.741727	0.352636	99.81445	83.0136	77.9

Sample	Sample type	core/ rim	n=	Clinopyroxene averages wt%												
				SiO_2	TiO_2	Al_2O_3	Cr_2O_3	Fe_2O_3	MgO	CaO	MnO	FeO	Na_2O	Total	Mg# cpx	An plag
UAE561	Layered gabbro	r	11	52.14264	0.540364	2.350909	0.236909	1.235091	15.38955	21.98318	0.122182	5.372818	0.376545	99.75018	83.62332	78.7
UAE568	Layered gabbro	c	11	52.05282	0.521	2.151182	0.174091	1.363455	15.79009	21.49927	0.132091	5.149545	0.375455	99.209	84.53073	75
UAE568	Layered gabbro	r	11	51.21918	0.695273	2.982818	0.200455	2.461364	15.57964	20.952	0.142545	4.486545	0.607727	99.32755	86.08711	76.5
UAE591	Layered gabbro	c	11	51.99691	0.303091	2.732455	0.886455	0.883727	16.80791	21.74609	0.084182	3.382636	0.251	99.07445	89.86277	89.8
UAE591	Layered gabbro	r	11	52.19682	0.295818	2.559727	0.820455	0.914273	16.70036	22.15864	0.089	3.170091	0.264636	99.16982	90.38737	90.6
UAE2815	Layered gabbro	c	11	51.66627	0.701364	2.493091	0.083727	0.055364	14.00282	21.14427	0.150364	7.960091	0.411273	98.66864	75.82843	66.4
UAE2815	Layered gabbro	r	11	51.84936	0.649727	2.341364	0.083455	0.054636	13.83873	21.72136	0.154182	7.595273	0.418727	98.70682	76.44895	67.7
UAE2390	Layered gabbro	c	12	52.06575	0.349667	2.346	0.03	1.320583	15.34783	22.66817	0.106167	4.6035	0.316333	99.154	85.5846	87
UAE2390	Layered gabbro	r	12	51.84575	0.38025	2.4015	0.048	1.518167	15.32383	22.658	0.103667	4.44325	0.312583	99.035	86.01115	88.4
UAE4519	Layered gabbro	c	7	51.73629	0.237571	2.181	0.237714	1.140857	16.15257	21.75257	0.100571	4.289143	0.222143	98.05043	87.04062	87.7
UAE4519	Layered gabbro	r	7	52.03571	0.229429	1.833857	0.187714	1.599571	17.03243	21.07143	0.131714	4.197571	0.160571	98.48	87.83245	87.6
UAE263	MTZ gabbro	c	10	50.8618	0.1524	2.8015	1.1509	2.9454	16.3899	23.1068	0.0548	0.515	0.4077	98.3862	98.26596	83.6
UAE263	MTZ gabbro	r	10	51.5723	0.1369	2.5955	0.9788	2.1958	16.6206	22.9368	0.0449	0.9811	0.3786	98.4413	96.80042	85.6
UAE276	MTZ gabbro	c	9	52.26156	0.222667	3.312889	0.578	0.726444	16.34089	23.077	0.044889	2.577667	0.297667	99.43967	91.86592	88.9
UAE276	MTZ gabbro	r	10	52.7607	0.2351	2.7712	0.6605	0.2872	16.6416	22.9169	0.049	2.8781	0.2781	99.4784	91.15284	89.3
UAE322	MTZ gabbro	c	8	52.66188	0.108125	2.458125	0.577375	0.734	16.1005	23.36288	0.082625	3.021375	0.283375	99.39025	90.47314	85.1
UAE322	MTZ gabbro	r	6	53.183	0.072833	1.862	0.417	0.775833	16.48767	23.7235	0.0875	2.630833	0.250167	99.49033	91.7657	86.5
UAE340	MTZ gabbro	c	9	51.431	0.442889	3.092556	0.939889	1.474222	15.75622	23.32656	0.081444	1.969444	0.404889	98.91911	93.43459	81.5
UAE340	MTZ gabbro	r	7	51.80443	0.317143	2.485714	0.698143	1.358143	16.03514	23.32071	0.054571	1.990429	0.372714	98.43714	93.49005	82.4
UAE349	MTZ gabbro	c	10	52.3723	0.1207	2.6726	0.5733	0.8114	16.2993	23.402	0.0539	2.5129	0.2326	99.051	92.02511	93.1
UAE349	MTZ gabbro	r	10	52.3049	0.1226	2.5002	0.5757	0.9897	16.3581	23.3749	0.0478	2.3938	0.2359	98.9036	92.41599	93.8
UAE277	Wehrlite	c	10	53.4422	0.2789	3.2902	1.1092	0	16.7446	22.6981	0.0563	2.8134	0.3321	100.765	91.38474	88.3
UAE277	Wehrlite	r	10	53.6336	0.2951	3.0661	1.0241	0.0352	16.5827	23.4592	0.0701	2.6323	0.3185	101.1169	91.82767	88.4
UAE342	Wehrlite	c	6	54.253	0.034667	1.7045	0.562667	0.039167	17.60517	22.277	0.088167	3.590667	0.125833	100.2808	89.75287	
UAE342	Wehrlite	r	6	54.02317	0.060333	1.6395	0.620333	0.177667	17.2845	23.32333	0.079667	3.060667	0.109167	100.3783	90.97549	
UAE225	Wehrlite	c	10	53.2424	0.3814	3.2103	1.1368	0	16.0786	22.8879	0.0727	2.84	0.4228	100.2729	90.97666	82.1
UAE225	Wehrlite	r	9	53.67	0.317556	2.889111	0.91	0	16.30989	23.27344	0.077444	2.714556	0.362222	100.5242	91.46722	84.1
UAE469	Wehrlite	c	5	53.0488	0.1468	2.203	0.845	0.2762	16.5432	22.299	0.0794	4.0804	0.2438	99.7656	87.82338	90.5
UAE469	Wehrlite	r	6	52.833	0.328833	2.324333	0.674	0.171833	15.83483	22.19967	0.083	5.193167	0.317333	99.96	84.45672	89.7
UAE422	Wehrlite	c	10	52.2586	0.6044	3.1334	1.0213	0.0959	16.5033	21.9185	0.0516	3.115	0.3772	99.0792	90.41233	85.5
UAE422	Wehrlite	r	10	52.5363	0.599	2.9949	0.9258	0	16.4643	22.244	0.0629	3.0455	0.3799	99.2526	90.59226	85.4
UAE474	Wehrlite	c	10	54.5477	0.13	1.9633	0.6808	0.017	17.628	22.9111	0.0675	2.9651	0.164	101.0745	91.37046	
UAE474	Wehrlite	r	10	54.4483	0.1462	1.9886	0.6555	0	17.5163	23.1609	0.0508	2.9231	0.1638	101.0535	91.44166	
UAE3055	Wehrlite	c	14	52.607	0.317357	2.627714	0.806143	0.177286	16.83386	21.53314	0.070857	4.2755	0.228643	99.4775	87.52037	84.6
UAE3055	Wehrlite	r	14	52.51014	0.367571	2.713071	0.845214	0.186429	16.73957	21.48093	0.099286	4.405786	0.2455	99.5935	87.13538	84.1
UAE3994	Wehrlite	c	5	52.6984	0.236	2.057	0.7618	0.9512	16.0756	22.9158	0.0744	3.0466	0.4518	99.2686	90.39131	79.7
UAE3994	Wehrlite	r	6	53.07417	0.179	1.754167	0.656167	0.617667	16.429	22.70783	0.072833	3.294667	0.396667	99.18217	89.88036	77.6
UAE131	Younger gabbro	c	10	51.9149	0.4223	2.1347	0.2117	0.6338	14.7799	21.1706	0.1623	7.1515	0.2961	98.8778	78.63411	79.2
UAE131	Younger gabbro	r	7	52.14943	0.436143	1.877429	0.103	0.427714	14.791	21.15957	0.182571	7.272429	0.313429	98.71271	78.36519	78.1
UAE488	Younger gabbro	c	6	55.83183	0.116667	1.949167	0.024833	0	19.39583	12.03117	0.177833	7.997167	0.199	97.7235	81.14271	86.1
UAE488	Younger gabbro	r	6	54.69717	0.1675	2.947833	0.031667	0	17.66233	12.55733	0.149167	9.209667	0.252667	97.67533	77.35122	86

Sample	Sample type	core/ rim	n=	Clinopyroxene averages wt%												
				SiO_2	TiO_2	Al_2O_3	Cr_2O_3	Fe_2O_3	MgO	CaO	MnO	FeO	Na_2O	Total	Mg# cpx	An plag
UAE552	Younger gabbro	c	11	51.34273	0.658727	2.540455	0.247909	2.047818	15.19845	22.259	0.104909	4.345	0.416091	99.16109	86.18219	64.6
UAE552	Younger gabbro	r	11	51.55691	0.603727	2.328727	0.234636	2.170273	15.30618	21.83336	0.122909	4.832545	0.417182	99.40645	84.94075	64.5
UAE644	Younger gabbro	c	9	51.20844	0.345222	1.801	0.174333	3.181222	15.31878	22.93222	0.122222	3.554111	0.254889	98.89244	88.47395	88.2
UAE644	Younger gabbro	r	8	51.04188	0.3885	1.88025	0.24675	2.84625	15.35838	22.29425	0.10175	4.08675	0.27125	98.516	87.00114	87.7
UAE759	Younger gabbro	c	8	51.16113	0.369625	1.09175	0.01625	1.143875	11.12138	20.28863	0.407875	13.92563	0.29225	99.81838	58.72557	35.7
UAE769	Younger gabbro	c	9	51.80711	0.344889	1.899556	0.007778	1.284333	14.08978	21.40678	0.216667	8.326778	0.253556	99.63722	75.10083	87.6
UAE769	Younger gabbro	r	10	51.721	0.3822	1.9181	0.0182	0.92	14.0431	21.6309	0.2018	8.1783	0.2297	99.2433	75.3644	88.4
UAE2806	Younger gabbro	c	10	51.6429	0.5384	2.387	0.1614	1.9452	15.2422	22.212	0.1375	4.8168	0.3574	99.4408	84.92695	72.9
UAE2806	Younger gabbro	r	7	51.72457	0.531571	2.307714	0.210857	1.644286	15.04057	22.57671	0.135571	4.894	0.337571	99.40343	84.57408	74.6
UAE2824	Younger gabbro	c	10	52.0061	0.3502	1.4433	0.1073	1.0348	14.2238	20.5677	0.1877	9.1685	0.3008	99.3902	73.44341	78.2
UAE2824	Younger gabbro	r	8	51.67438	0.39625	1.601625	0.1225	1.624625	14.00138	21.55888	0.201625	7.95575	0.304625	99.44163	75.8287	78.7
UAE595	Younger gabbro	c	11	52.655	0.380273	2.339182	0.354091	0.152091	15.63927	21.94464	0.159091	5.301364	0.305727	99.23073	84.02907	77.3
UAE595	Younger gabbro	r	9	52.91222	0.299444	1.958889	0.316444	0.300222	15.39867	22.81133	0.141333	5.071333	0.298111	99.508	84.38814	79.7
UAE740	Younger gabbro	c	11	52.72891	0.413455	2.085909	0.062455	0.686182	16.56309	20.01827	0.176636	6.871455	0.258364	99.86473	81.11922	84.2
UAE740	Younger gabbro	r	11	52.42645	0.505909	2.295909	0.093909	1.073091	15.61773	21.78864	0.155727	5.645091	0.34	99.94245	83.14537	82.9
UAE2264	Younger gabbro	?c	7	55.083	0.082714	0.728286	0.025	0	16.87114	25.82829	0.001429	1.754429	0.073857	100.4481	94.49146	96.2
UAE2372	Younger gabbro	c	9	51.66256	0.262111	1.190222	0.032778	0.947556	13.66689	21.40167	0.223111	8.718111	0.278333	98.38333	73.65136	59.6
UAE2372	Younger gabbro	r	10	51.6591	0.2584	1.1869	0.0397	1.0354	13.6976	21.2897	0.2113	8.7596	0.2894	98.4271	73.59727	57.5
UAE2374	Younger gabbro	c	7	52.12171	0.251	1.179286	0.088143	0.647714	14.094	21.85129	0.168714	8.043857	0.263429	98.70914	75.75137	76.6
UAE2374	Younger gabbro	r	7	52.16871	0.248286	1.131143	0.082429	0.700571	14.19029	21.774	0.166571	8.004571	0.268286	98.73486	75.95971	76.9
UAE2386	Younger gabbro	c	10	51.8194	0.2608	2.1268	0.0977	1.5827	16.1244	21.4943	0.114	4.8548	0.2052	98.6801	85.54228	90
UAE2386	Younger gabbro	r	10	52.0145	0.2604	1.9973	0.0892	1.5656	16.3174	21.1527	0.135	5.1904	0.1986	98.9211	84.86243	91
UAE4820	Younger gabbro	c	9	52.05444	0.274	1.823222	0.017556	1.480111	16.06833	20.83344	0.146222	6.104	0.196	98.99733	82.43632	89.4
UAE4820	Younger gabbro	r	9	52.00156	0.312222	1.696222	0.020333	1.514889	15.61578	21.66244	0.131667	5.761556	0.211889	98.92856	82.84927	89.5
UAE4828	Younger gabbro	c	12	51.878	0.342083	1.525083	0.181333	1.013917	14.64775	21.41592	0.158083	7.37925	0.261083	98.8025	77.9661	87.5
UAE4828	Younger gabbro	r	9	51.98422	0.307667	1.388111	0.161222	0.808667	14.56267	21.45256	0.161556	7.685444	0.248	98.76011	77.14916	87.1
UAE3040	Younger gabbro	c	11	51.64036	0.480818	2.492182	0.290364	1.421182	16.38027	21.25655	0.099364	4.462	0.257	98.78009	86.73221	80.6
UAE3040	Younger gabbro	r	11	51.76945	0.417818	2.355545	0.309818	1.524636	16.46309	21.38745	0.101455	4.243273	0.256818	98.82936	87.37347	78.8
UAE3982	Younger gabbro	c	7	50.94243	0.641857	2.444429	0.136571	1.857429	14.80629	22.03671	0.121571	4.898143	0.399	98.28443	84.34821	95.1
UAE3982	Younger gabbro	r	8	50.75275	0.6745	2.447625	0.116125	2.382875	14.823	22.14475	0.13925	4.5115	0.39925	98.39163	85.40916	97.1
UAE3969	Younger gabbro	c	9	52.248	0.482889	1.966	0.013333	0.133778	14.15956	21.09156	0.198444	9.013222	0.245222	99.552	73.68421	85.7
UAE3969	Younger gabbro	r	9	52.26444	0.490222	1.819222	0.018778	0.181778	14.26989	20.98089	0.190444	9.030556	0.243111	99.48933	73.79652	85.6
UAE3979	Younger gabbro	c	8	53.23063	0.297625	1.89275	0.06425	0.029375	16.56763	20.5305	0.10475	6.53275	0.183875	99.43413	81.8918	88
UAE3979	Younger gabbro	r	9	53.09333	0.285667	1.868778	0.089333	0.065667	16.07478	21.15822	0.164444	6.390333	0.199222	99.38978	81.76126	88.6
UAE3987	Younger gabbro	c	8	52.5255	0.360125	1.345625	0.018625	0.05875	13.97313	21.297	0.17425	9.305625	0.24775	99.30638	72.79711	84.6
UAE3987	Younger gabbro	r	10	51.9807	0.4676	1.621	0.0306	0.5462	13.949	20.9137	0.1665	9.3872	0.2616	99.3241	72.58874	83.7
UAE2376	Younger gabbro	c	8	53.5675	0.286875	1.4445	0.28125	0	15.46238	22.49225	0.106625	5.740125	0.253875	99.63538	82.75904	91
UAE2376	Younger gabbro	r	10	53.7199	0.2312	1.2253	0.257	0	15.507	22.5453	0.1018	5.6253	0.2498	99.4626	83.07528	90.7
UAE3182	Younger gabbro	c	9	53.00133	0.271556	1.847222	0.528444	0.010556	15.11933	22.214	0.099444	5.939333	0.320889	99.35211	81.93323	85.6
UAE3182	Younger gabbro	r	8	53.26538	0.31025	1.578375	0.325625	0	15.17438	22.08575	0.11425	6.0585	0.284875	99.19738	81.69855	84.5

Table 3 (may be supplementary)

Sample No.	UAE	3079	3102	3164	3132	3136	2300	2269	2307	2312	3125	3137	3167	3180	3155	4843	2261	2266	2270	2371	4066	343
Rock type		Pillow basalt	Pillow basalt	Pillow basalt	Pillow basalt	Pillow basalt	Sheeted dyke complex	Sheeted dyke complex	Sheeted dyke complex	Sheeted dyke complex	Sheeted dyke complex	Sheeted dyke complex	Sheeted dyke complex	Sheeted dyke complex	Sheeted dyke complex	Sheeted Dyke Complex	Dyke from dyke rooting zone	Dyke from dyke rooting zone	Dyke from dyke rooting zone	Dyke from dyke rooting zone	Dyke from dyke rooting zone	Later dyke
Block		Aswad	Aswad	Aswad	Aswad	Aswad	Aswad	Aswad	Aswad	Aswad	Aswad	Aswad	Aswad	Aswad	Aswad	Aswad	Aswad	Aswad	Aswad	Aswad	Khor Fakkan	Khor Fakkan
SiO_2		43.80	57.04	48.43	47.27	61.50	49.86	48.92	48.38	61.90	50.61	50.04	52.91	52.11	51.07	49.55	47.67	48.74	48.16	50.35	63.79	45.08
TiO_2		1.14	1.60	0.83	0.84	1.45	0.85	1.15	0.96	1.33	1.70	1.63	1.08	1.75	0.90	0.94	0.87	0.92	0.73	1.41	0.91	0.17
Al_2O_3		16.36	14.11	15.08	16.39	13.77	15.38	14.88	15.59	15.20	14.34	14.97	15.96	14.91	16.07	17.46	15.36	15.96	15.08	14.60	14.54	11.80
Fe_2O_3		10.06	11.72	9.64	8.87	7.56	9.43	10.96	9.55	9.05	12.16	12.46	10.10	13.31	8.80	8.13	9.54	9.24	8.48	13.07	7.08	10.61
MnO		0.15	0.26	0.18	0.16	0.08	0.15	0.13	0.15	0.10	0.17	0.24	0.14	0.37	0.17	0.15	0.14	0.13	0.15	0.23	0.05	0.20
MgO		8.83	5.09	8.06	10.14	2.05	7.82	7.50	7.73	1.89	6.62	6.33	6.01	5.23	7.71	8.40	8.23	8.40	8.81	6.03	1.71	13.28
CaO	wt %	11.74	2.36	12.99	11.46	6.01	12.50	12.44	12.26	5.85	7.76	8.88	7.67	7.01	9.07	12.92	13.84	13.39	15.01	11.13	6.67	14.55
Na_2O		1.87	4.51	2.74	2.06	3.74	2.36	2.39	2.74	4.98	4.10	4.00	2.97	3.47	4.02	1.94	1.68	2.20	1.37	3.07	4.23	0.18
K_2O		0.12	0.07	0.23	0.07	0.08	0.01	0.02	0.03	0.02	0.17	0.10	0.26	0.11	0.07	0.01	0.04	0.07	0.00	0.00	0.12	0.00
P_2O_5		0.11	0.22	0.06	0.06	0.16	0.06	0.09	0.07	0.32	0.16	0.13	0.10	0.18	0.09	0.07	0.06	0.06	0.05	0.10	0.17	0.01
Loss On Ignition		4.98	2.96	3.44	1.73	2.36	0.88	0.35	1.74	0.16	1.70	2.05	2.99	2.28	2.52	0.71	1.32	0.44	1.64	0.56	0.56	3.12
Total		99.17	99.94	97.46	99.04	98.76	99.32	98.82	99.20	100.78	99.49	100.82	100.17	100.73	100.50	100.27	98.75	99.55	99.46	100.57	99.84	99.01
V		259.47	155.82	247.65	214.14	251.31	231.17	261.90	221.87	58.73	297.24	321.62	269.87	360.31	232.52	190.58	246.13	213.87	218.81	304.29	62.10	274.53
^{52}Cr		275.85	17.12	381.87	392.49	41.60	239.02	209.26	308.01	32.62	67.03	17.31	11.96	18.38	187.42	484.47	276.81	283.50	344.67	55.29	32.29	988.62
^{53}Cr							243.56	215.06	313.79	33.06							284.88	288.04	357.05	57.14		880.68
Mn		0.15	0.23	0.17	0.15	0.08	0.15	0.13	0.15	0.09	0.16	0.20	0.14	0.33	0.16	0.14	0.13	0.12	0.14	0.22	0.05	0.19
Co		46.65	15.86	42.81	45.23	21.55	36.81	41.80	39.17	13.12	40.51	38.19	35.55	37.67	31.97	37.47	39.78	40.95	40.31	41.88	21.77	51.64
^{60}Ni		92.51	12.03	77.62	118.47	3.51	100.58	91.62	102.16	7.42	49.31	31.49	20.30	8.68	68.05		110.63	126.87	160.30	46.17	0.01	377.15
^{62}Ni		85.24	27.20	71.43	103.87	16.81	96.91	91.27	96.38	18.32	59.83	42.67	22.15	23.47	62.30	517.57	108.57	122.09	150.32	52.41	3.50	324.56
Zn		37.77	90.61	49.91	36.22	65.76	38.86	38.70	52.76	56.69	35.37	41.40	76.75	87.66	46.37	58.74	36.05	35.50	28.79	58.47	9.60	41.34
Ga		15.59	17.62	13.73	14.28	18.96	16.49	17.29	16.44	22.64	16.33	17.07	17.11	18.99	15.40	15.15	15.43	15.79	13.46	18.73	16.99	8.64
Rb		1.30	0.63	2.95	0.27	0.45	0.22	0.18	0.40	0.43	1.74	0.29	4.93	0.94	0.22	0.16	0.08	0.21	0.24	0.20	0.97	0.49
Sr		189.31	53.29	165.08	144.46	83.14	124.08	143.79	164.57	171.86	154.65	385.74	200.59	135.24	170.74	122.10	225.20	126.82	106.01	138.84	173.00	24.27
Y		29.65	52.46	23.50	22.06	34.56	24.26	29.18	24.73	64.92	43.18	35.70	28.11	43.57	26.06	22.15	22.29	22.70	21.20	34.16	33.12	5.42
Zr		84.34	159.81	40.09	50.33	102.99	46.65	65.67	53.91	181.61	121.63	80.92	76.46	114.56	65.00	52.96	43.36	49.31	37.82	74.20	89.56	3.01
Nb		2.66	3.33	0.54	0.62	1.89	1.01	1.58	1.08	4.05	3.37	2.07	1.33	2.68	1.14	0.37	0.88	0.97	0.65	1.40	3.07	0.26
Cs		0.04	0.03	0.02	0.03	0.01	0.02	0.00	0.01	0.01	0.07	0.00	0.10	0.02	0.00	0.08	0.00	0.01	0.01	0.01	0.02	0.02
Ba		7.32	36.93	30.44	153.22	3.03	13.23	8.49	25.50	33.05	16.56	16.89	53.89	15.88	23.30	10.67	9.42	12.00	16.91	11.77	25.94	8.31
La		3.21	4.67	1.34	2.24	4.07	2.15	3.72	2.03	7.41	4.50	3.22	2.91	4.41	2.87	1.47	1.72	2.08	1.39	2.66	3.94	0.32
Ce	parts per million	9.50	14.34	4.34	5.98	12.45	7.01	9.19	6.99	24.19	13.56	9.91	8.54	13.63	7.81	5.37	5.78	6.88	4.88	9.43	10.02	0.97
Pr		1.64	2.51	0.85	1.07	2.20	1.44	1.84	1.44	4.73	2.34	1.78	1.51	2.43	1.38	1.07	1.22	1.42	1.05	1.95	1.64	0.13
Nd		8.49	12.80	4.77	5.50	11.20	6.25	7.98	6.37	20.08	12.12	9.41	7.90	12.74	7.37	5.84	5.46	6.17	4.79	8.64	8.22	0.47
Sm		2.95	4.59	1.90	2.00	3.90	2.25	2.73	2.32	6.66	4.25	3.34	2.74	4.32	2.54	2.17	1.97	2.14	1.77	3.10	2.81	0.19
Eu		1.06	1.51	0.77	0.77	1.38	0.83	1.02	0.88	2.14	1.29	1.22	1.00	1.50	0.95	0.84	0.76	0.85	0.65	1.13	1.02	0.07
Gd		3.77	6.29	2.76	2.68	4.98	2.91	3.63	3.00	8.21	5.44	4.51	3.58	5.72	3.31	2.78	2.68	2.83	2.45	4.08	3.76	0.36
Tb		0.69	1.17	0.53	0.49	0.87	0.54	0.66	0.55	1.45	0.99	0.83	0.66	1.07	0.62	0.51	0.50	0.52	0.46	0.75	0.72	0.08
Dy		4.72	8.09	3.77	3.45	5.87	3.76	4.54	3.84	9.87	6.83	5.79	4.59	7.25	4.23	3.53	3.46	3.56	3.25	5.22	5.11	0.72
Ho		0.95	1.64	0.74	0.71	1.13	0.75	0.90	0.76	1.96	1.36	1.13	0.89	1.41	0.83	0.69	0.69	0.70	0.65	1.05	1.02	0.17
Er		2.82	5.03	2.31	2.14	3.33	2.40	2.87	2.44	6.28	4.12	3.44	2.71	4.27	2.50	1.95	2.18	2.24	2.11	3.35	3.24	0.60
Tm		0.45	0.81	0.37	0.34	0.51	0.38	0.45	0.39	0.99	0.66	0.55	0.43	0.68	0.40	0.33	0.34	0.35	0.33	0.53	0.54	0.11
Yb		2.83	5.07	2.37	2.16	3.24	2.28	2.76	2.31	6.03	4.17	3.60	2.84	4.45	2.59	2.14	2.13	2.12	2.08	3.22	3.43	0.73
Lu		0.44	0.78	0.35	0.32	0.47	0.37	0.43	0.37	0.94	0.70	0.64	0.42	0.64	0.42	0.29	0.37	0.33	0.33	0.52	0.52	0.13
Hf		2.18	4.38	1.26	1.22	3.09	1.49	1.87	1.57	5.15	3.19	2.45	2.18	3.33	1.81	1.40	1.31	1.46	1.21	2.24	2.46	0.11
Ta		0.15	0.21	0.05	0.07	0.13	0.07	0.11	0.07	0.26	0.22	0.15	0.10	0.19	0.09	0.04	0.06	0.07	0.05	0.09	0.21	0.02
Pb		11.91	9.83	7.69	12.22	6.47	0.27	0.46	12.47	0.41	10.74	10.27	8.66	12.83	9.99	6.20	5.22	0.27	0.47	2.33	4.63	2.97
Th		0.18	0.34	0.04	0.05	0.21	0.01	0.07	0.00	0.01	0.27	0.17	0.20	0.23	0.14	0.03	0.08	0.13	0.29	0.08	0.44	0.11
U		0.09	0.28	0.04	0.04	0.18	0.00	0.03	0.00	0.00	0.12	0.10	0.12	0.10	0.09	0.02	0.03	0.05	0.13	0.05	0.29	0.06

Sample No.	UAE	104	556	2326	2175	399	466	496	3059	3092	3971	2378	3989	4311	2306	2311	2325	3115	3146	3183	2132	2119
Rock type		Later dyke	Later dyke	Later dyke	Later dyke	Later dyke	Later dyke	Later dyke	Later dyke	Later dyke	Later dyke	Later dyke	Later dyke	Later dyke	Later dyke	Later dyke	Later dyke	Later dyke	Later dyke	Later dyke	Later dyke	Later dyke
Block		Khor Fakkan	Khor Fakkan	Khor Fakkan	Khor Fakkan	Khor Fakkan	Aswad	Aswad	Aswad	Aswad	Aswad	Aswad	Aswad	Aswad	Aswad	Aswad	Aswad	Aswad	Aswad	Aswad	Khor Fakkan	Khor Fakkan
SiO_2	wt %	50.81	48.75	53.59	54.14	56.53	52.78	53.09	54.69	50.47	56.78	55.24	58.16	52.88	47.73	47.76	46.86	49.29	48.38	47.48	47.23	52.86
TiO_2		0.18	0.19	0.17	0.44	0.45	0.33	0.35	0.83	0.47	0.48	0.41	0.78	0.50	0.92	0.44	0.81	1.35	0.88	1.00	0.38	0.15
Al_2O_3		10.17	15.40	14.73	14.07	14.40	15.83	14.50	14.65	16.12	15.24	16.04	13.72	14.38	14.68	14.46	18.06	16.19	16.12	15.50	15.10	13.47
Fe_2O_3		9.10	9.48	9.29	10.97	12.05	8.14	8.87	11.50	8.57	8.72	8.36	9.30	10.28	10.36	8.40	8.40	10.14	8.91	11.13	9.25	9.76
MnO		0.16	0.15	0.17	0.18	0.18	0.09	0.15	0.10	0.21	0.15	0.09	0.16	0.16	0.16	0.13	0.17	0.16	0.18	0.21	0.16	0.17
MgO		15.02	9.69	8.74	6.13	4.68	8.36	9.22	4.39	8.42	6.55	6.54	5.97	8.02	9.03	9.93	8.10	7.16	8.45	9.17	8.13	9.31
CaO		10.27	11.71	11.06	9.31	9.93	13.60	11.79	7.56	11.70	10.74	11.64	8.76	10.87	13.45	15.81	14.26	11.43	12.55	13.89	12.21	12.68
Na_2O		1.04	1.02	1.46	3.21	1.36	0.92	1.48	3.18	1.99	1.79	1.23	2.27	1.03	1.95	1.13	2.05	2.73	2.39	1.18	1.46	0.52
K_2O		0.02	0.04	0.15	0.06	0.16	0.03	0.18	0.23	0.16	0.04	0.08	0.04	0.00	0.01	0.00	0.18	0.06	0.08	0.05	0.02	0.00
P_2O_5		0.03	0.03	0.01	0.02	0.04	0.04	0.04	0.05	0.04	0.02	0.03	0.04	0.03	0.01	0.00	0.06	0.15	0.07	0.05	0.01	0.01
Loss On Ignition		1.88	2.09	0.81	0.91	0.73	0.56	0.53	1.87	2.14	0.45	1.28	0.38	1.16	0.99	0.51	0.84	0.16	1.99	0.19	0.63	0.64
Total		98.67	98.56	100.17	99.45	100.52	100.68	100.17	99.05	100.29	100.96	100.93	99.59	99.30	99.30	98.57	99.79	98.82	99.99	99.85	94.59	99.57
V	parts per million	216.00	299.00	268.12	321.06	459.00	214.00	228.00	390.32	231.67	285.00	281.80	279.92	271.69	247.64	255.88	187.82	270.15	248.88	299.50	248.30	268.80
^{52}Cr		1250.00	353.00	447.45	80.47	77.00	121.00	318.00	46.04	183.20	114.02	157.80	317.78	274.15	396.27	303.06	456.02	169.21	311.57	139.56	133.40	427.20
^{53}Cr					84.13										397.47	307.99					130.00	429.90
Mn					0.16					0.20	0.15	0.09	0.15	0.16	0.16	0.12		0.15	0.17	0.20	0.15	0.17
Co		59.00	35.00	45.03	33.44	34.00	38.00	41.00	36.93	35.67	37.60	36.78	32.66	43.17	47.57	45.65	37.79	39.00	39.26	48.38	40.28	39.38
^{60}Ni		280.00	80.00		47.97	13.00	43.00	84.00		58.00	97.40	63.23	93.77	95.81	125.25	131.95		73.56	105.26	74.96	35.55	51.66
^{62}Ni					44.46					46.44	81.47	54.51	84.39	83.12	116.75	115.06		72.95	92.27	69.91	34.99	48.31
Zn				54.13	38.83				11.80	125.28	41.69	13.60	53.66	60.71	33.54	27.71	71.98	22.44	57.29	32.07	32.58	40.60
Ga		8.03	11.34	13.10	13.15	14.09	12.19	11.84	15.28	12.99	14.40	13.79	13.47	13.14	15.54	13.69	13.59	16.51	14.13	15.36	12.63	11.54
Rb		0.31	0.73	5.50	0.43	1.87	0.13	5.56	1.88	1.71	1.31	0.37	0.24	0.92	0.21	0.12	0.52	0.41	0.21	0.09	0.36	0.26
Sr		42.09	85.11	88.22	170.15	64.47	215.96	89.97	164.00	96.15	89.14	143.60	74.48	78.63	170.94	73.03	387.60	147.82	147.59	106.83	96.80	56.79
Y		6.20	5.26	6.72	11.73	10.12	9.29	11.17	20.15	13.84	15.97	14.27	17.59	13.16	18.55	14.26	17.27	29.25	23.47	19.85	8.73	5.71
Zr		6.38	11.59	12.99	14.70	16.41	11.06	20.22	39.15	28.74	31.46	23.22	36.83	19.85	11.73	1.12	25.84	26.74	40.25	16.70	6.37	1.93
Nb		0.36	0.84	1.26	0.76	0.77	0.28	0.51	1.30	1.17	1.03	0.94	1.44	0.30	0.06	0.02	0.32	1.10	0.86	0.35	0.14	0.22
Cs		0.01	0.01	0.30	0.01		0.00	0.14	0.04	0.05	0.05	0.03	0.03	0.08	0.00	0.00	0.01	0.08	0.01	0.01	0.03	0.04
Ba		20.59	14.93	21.35	7.45	18.44	10.76	37.33	20.94	35.71	28.28	2.72	17.69	26.98	108.85	4.59	13.48	16.06	20.57	3.35	20.83	8.76
La		0.21	0.50	1.11	0.91		0.35	0.55	1.82	0.88	1.05	1.08	1.00	0.61	0.49	0.07	0.79	2.39	1.88	0.75	0.48	0.13
Ce		0.53	1.15	2.39	2.63	1.90	1.11	1.57	4.86	2.73	2.75	2.85	2.96	1.68	2.12	0.85	2.83	6.81	6.00	2.83	1.04	0.28
Pr		0.09	0.14	0.28	0.48	0.31	0.21	0.27	0.75	0.49	0.49	0.45	0.53	0.31	0.58	0.15	0.62	1.35	1.11	0.61	0.30	0.12
Nd		0.50	0.64	1.25	2.02	1.53	1.35	1.70	4.20	2.73	2.69	2.23	2.81	1.83	3.10	1.00	3.87	7.81	5.96	3.84	1.46	0.49
Sm		0.25	0.24	0.39	0.72	0.52	0.60	0.69	1.56	1.08	1.06	0.86	1.14	0.79	1.48	0.67	1.58	2.99	2.17	1.66	0.64	0.23
Eu		0.10	0.11	0.17	0.28	0.23	0.25	0.27	0.58	0.43	0.40	0.28	0.45	0.33	0.71	0.31	0.71	1.15	0.83	0.76	0.30	0.11
Gd		0.49	0.40	0.55	1.08	0.83	0.96	1.10	2.13	1.53	1.58	1.31	1.77	1.30	2.14	1.26	2.12	3.93	2.93	2.53	0.96	0.41
Tb		0.11	0.09	0.12	0.22	0.18	0.19	0.22	0.41	0.29	0.31	0.26	0.36	0.27	0.41	0.27	0.43	0.70	0.54	0.48	0.18	0.10
Dy		0.85	0.69	0.89	1.64	1.42	1.40	1.63	2.94	2.10	2.31	1.99	2.65	1.98	2.93	2.11	2.84	4.82	3.79	3.45	1.31	0.78
Ho		0.21	0.17	0.22	0.35	0.34	0.31	0.37	0.65	0.43	0.47	0.42	0.55	0.42	0.58	0.45	0.57	0.95	0.74	0.66	0.27	0.18
Er		0.67	0.57	0.71	1.22	1.12	0.96	1.15	1.95	1.34	1.53	1.39	1.75	1.31	1.86	1.47	1.67	2.78	2.29	2.02	0.87	0.63
Tm		0.11	0.10	0.13	0.21	0.18	0.16	0.19	0.32	0.21	0.26	0.24	0.30	0.22	0.29	0.24	0.26	0.43	0.37	0.32	0.15	0.12
Yb		0.78	0.71	0.90	1.37	1.27	1.03	1.23	2.08	1.36	1.72	1.57	2.00	1.44	1.75	1.47	1.63	2.66	2.38	2.04	0.89	0.80
Lu		0.13	0.12	0.16	0.23	0.22	0.16	0.20	0.34	0.21	0.26	0.27	0.31	0.29	0.28	0.24	0.25	0.42	0.35	0.29	0.14	0.15
Hf		0.22	0.26	0.36	0.49	0.46	0.44	0.61	1.20	0.87	0.89	0.72	1.10	0.63	0.58	0.19	0.86	0.90	1.43	0.59	0.30	0.10
Ta		0.02	0.07	0.11	0.05	0.05	0.02	0.04	0.10	0.07	0.06	0.08	0.09	0.03	0.01	0.00	0.03	0.09	0.07	0.04	0.01	0.02
Pb		0.50	0.22	0.79	0.51		0.51	0.29		13.88	3.73	7.89	6.75	6.87	1.83	7.23		5.93	8.82	4.49	6.12	1.91
Th		0.03	0.16	0.31	0.03	0.19	0.05	0.08	0.23	0.10	0.11	0.19	0.13	0.05	0.08	0.42	0.01	0.01	0.09	0.01	7.02	0.06
U		0.02	0.15	0.27	0.03	0.10	0.03	0.07	0.18	0.07	0.11	0.17	0.15	0.05	0.03	0.18	0.01	0.01	0.05	0.01	3.59	0.02

Sample No.	UAE	2130	2172	2178	2331	285	105	2164	2341	2147	2338	2370	2361	350	3143	2094	580	3984	3999	4050	3982	517
Rock type		Later dyke	Later dyke	Later dyke	Later dyke	Later dyke	Later dyke	Enriched dyke	Enriched dyke	Enriched dyke	Enriched dyke	Enriched dyke	Enriched dyke	Enriched dyke	Enriched dyke	Enriched dyke	Younger gabbro	Younger gabbro	Younger gabbro	Younger gabbro	Younger gabbro	Younger gabbro
Block		Khor Fakkan	Khor Fakkan	Khor Fakkan	Khor Fakkan	Khor Fakkan	Khor Fakkan	Khor Fakkan	Khor Fakkan	Khor Fakkan	Khor Fakkan	Khor Fakkan	Khor Fakkan	Khor Fakkan	Aswad	Aswad?	Aswad	Aswad	Aswad	Aswad	Aswad	Aswad
SiO_2		50.06	46.79	51.24	49.15	47.85	45.15	46.75	50.11	58.89	46.39	48.39	47.33	46.61	41.45	46.88	45.94	47.62	47.48	48.34	47.28	44.98
TiO_2		0.46	0.23	0.16	0.41	0.29	0.70	0.28	1.78	0.18	1.25	1.64	0.94	1.38	3.14	1.32	0.13	0.24	0.85	0.13	0.28	0.18
Al_2O_3		15.88	15.51	12.58	15.91	16.16	16.95	17.06	15.06	16.59	16.51	14.45	17.38	16.71	10.35	15.63	16.30	14.92	18.52	18.36	21.06	12.32
Fe_2O_3		10.59	9.33	9.58	7.86	10.93	11.36	9.02	12.46	7.91	10.08	12.63	9.64	7.99	12.78	10.09	4.22	7.68	5.12	4.69	4.01	9.44
MnO		0.17	0.18	0.16	0.14	0.18	0.14	0.16	0.19	0.13	0.16	0.19	0.18	0.14	0.15	0.16	0.08	0.13	0.10	0.08	0.05	0.14
MgO	wt %	7.47	11.24	10.25	9.08	9.24	9.30	9.58	6.32	3.26	7.31	6.32	7.63	9.81	6.92	8.26	13.62	11.60	7.65	9.92	7.59	18.03
CaO		12.80	15.93	12.45	14.28	13.11	13.61	11.63	10.49	8.25	10.86	10.54	10.45	14.48	15.44	11.32	16.25	15.29	16.53	17.03	18.21	11.43
Na_2O		1.25	1.07	1.68	2.06	0.92	1.30	1.10	3.45	1.55	2.99	3.37	2.69	1.54	2.83	3.16	0.81	0.97	1.25	0.92	0.73	0.60
K_2O		0.01	0.00	0.02	0.00	0.01	0.01	0.07	0.14	0.37	0.53	0.35	0.32	0.27	0.16	0.16	0.00	0.00	0.01	0.03	0.00	0.00
P_2O_5		0.02	0.00	0.00	0.00	0.03	0.03	0.00	0.21	0.02	0.18	0.22	0.09	0.18	1.20	0.21	0.00	0.00	0.11	0.00	0.00	0.03
Loss On Ignition		0.52	0.56	1.06	1.30	0.18	1.47	0.48	1.57	1.47	2.79	1.79	1.74	3.19	5.89	2.84	2.54	1.55	1.27	1.40	0.84	1.67
Total		99.24	100.84	99.18	100.19	98.90	100.02	96.14	101.80	98.63	99.05	99.88	99.01	102.30	100.33	100.04	99.88	100.00	98.89	100.92	100.06	98.82
V		281.30	171.83	232.32	183.22	291.00	393.00	56.33	255.28	228.50	190.61	246.62	150.99	222.20	290.76	215.36	98.81	177.18	201.99	96.39	117.70	751.00
^{52}Cr		100.40	278.07	566.45	195.63	164.00	152.00	169.22	124.45	69.43	205.95	130.21	245.10	287.41	623.98	372.13	1401.44	499.35	221.62	602.15	309.33	70.00
^{53}Cr		97.67	283.54	567.93	197.99			174.21	128.96	66.47	209.07	132.04	257.67				1354.92					
Mn		0.16	0.17	0.16	0.13			0.05	0.18	0.13	0.15	0.18	0.17		0.15		0.07	0.13	0.09	0.08	0.05	
Co		41.59	51.70	43.09	42.50	47.00	55.00	7.37	39.77	22.61	41.55	39.95	42.00	35.92	48.14	42.77	37.74	50.73	27.84	35.29	24.58	31.00
^{60}Ni		25.72	102.60	128.78	109.76	39.00	74.00	9.40	54.42	3.43	101.62	58.34	141.36		150.78		407.39	181.81	76.76	147.51	89.11	440.00
^{62}Ni		26.74	91.20	118.15	96.06			7.59	65.67	3.00	98.69	65.32	140.35		160.02		354.74	153.09	69.79	125.41	76.22	
Zn		32.68	25.00	31.48	32.86			63.66	89.17	49.97	74.94	90.65	53.97	54.35	75.85	72.65	24.12	38.55	17.62	33.94	9.40	
Ga		14.74	12.17	10.44	14.46	12.01	13.69	13.69	19.84	14.69	16.94	18.23	16.08	15.89	15.37	14.53	9.18	11.42	13.20	10.38	13.84	7.60
Rb		0.15	0.02	0.27	0.23	0.01	0.03	2.86	2.13	6.93	7.35	8.88	8.92	0.85	2.46	3.73	0.09	0.30	0.06	0.00	0.01	0.06
Sr		102.30	106.75	84.28	120.49	77.68	112.56	182.45	222.42	112.50	433.37	398.53	194.65	334.50	624.83	394.10	119.41	126.08	241.02	129.85	199.91	69.44
Y		10.67	7.00	6.37	10.54	7.12	5.34	28.56	37.69	10.85	25.94	35.97	21.75	24.25	29.44	26.40	4.81	7.43	15.16	3.83	7.25	5.26
Zr		9.24	0.31	1.22	5.66	1.35	3.28	71.18	144.34	21.56	95.98	123.97	63.34	119.50	233.55	99.89	3.89	1.31	5.66	0.25	4.74	3.24
Nb		0.22	0.01	0.13	0.01	0.24	0.07	15.46	12.54	3.41	11.70	13.62	4.91	10.12	87.76	11.95	0.14	0.01	0.16	0.01	0.00	0.03
Cs		0.05	0.00	0.01	0.00			0.11	0.02	0.11	0.24	1.68	0.26	0.02	0.01	6.71	0.08	0.03	0.02	0.02	0.00	
Ba	parts per million	5.15	1.91	2.97	7.61	12.61	12.53	40.84	78.01	88.63	241.23	258.43	24.66	18.57	314.15	435.20	18.59	2.58	1.40	1.45	1.73	2.03
La		0.64	0.14	0.15	0.28			17.33	13.09	5.29	12.41	15.44	5.44	10.03	77.43	13.66	0.23	0.09	0.76	0.01	0.25	
Ce		1.77	0.73	0.89	1.15	0.36	0.73	40.90	31.32	11.76	28.48	34.70	12.94	21.31	150.41	28.19	1.00	0.40	2.18	0.20	0.70	0.76
Pr		0.38	0.15	0.10	0.32	0.09	0.14	5.14	4.89	1.53	4.26	5.17	2.07	2.93	17.91	3.42	0.19	0.11	0.45	0.06	0.17	0.16
Nd		1.78	0.90	0.50	1.80	0.62	0.83	15.72	17.65	4.59	14.68	17.99	7.88	12.14	66.19	15.49	0.93	0.84	2.78	0.44	1.13	1.02
Sm		0.78	0.49	0.28	0.89	0.34	0.36	3.82	4.73	1.09	3.72	4.63	2.27	3.33	11.86	3.82	0.38	0.49	1.23	0.25	0.57	0.43
Eu		0.34	0.29	0.14	0.50	0.22	0.28	0.87	1.64	0.32	1.34	1.62	0.98	1.15	3.43	1.37	0.19	0.33	0.69	0.20	0.28	0.23
Gd		1.13	0.78	0.51	1.32	0.65	0.60	3.78	5.41	1.23	3.96	5.27	2.83	3.71	9.83	4.07	0.57	0.85	1.84	0.44	0.92	0.63
Tb		0.22	0.16	0.11	0.25	0.14	0.12	0.64	0.93	0.21	0.65	0.89	0.49	0.67	1.24	0.67	0.11	0.17	0.35	0.09	0.18	0.12
Dy		1.62	1.15	0.88	1.74	1.04	0.90	4.08	5.95	1.56	4.20	5.79	3.33	4.15	6.24	4.22	0.75	1.24	2.50	0.63	1.24	0.90
Ho		0.33	0.23	0.19	0.34	0.24	0.20	0.76	1.14	0.31	0.80	1.10	0.66	0.80	0.97	0.87	0.15	0.24	0.50	0.12	0.24	0.18
Er		1.08	0.70	0.68	1.05	0.74	0.55	2.53	3.60	1.08	2.53	3.46	2.12	2.34	2.44	2.41	0.48	0.70	1.51	0.35	0.72	0.49
Tm		0.18	0.11	0.11	0.16	0.12	0.08	0.43	0.56	0.19	0.39	0.54	0.33	0.36	0.33	0.37	0.07	0.11	0.24	0.05	0.11	0.08
Yb		1.11	0.66	0.79	0.93	0.79	0.53	2.72	3.35	1.24	2.29	3.25	2.03	2.28	1.95	2.24	0.42	0.64	1.51	0.30	0.67	0.53
Lu		0.18	0.10	0.13	0.15	0.13	0.08	0.43	0.52	0.22	0.36	0.50	0.32	0.34	0.26	0.35	0.07	0.11	0.21	0.03	0.10	0.08
Hf		0.42	0.09	0.12	0.33	0.09	0.12	2.47	3.59	0.69	2.33	3.13	1.63	2.49	5.40	2.16	0.16	0.09	0.24	0.04	0.19	0.12
Ta		0.02	0.00	0.01	0.00	0.01		1.61	0.64	0.30	0.56	0.65	0.25	0.60	4.47	0.58	0.01	0.01	0.03	0.01	0.01	
Pb		2.05	0.90	5.95	0.71			0.04	4.73	6.55	1.68	2.45	6.12	0.18	33.01	1.63	1.29	12.35	3.26	7.17	3.90	
Th		0.08	0.13	0.05	1.35	0.04	0.06	0.01	0.00	1.52	1.43	0.11	19.08	1.15	7.12	1.45	0.03	0.00	0.00	0.00	0.00	0.01
U		0.04	0.08	0.04	0.32	0.00	0.05	-0.01	0.00	0.61	0.36	0.04	2.20	0.28	1.44	0.33	0.01	0.01	0.01	0.00	0.00	0.01

Sample No.	UAE	479	488	450	460	461	462	4021	2113	3970	4018	530	4868	4853	3181	4313	4338	4012	4306	2384	2334	3987
Rock type		Younger gabbro	Younger gabbro	Younger gabbro	Younger gabbro	Younger gabbro	Younger gabbro	Younger gabbro	Younger gabbro	Younger gabbro	Younger gabbro	Younger gabbro	Younger gabbro	Younger gabbro	Younger gabbro	Younger gabbro	Younger gabbro	Younger gabbro	Younger gabbro	Younger gabbro	Younger gabbro	Younger gabbro
Block		Aswad	Aswad	Aswad	Aswad	Aswad	Aswad	Aswad	Aswad	Aswad	Aswad	Aswad	Aswad	Aswad	Aswad	Aswad	Aswad	Aswad	Aswad	Aswad	Khor Fakkan	Aswad
SiO_2		44.71	43.25	50.55	47.35	53.04	48.05	51.65	40.23	51.69	51.07	52.30	47.08	55.10	47.86	51.11	48.27	48.88	48.77	50.75	48.96	48.59
TiO_2		0.07	0.10	0.17	0.81	0.18	0.14	0.27	0.02	1.74	0.34	0.33	0.27	0.26	1.40	0.39	0.14	0.82	0.14	0.21	0.99	0.40
Al_2O_3		25.56	18.66	10.36	16.85	18.29	19.07	15.37	20.94	18.87	15.31	13.30	26.44	13.92	15.18	16.72	24.43	15.24	18.94	13.10	14.51	15.38
Fe_2O_3		2.15	4.59	3.83	13.34	6.20	5.22	7.43	4.90	2.47	7.52	9.64	3.53	7.97	10.76	6.88	2.22	9.60	4.95	7.63	9.26	9.74
MnO		0.03	0.08	0.08	0.20	0.10	0.10	0.13	0.07	0.05	0.12	0.15	0.05	0.14	0.15	0.13	0.04	0.16	0.11	0.16	0.12	0.18
MgO	wt %	5.16	9.35	13.37	7.98	7.83	9.25	9.49	14.29	3.06	9.75	8.58	5.47	8.67	9.22	9.20	5.22	9.69	10.69	14.24	8.19	9.79
CaO		17.24	12.73	20.78	12.79	13.28	16.69	12.56	12.59	15.18	12.33	11.68	14.95	12.00	14.48	11.09	17.91	14.44	15.03	12.42	14.97	14.12
Na_2O		1.02	0.90	0.44	1.28	1.08	0.59	1.11	1.07	3.63	1.86	1.74	1.28	1.69	1.23	2.21	1.41	1.58	0.73	1.12	2.19	0.71
K_2O		0.00	0.00	0.01	0.02	0.01	0.01	0.02	0.00	0.03	0.11	0.34	0.01	0.08	0.07	0.61	0.03	0.00	0.04	0.06	0.03	0.08
P_2O_5		0.04	0.03	0.02	0.06	0.03	0.03	0.00	0.03	0.48	0.01	0.05	0.00	0.01	0.11	0.01	0.00	0.01	0.00	0.02	0.04	0.00
Loss On Ignition		1.67	1.74	0.77	0.01	0.57	0.48	0.90	5.14	1.13	1.60	0.88	0.61	1.00	0.36	1.63	1.62	0.52	0.53	1.33	0.38	0.02
Total		97.65	91.43	100.37	100.58	100.61	99.63	98.92	99.28	98.33	100.02	98.99	99.68	100.86	100.82	99.98	101.28	100.92	99.94	101.03	99.63	99.03
V		46.00	63.00		405.00	145.00	136.00	193.40	50.67	118.53	218.12	246.91	51.73	206.88	326.05	193.77	65.39	250.37	115.35	179.10	297.69	283.49
^{52}Cr		189.00	134.00		103.00	42.00	47.00	507.51	1075.00	7.25	398.29	620.67	75.62	595.51	282.22	131.18	726.56	356.40	233.95	882.50	226.20	124.40
^{53}Cr									1013.00													
Mn								0.13	0.06	0.05	0.13		0.05	0.14	0.14	0.12	0.04	0.16	0.11	0.15		0.18
Co		13.00	31.00		50.00	36.00	36.00	40.01	46.67	13.97	35.81	38.52	26.05	36.58	51.60	31.29	15.82	45.64	32.96	42.91	43.62	45.60
^{60}Ni		39.00	191.00		46.00	17.00	24.00	107.28	575.80	29.97	90.71		78.66		116.06	91.19	761.45	112.17	93.75	193.50		72.23
^{62}Ni								92.68	515.80	41.83	79.39		67.94		109.37	78.42		101.35	75.93	161.30		63.29
Zn								39.88	16.58	4.41	31.07	50.12	3.85	62.07	38.85	29.35	7.02	37.79	20.96	23.01	25.21	76.18
Ga		12.86	10.28		16.61	12.77	10.38	11.95	10.48	16.74	11.09	10.53	13.45	11.91	14.98	11.99	12.64	13.91	12.51	9.64	14.70	12.14
Rb		0.11	0.10		0.03	0.08	0.13	0.34	0.14	0.01	0.73	1.19	0.31	0.66	0.50	10.28	0.10	0.32	0.22	0.02	0.20	0.40
Sr		217.18	59.74		104.04	97.60	78.88	73.14	268.90	363.00	120.51	264.10	214.82	107.06	140.79	182.28	129.18	146.44	92.39	92.16	141.60	71.49
Y		1.60	3.31		12.12	10.13	4.25	8.48	1.95	47.61	8.33	10.52	6.01	13.30	26.70	10.63	3.42	16.15	3.75	8.30	20.32	9.37
Zr		0.35	0.25		3.44	14.02	2.32	11.19	0.01	64.60	9.26	20.33	16.22	22.56	39.77	16.18	4.92	12.10	1.64	9.21	21.75	4.48
Nb		0.01	0.01		0.34	0.32	0.02	0.30	0.02	1.83	0.29	0.25	0.04	0.17	1.51	0.11	0.01	0.08	0.01	0.09	0.41	0.54
Cs					0.00	0.00		0.03	0.05	0.00	0.03	0.02	0.15	0.06	0.07	0.29	0.03	0.04	0.02	0.00	0.00	0.05
Ba		1.46	3.10		3.76	7.91	1.96	40.41	30.95	9.81	18.00	20.99	10.27	26.96	13.68	20.95	7.19	14.00	4.55	11.76	6.05	3.55
La	parts per million				0.35	0.48		0.13	0.04	2.95	0.42	0.53	0.68	0.60	1.78	0.49	0.20	0.52	0.13	0.35	0.85	0.03
Ce		0.29	0.18		1.15	1.46	0.46	1.00	0.16	10.33	1.37	1.46	2.10	1.84	5.68	1.71	0.81	1.97	0.36	0.87	2.95	0.69
Pr		0.07	0.05		0.24	0.27	0.11	0.19	0.04	2.15	0.26	0.28	0.37	0.36	1.11	0.33	0.15	0.43	0.08	0.16	0.60	0.16
Nd		0.33	0.31		1.68	1.55	0.59	1.03	0.20	12.98	1.31	1.57	1.90	1.98	6.36	1.85	0.84	2.72	0.50	0.95	3.96	1.09
Sm		0.14	0.17		0.85	0.70	0.29	0.46	0.11	4.96	0.53	0.67	0.66	0.86	2.46	0.75	0.33	1.32	0.22	0.45	1.74	0.57
Eu		0.18	0.16		0.50	0.25	0.15	0.21	0.10	1.30	0.24	0.27	0.36	0.30	0.87	0.31	0.22	0.65	0.18	0.18	0.77	0.29
Gd		0.22	0.30		1.39	1.07	0.45	0.75	0.18	6.88	0.84	1.01	0.81	1.30	3.51	1.07	0.45	1.96	0.37	0.75	2.43	0.94
Tb		0.04	0.07		0.28	0.21	0.09	0.16	0.04	1.21	0.17	0.22	0.14	0.26	0.67	0.22	0.08	0.38	0.08	0.16	0.47	0.20
Dy		0.30	0.52		1.97	1.48	0.70	1.25	0.31	8.01	1.28	1.60	1.00	1.97	4.55	1.59	0.60	2.72	0.59	1.17	3.26	1.52
Ho		0.06	0.11		0.43	0.33	0.15	0.26	0.07	1.49	0.26	0.34	0.19	0.41	0.88	0.33	0.12	0.53	0.12	0.25	0.70	0.31
Er		0.17	0.36		1.29	1.01	0.45	0.86	0.22	4.27	0.83	1.09	0.59	1.25	2.67	1.02	0.33	1.60	0.36	0.82	1.99	0.96
Tm		0.03	0.05		0.20	0.16	0.07	0.14	0.04	0.62	0.13	0.19	0.09	0.22	0.43	0.17	0.06	0.25	0.06	0.14	0.31	0.16
Yb		0.16	0.39		1.30	1.03	0.48	0.95	0.30	3.84	0.88	1.23	0.57	1.46	2.72	1.07	0.35	1.55	0.38	0.89	1.90	1.05
Lu		0.03	0.07		0.21	0.16	0.09	0.10	0.03	0.52	0.12	0.20	0.10	0.23	0.58	0.16	0.05	0.23	0.08	0.14	0.30	0.12
Hf		0.02	0.03		0.16	0.51	0.10	0.36	0.01	1.56	0.31	0.54	0.44	0.71	1.20	0.51	0.11	0.45	0.06	0.34	0.80	0.17
Ta					0.01	0.02		0.03	0.00	0.08	0.02	0.03	0.02	0.02	0.11	0.03	0.01	0.02	0.01	0.03	0.03	0.02
Pb					0.00	0.11		5.97	1.53	2.99	5.74		7.01	4.86	9.11	4.20	4.42	4.21	4.80	5.16	0.12	14.83
Th		0.00	0.00		0.01	0.05	0.03	0.05	0.00	0.03	0.04	0.07	0.01	0.08	0.03	0.04	0.01	0.01	0.00	0.05	0.01	0.00
U		0.00	0.00		0.01	0.05	0.03	0.08	0.01	0.06	0.05	0.06	0.01	0.07	0.03	0.04	0.00	0.01	0.00	0.04	0.01	0.01

Sample No.	UAE	4025	2373	2375	2382	2386	4525	4820	3979	4517	4323	4334	569	3040	3093	2325	3031	3055	3107	3145	2121	2348
Rock type		Younger gabbro	Younger gabbro	Younger gabbro	Younger gabbro	Younger gabbro	Younger gabbro	Younger gabbro	Younger gabbro	Younger gabbro	Younger gabbro	Younger gabbro	Younger gabbro	Younger gabbro	Younger gabbro	High-level gabbro	High-level gabbro	High-level gabbro	High-level gabbro	High-level gabbro	High-level gabbro	High-level gabbro
Block		Aswad	Aswad	Aswad	Aswad	Aswad	Fizh	Aswad	Aswad	Aswad	Aswad	Aswad		Aswad	Aswad	Aswad	Aswad	Aswad	Aswad	Aswad	Khor Fakkan	Khor Fakkan
SiO_2		49.74	41.78	50.75	46.50	48.32	49.27	48.04	48.53	47.90	40.20	50.63	46.98	47.59	51.63	46.19	47.62	46.48	49.81	46.51	49.94	48.07
TiO_2		0.10	4.49	0.20	0.27	0.12	0.12	0.12	0.12	0.09	0.30	0.20	0.06	0.44	0.21	0.26	0.20	0.36	1.08	0.27	0.28	0.13
Al_2O_3		14.39	13.31	12.71	17.14	15.59	20.06	15.75	18.44	15.88	15.67	10.18	19.92	16.07	18.01	18.87	21.10	8.09	16.79	22.34	16.78	12.32
Fe_2O_3		5.93	13.54	7.97	8.38	5.84	5.38	6.76	4.80	5.13	16.42	7.89	7.87	7.16	5.06	6.48	3.69	9.57	9.09	4.31	8.50	9.17
MnO		0.12	0.25	0.16	0.16	0.13	0.11	0.13	0.11	0.10	0.09	0.14	0.14	0.13	0.07	0.11	0.08	0.18	0.15	0.08	0.07	0.17
MgO	wt %	13.19	9.43	13.74	10.32	13.56	9.26	11.36	10.29	12.02	12.11	16.59	9.83	11.25	8.31	9.63	9.12	21.46	7.37	7.06	7.01	12.36
CaO		15.74	11.84	13.91	14.35	16.36	14.67	14.60	15.18	16.71	10.39	11.75	14.69	14.57	10.79	15.00	17.41	12.42	11.59	16.48	12.47	15.92
Na_2O		0.34	2.26	0.94	0.92	0.44	1.03	0.62	0.73	0.48	0.75	0.67	0.31	1.36	3.63	1.39	1.14	0.63	2.97	1.52	2.27	0.27
K_2O		0.07	0.77	0.06	0.05	0.06	0.02	0.04	0.00	0.03	0.03	0.10	0.00	0.08	0.13	0.00	0.05	0.07	0.11	0.07	0.00	0.00
P_2O_5		0.00	2.17	0.02	0.02	0.02	0.01	0.00	0.00	0.00	0.01	0.01	0.00	0.04	0.02	0.00	0.02	0.02	0.07	0.02	0.00	0.00
Loss On Ignition		1.27	0.09	0.13	1.23	0.52	0.79	0.87	0.58	0.52	3.23	1.10	0.21	0.87	1.20	1.51	0.87	1.99	1.84	1.17	0.93	0.24
Total		100.87	99.92	100.58	99.34	100.96	100.72	98.29	98.77	98.86	99.19	99.26	100.01	99.56	99.06	99.44	101.29	101.26	100.87	99.85	98.25	98.68
V		127.19	368.70	212.70	266.90	140.30	110.36	138.89	106.98	130.91	199.94	220.43	145.19	152.40	143.43	113.10	130.74	162.17	265.01	108.03	251.20	256.57
^{52}Cr		730.46	188.60	971.70	139.90	260.90	56.34	65.90	206.93	650.74	451.46	1393.72	21.14	408.48	73.58	457.14	1666.09	2070.87	121.93	447.00	73.14	498.52
^{53}Cr													21.01			459.31					68.99	512.70
Mn		0.12	0.23	0.16	0.16	0.13	0.11	0.13	0.11	0.10	0.08	0.14	0.14	0.13	0.07	0.11	0.08	0.18	0.15	0.08	0.08	0.18
Co		39.19	57.59	46.34	47.59	42.07	34.28	44.07	30.66	43.81	158.22	58.19	50.45	45.74	31.31	38.60	29.35	76.86	38.20	24.90	40.73	59.02
^{60}Ni		121.38	147.20	175.60	78.02	116.20	49.89	122.31	94.86	205.92	141.52	383.70	119.71	152.54	55.67	124.25	165.30	618.98	52.34	121.31	16.14	124.80
^{62}Ni		106.34	184.70	146.10	66.62	94.14	39.22	103.84	76.81	178.86	123.37	337.63	102.75	127.23	43.19	109.34	134.30	507.85	49.85	98.68	14.21	114.74
Zn		23.17	130.20	30.02	43.62	18.06	19.05	25.54	21.80	22.28	35.73	52.43	27.59	40.43	10.15	23.86	112.42	51.64	21.67	26.27	23.66	31.61
Ga		8.09	23.97	9.88	12.39	9.26	12.97	10.52	11.57	9.58	14.77	9.38	11.77	11.67	11.12	14.32	12.66	7.03	16.04	13.93	14.16	8.90
Rb		0.06	28.82	0.16	0.36	0.08	0.42	0.28	0.01	0.18	0.26	2.78	0.17	0.44	0.54	0.16	3.04	0.51	0.72	0.42	0.44	0.10
Sr		47.94	1027.00	62.46	82.95	62.80	116.86	72.42	131.15	56.68	108.53	55.36	42.79	137.22	132.94	167.45	81.30	53.74	155.98	141.51	152.40	44.55
Y		2.82	43.52	7.47	7.15	3.86	2.90	3.66	3.44	3.17	7.62	7.82	2.10	11.69	6.54	5.84	6.15	9.70	29.10	7.20	9.12	3.31
Zr		2.22	265.00	13.20	3.78	8.87	4.93	19.42	9.11	13.06	5.46	16.92	0.69	53.73	14.55	1.06	11.96	23.92	72.39	9.45	4.56	0.38
Nb		0.46	99.47	1.81	0.50	0.25	0.19	3.47	1.14	2.05	0.26	1.66	0.01	3.33	1.51	0.02	1.42	1.47	1.02	0.22	0.12	0.01
Cs		0.01	0.34	0.02	0.02	0.02	0.14	0.05	0.02	0.01	0.07	0.09	0.01	0.01	0.01	0.01	0.63	0.02	0.09	0.05	0.02	0.00
Ba		2.51	3049.00	1.45	0.42	0.01	6.15	4.53	3.27	7.08	7.86	15.59	4.79	37.47	12.31	10.85	8.44	6.37	11.95	8.53	17.91	6.22
La		0.07	226.80	0.21	0.05	0.01	0.06	0.07	0.08	0.05	0.02	0.18	0.03	1.00	0.16	0.11	0.71	1.32	2.08	0.40	0.69	0.03
Ce	parts per million	0.21	387.10	0.77	0.35	0.17	0.30	0.24	0.32	0.17	0.22	0.51	0.10	2.80	0.64	0.75	1.13	1.68	7.16	1.27	1.19	0.11
Pr		0.05	40.76	0.15	0.09	0.04	0.06	0.05	0.07	0.03	0.08	0.09	0.02	0.50	0.13	0.14	0.20	0.33	1.36	0.25	0.28	0.04
Nd		0.29	137.60	0.95	0.67	0.33	0.36	0.36	0.42	0.26	0.69	0.57	0.14	2.69	0.82	0.87	1.11	1.91	7.42	1.49	1.27	0.24
Sm		0.16	21.82	0.45	0.39	0.21	0.18	0.18	0.19	0.16	0.49	0.33	0.08	1.02	0.42	0.48	0.45	0.81	2.73	0.63	0.55	0.15
Eu		0.10	6.56	0.20	0.22	0.12	0.14	0.13	0.17	0.11	0.18	0.14	0.08	0.47	0.18	0.34	0.27	0.33	0.93	0.39	0.25	0.09
Gd		0.45	17.63	0.73	0.70	0.36	0.31	0.33	0.35	0.32	0.81	0.62	0.16	1.45	0.67	0.75	0.68	1.15	3.74	0.90	0.86	0.28
Tb		0.05	1.96	0.14	0.14	0.08	0.06	0.07	0.07	0.07	0.17	0.14	0.04	0.27	0.14	0.14	0.13	0.22	0.66	0.17	0.18	0.06
Dy		0.45	9.34	1.11	1.09	0.59	0.46	0.56	0.54	0.51	1.27	1.10	0.29	1.92	1.01	1.00	0.95	1.55	4.54	1.18	1.33	0.50
Ho		0.09	1.40	0.23	0.22	0.12	0.10	0.12	0.11	0.10	0.25	0.23	0.06	0.38	0.21	0.19	0.20	0.32	0.93	0.23	0.28	0.11
Er		0.29	3.51	0.75	0.71	0.38	0.28	0.36	0.34	0.31	0.73	0.75	0.22	1.11	0.66	0.58	0.59	0.94	2.81	0.69	0.94	0.36
Tm		0.05	0.46	0.13	0.12	0.06	0.05	0.06	0.05	0.05	0.11	0.13	0.04	0.17	0.11	0.09	0.09	0.15	0.45	0.10	0.16	0.06
Yb		0.29	2.55	0.82	0.75	0.37	0.28	0.38	0.35	0.31	0.65	0.88	0.26	1.07	0.69	0.49	0.57	0.91	2.96	0.66	0.99	0.37
Lu		0.04	0.33	0.13	0.11	0.06	0.04	0.05	0.06	0.04	0.09	0.13	0.05	0.16	0.12	0.07	0.10	0.13	0.43	0.09	0.17	0.06
Hf		0.06	5.96	0.32	0.12	0.28	0.12	0.37	0.18	0.23	0.18	0.44	-0.01	1.47	0.38	0.12	0.31	0.62	2.02	0.29	0.26	0.01
Ta		0.01	4.58	0.04	0.02	0.01	0.02	0.08	0.05	0.06	0.02	0.09	0.00	0.14	0.07	0.00	0.07	0.07	0.09	0.03	0.01	0.00
Pb		10.00	8.34	4.74	8.23	6.49	8.62	8.08	8.95	6.64	11.96	5.71	1.00	11.88	10.66	0.24	31.51	7.43	6.95	8.62	2.67	0.82
Th		0.00	17.21	0.03	0.01	0.02	0.01	0.05	0.03	0.05	0.00	0.05	0.01	0.10	0.04	0.00	0.05	0.04	0.08	0.01	0.13	7.38
U		0.00	5.15	0.00	0.00	0.00	0.00	0.00	0.01	0.00	0.03	0.08	0.00	0.04	0.03	0.00	0.04	0.05	0.06	0.03	0.08	0.90

Sample No.	UAE	2343	554	557	103	131	2201	249	34	2239	219	559	300	552	203	2381	3995	4006	3929	4508	3997	4030
Rock type		High-level gabbro	High-level gabbro	High-level gabbro	High-level gabbro	High-level gabbro	High-level gabbro	High-level gabbro	High-level gabbro	High-level gabbro	High-level gabbro	High-level gabbro	High-level gabbro	High-level gabbro	High-level gabbro	Layered gabbro	Layered gabbro	Layered gabbro	Layered gabbro	Layered gabbro	Layered gabbro	Layered gabbro
Block		Khor Fakkan	Khor Fakkan	Khor Fakkan	Khor Fakkan	Khor Fakkan	Khor Fakkan	Khor Fakkan	Khor Fakkan	Khor Fakkan	Khor Fakkan	Khor Fakkan	Khor Fakkan	Khor Fakkan	Khor Fakkan	Aswad	Aswad	Aswad	Fizh	Aswad	Aswad	Aswad
SiO_2	wt %	47.31	50.08	44.50	44.07	47.21	45.35	46.80	46.60	49.35	48.21	45.25	45.95	49.14	46.92	45.41	46.78	48.10	57.53	48.56	47.88	50.42
TiO_2	wt %	0.17	0.30	0.14	1.16	0.34	0.76	0.13	0.11	0.05	0.04	0.08	0.21	0.27	0.26	0.15	0.12	0.17	0.97	0.10	0.14	0.19
Al_2O_3	wt %	17.37	16.83	19.38	19.58	16.17	16.41	16.40	16.20	18.08	16.46	24.23	15.69	17.45	15.97	15.54	21.25	15.99	14.62	13.37	18.67	11.86
Fe_2O_3	wt %	7.27	5.52	5.84	12.40	8.08	11.55	5.70	5.84	5.27	5.92	5.53	7.38	5.50	8.57	5.26	3.51	5.62	10.66	3.54	3.60	7.57
MnO	wt %	0.14	0.08	0.08	0.11	0.13	0.14	0.10	0.10	0.11	0.10	0.07	0.13	0.09	0.13	0.10	0.06	0.11	0.15	0.08	0.07	0.21
MgO	wt %	10.25	9.83	14.46	5.65	10.35	9.08	11.58	12.35	11.25	13.23	10.00	11.17	9.82	10.59	15.45	9.00	12.37	2.58	12.29	9.91	13.24
CaO	wt %	16.02	15.34	10.89	14.59	14.79	13.87	17.65	17.21	16.44	16.33	12.89	16.45	14.66	16.14	15.46	17.30	16.60	5.15	19.34	17.61	15.05
Na_2O	wt %	0.76	2.03	1.38	1.72	1.27	1.08	0.54	0.46	0.26	0.25	1.39	0.66	2.00	0.83	0.85	1.13	1.04	5.36	0.33	1.22	0.43
K_2O	wt %	0.00	0.04	0.04	0.01	0.00	0.01	0.00	0.00	0.00	0.00	0.01	0.00	0.02	0.00	0.05	0.04	0.02	0.01	0.01	0.02	0.01
P_2O_5	wt %	0.00	0.03	0.04	0.04	0.03	0.04	0.03	0.05	0.03	0.03	0.04	0.03	0.03	0.03	0.02	0.00	0.00	0.08	0.01	0.00	0.00
Loss On Ignition	wt %	0.30	1.24	3.44	0.03	0.20	0.82	0.42	1.73	0.42	0.82	1.76	0.01	1.76	0.15	1.35	1.66	0.51	1.79	0.43	0.60	1.13
Total	wt %	99.60	101.31	100.19	99.37	98.58	99.10	99.36	100.65	101.26	101.39	101.26	97.67	100.74	99.60	99.64	100.84	100.52	98.89	98.07	99.73	100.11
V	parts per million	145.45	151.00	37.00	756.00	212.00	489.00	127.00	135.00		115.00	20.00	160.00	124.00	201.00	105.40	77.15	122.53	227.53	124.36	107.85	208.70
^{52}Cr	parts per million	237.04	874.00	219.00	43.00	371.00	57.00	317.00	329.00		306.00	69.00	362.00	386.00	109.00	148.80	1421.77	672.36	17.62	751.82	241.12	786.79
^{53}Cr	parts per million	246.10																	17.01			
Mn	parts per million	0.14														0.11	0.06	0.11	0.13	0.08	0.07	0.20
Co	parts per million	46.52	32.00	51.00	51.00	56.00	55.00	42.00	48.00		49.00	45.00	53.00	38.00	37.00	49.74	30.07	46.88	21.75	32.72	30.63	43.40
^{60}Ni	parts per million	144.56	146.00	449.00	18.00	131.00	29.00	99.00	115.00		132.00	249.00	78.00	96.00	28.00	148.60	229.05	182.09	0.01	115.65	136.92	158.56
^{62}Ni	parts per million	135.26														124.40	198.01	152.80	3.50	97.48	115.66	133.39
Zn	parts per million	28.04														24.31	18.67	27.74	37.04	16.51	15.50	39.67
Ga	parts per million	13.13	11.41	10.10	17.28	11.87	13.72	8.76	9.06		6.90	12.98	9.90	12.29	10.87	9.10	11.04	10.55	19.76	8.03	11.08	8.59
Rb	parts per million	0.04	0.47	0.22	0.06	0.17	0.03	0.15	0.05		0.11	0.00	0.01	0.04	0.03	0.27	0.76	0.05	0.43	0.28	0.33	0.24
Sr	parts per million	97.69	125.85	110.23	137.35	127.38	123.85	75.12	82.38		32.27	129.56	81.18	152.41	114.18	89.94	151.60	87.44	63.43	93.94	132.06	65.96
Y	parts per million	5.52	8.20	2.94	4.38	8.82	4.83	4.26	3.39		1.09	1.37	6.00	7.11	6.10	4.65	3.14	5.36	26.01	3.21	4.34	7.05
Zr	parts per million	0.17	7.56	3.47	2.64	7.48	2.34	1.49	1.16		0.49	0.74	2.14	4.37	3.55	4.84	1.56	1.19	55.97	1.06	8.23	5.00
Nb	parts per million	0.01	0.20	0.10	0.05	0.12	0.04	0.01	0.16		0.02	0.03	0.00	0.06	0.04	0.19	0.01	0.00	0.93	0.11	0.46	0.02
Cs	parts per million	0.06	0.01						0.00							0.03	0.05	0.00	0.01	0.02	0.08	0.02
Ba	parts per million	3.16	3.74	1.95	2.75	34.41	14.66	0.35	36.90		1.73	2.10	0.43	0.82	0.00	0.29	1.25	3.35	9.20	4.44	0.84	2.92
La	parts per million	0.08	0.35						0.04							0.07	0.09	0.15	2.42	0.06	0.05	0.17
Ce	parts per million	0.65	1.15	0.99	0.50	1.31	0.46	0.31	0.18		0.04	0.71	0.80	1.12	0.59	0.43	0.43	0.41	7.49	0.16	0.42	0.69
Pr	parts per million	0.10	0.23	0.15	0.10	0.27	0.11	0.08	0.05		0.01	0.12	0.18	0.22	0.14	0.10	0.10	0.09	1.41	0.05	0.10	0.14
Nd	parts per million	0.61	1.49	0.84	0.65	1.69	0.69	0.57	0.39		0.04	0.58	1.01	1.33	0.92	0.69	0.60	0.68	6.15	0.35	0.66	0.86
Sm	parts per million	0.34	0.68	0.28	0.31	0.68	0.36	0.28	0.22		0.03	0.17	0.41	0.58	0.48	0.32	0.26	0.36	2.19	0.20	0.35	0.42
Eu	parts per million	0.23	0.39	0.24	0.26	0.39	0.28	0.18	0.14		0.04	0.26	0.24	0.40	0.29	0.20	0.20	0.23	0.73	0.12	0.24	0.18
Gd	parts per million	0.61	1.05	0.38	0.49	1.01	0.58	0.53	0.40		0.11	0.20	0.66	0.91	0.73	0.53	0.41	0.62	2.93	0.35	0.52	0.67
Tb	parts per million	0.13	0.20	0.07	0.10	0.19	0.12	0.10	0.08		0.02	0.04	0.14	0.16	0.14	0.11	0.08	0.12	0.54	0.08	0.10	0.14
Dy	parts per million	0.87	1.36	0.49	0.75	1.45	0.82	0.72	0.56		0.18	0.24	0.97	1.21	1.06	0.75	0.52	0.89	3.82	0.55	0.72	1.07
Ho	parts per million	0.18	0.28	0.10	0.16	0.31	0.18	0.15	0.12		0.04	0.05	0.21	0.24	0.23	0.14	0.10	0.17	0.77	0.11	0.14	0.22
Er	parts per million	0.57	0.80	0.29	0.46	0.88	0.55	0.45	0.35		0.13	0.14	0.61	0.65	0.64	0.43	0.29	0.50	2.53	0.31	0.41	0.68
Tm	parts per million	0.09	0.12	0.04	0.06	0.13	0.07	0.07	0.05		0.02	0.02	0.09	0.09	0.09	0.07	0.04	0.08	0.41	0.05	0.06	0.11
Yb	parts per million	0.51	0.73	0.29	0.45	0.88	0.50	0.42	0.31		0.14	0.14	0.63	0.64	0.63	0.40	0.25	0.47	2.54	0.26	0.37	0.72
Lu	parts per million	0.08	0.11	0.05	0.08	0.13	0.09	0.07	0.05		0.03	0.03	0.10	0.10	0.12	0.05	0.04	0.12	0.40	0.07	0.06	0.11
Hf	parts per million	0.06	0.30	0.10	0.10	0.25	0.13	0.07	0.07		0.01	0.03	0.09	0.19	0.15	0.16	0.08	0.08	1.80	0.04	0.24	0.16
Ta	parts per million	0.00	0.01						0.01							0.03	0.01	0.01	0.07	0.01	0.03	0.02
Pb	parts per million	5.22	0.01						0.22							5.47	7.94	4.05	2.00	10.56	7.40	5.91
Th	parts per million	8.89	0.02	0.02	0.03	0.03	0.01	0.01	0.01		0.01	0.00	0.00	0.01	0.01	0.00	0.00	0.00	0.33	0.00	0.01	0.02
U	parts per million	0.88	0.02	0.02	0.03	0.03	0.01	0.01	0.01		0.01	0.00	0.00	0.01	0.01	0.00	0.00	0.00	0.12	0.00	0.00	0.01

Sample No.	UAE	3975	644	487	2225	314	419	421	322	532	483	448	276	43	252	270	336	359	381	474	4027	4029
Rock type		Layered gabbro	Layered gabbro	Layered gabbro	Layered gabbro	Layered gabbro	Layered gabbro	Layered gabbro	Layered gabbro	Layered gabbro	Layered gabbro	Layered gabbro	Layered gabbro	Pyroxenite	Pyroxenite	Pyroxenite	Pyroxenite	Pyroxenite	Pyroxenite	Pyroxenite	Pyroxenite	Pyroxenite
Block		Aswad	Aswad	Aswad	Khor Fakkan	Khor Fakkan	Khor Fakkan	Khor Fakkan	Khor Fakkan	Aswad	Aswad	Aswad	Khor Fakkan	Khor Fakkan	Khor Fakkan	Khor Fakkan	Khor Fakkan	Khor Fakkan	Khor Fakkan	Khor Fakkan	Aswad	Aswad
SiO_2	wt %	55.11	51.09	47.36	46.54	46.87	45.81	46.50	43.92	47.98	46.69	42.65	48.28	53.99	51.02	54.82	50.86	53.92	52.56	51.88	52.00	51.84
TiO_2		0.39	0.21	0.31	0.17	0.16	0.12	0.05	0.02	0.15	0.06	0.04	0.10	0.03	0.06	0.07	0.20	0.01	0.05	0.11	0.16	0.20
Al_2O_3		14.68	12.10	14.77	18.24	20.28	19.29	23.88	19.44	16.53	24.26	21.41	18.84	0.93	2.85	1.08	3.16	0.63	1.63	1.82	2.29	5.92
Fe_2O_3		8.49	7.37	7.50	8.22	8.06	5.66	2.13	5.13	5.77	2.49	4.92	2.67	6.01	5.46	10.56	7.23	6.92	7.12	4.06	9.05	8.87
MnO		0.16	0.15	0.12	0.14	0.13	0.09	0.04	0.07	0.09	0.04	0.07	0.05	0.14	0.11	0.23	0.12	0.15	0.14	0.09	0.19	0.19
MgO		8.74	13.84	12.42	10.28	9.11	9.83	7.06	13.12	12.43	8.65	12.55	10.95	18.87	18.25	16.01	17.98	19.63	18.23	17.62	21.54	17.31
CaO		11.14	15.74	14.70	14.15	13.50	16.80	18.05	13.83	15.60	15.43	12.01	18.83	17.99	19.21	16.38	19.63	16.33	18.01	21.69	14.03	15.02
Na_2O		1.44	0.61	1.20	0.80	1.68	0.75	0.81	0.95	0.95	1.38	0.82	0.83	0.02	0.09	0.11	0.12	0.03	0.03	0.10	0.11	0.34
K_2O		0.02	0.00	0.01	0.01	0.00	0.06	0.06	0.04	0.00	0.07	0.02	0.01	0.03	0.04	0.01	0.04	0.04	0.03	0.03	0.01	0.01
P_2O_5		0.01	0.02	0.03	0.03	0.03	0.04	0.04	0.03	0.02	0.05	0.04	0.02	0.00	0.01	0.01	0.01	0.00	0.01	0.00	0.00	0.00
Loss On Ignition		0.77	0.31	2.29	0.32	0.08	0.31	0.73	2.47	0.47	2.29	3.39	0.57	0.78	1.20	0.19	0.80	0.20	0.60	0.51	0.27	0.61
Total		100.94	101.86	101.13	99.32	99.90	99.20	99.78	99.44	100.41	101.83	98.34	101.56	98.80	98.28	99.47	100.15	97.87	98.40	97.91	99.65	100.31
V	parts per million	266.48	199.00	149.00	117.00	78.00	97.00	59.00	33.00	120.00	43.00	26.00	101.00	115.00	165.00	296.00	232.00	105.00	199.00	147.00	206.61	254.68
^{52}Cr		369.57	541.00	901.00	103.00	46.00	265.00	1056.00	604.00	1008.00	799.00	2079.00	1403.00	3055.00	2801.00	1288.00	2725.00	2556.00	2250.00	3527.00	2351.37	1495.97
^{53}Cr																						
Mn		0.16																			0.18	0.19
Co		43.88	45.00	60.00	56.00	47.00	40.00	26.00	55.00	60.00	24.00	45.00	28.00	52.00	43.00	69.00	54.00	59.00	46.00	33.00	63.86	58.81
^{60}Ni		115.76	113.00	261.00	52.00	35.00	123.00	205.00	413.00	289.00	222.00	527.00	294.00	480.00	357.00	536.00	569.00	391.00	474.00	379.00	288.18	189.75
^{62}Ni		96.57																			255.59	166.56
Zn		67.38																			33.81	37.43
Ga		13.71	8.22	10.28	12.69	14.43	10.09	9.77	9.56	11.60	10.69	10.23	8.54	1.10	2.46	2.77	3.61	0.85	1.91	2.04	3.09	5.71
Rb		1.13	0.04	0.11	-0.02	0.03	0.31	0.02	0.06	0.01	0.06	0.00	0.01	0.73	0.17	0.07	0.01	0.02	0.00	0.00	0.19	0.23
Sr		90.08	95.42	102.98	116.88	146.82	135.10	112.20	162.98	113.66	160.87	100.10	93.47	41.81	19.24	3.33	12.10	0.00	0.00	2.01	10.20	26.24
Y		13.71	6.93	8.88	4.30	3.38	3.69	1.56	0.55	5.15	1.56	0.66	2.85	0.79	1.76	8.11	3.91	0.27	1.40	3.30	4.45	6.37
Zr		21.61	2.98	2.97	1.72	1.72	2.97	0.85	0.24	2.94	1.06	0.65	1.09	4.30	3.05	7.55	4.17	2.88	2.14	3.75	2.54	2.44
Nb		0.46	0.01	0.01	0.04	0.15	0.13	0.03	0.01	0.04	0.00	0.05	0.02	0.40	0.07	0.17	0.12	0.08	0.05	0.07	0.00	0.00
Cs		0.02				0.00															0.04	0.01
Ba		15.06	55.50	8.75	8.62	10.64	45.59	7.29	6.06	7.19	8.01	8.00	6.10	45.48	16.73	5.15	22.80	2.83	9.67	1.79	1.47	5.30
La		0.78				0.11															0.10	0.04
Ce		1.90	0.47	0.98	0.33	0.37	0.50	0.14	0.02	0.46	0.30	0.28	0.23	0.12	0.09	4.12	0.20	0.23	0.10	0.17	0.34	0.36
Pr		0.35	0.12	0.27	0.07	0.08	0.10	0.03	0.01	0.12	0.07	0.05	0.06	0.01	0.02	0.78	0.05	0.03	0.02	0.05	0.07	0.09
Nd		1.93	0.82	1.49	0.50	0.53	0.61	0.22	0.05	0.82	0.39	0.25	0.38	0.07	0.12	3.71	0.40	0.14	0.11	0.39	0.46	0.61
Sm		0.81	0.39	0.71	0.28	0.25	0.28	0.11	0.03	0.37	0.09	0.06	0.18	0.03	0.08	1.12	0.25	0.03	0.05	0.23	0.24	0.35
Eu		0.32	0.19	0.39	0.21	0.28	0.21	0.13	0.09	0.28	0.16	0.10	0.15	0.02	0.06	0.25	0.14	0.01	0.03	0.10	0.10	0.15
Gd		1.34	0.71	1.08	0.45	0.43	0.42	0.18	0.09	0.57	0.20	0.10	0.33	0.07	0.19	1.20	0.47	0.04	0.12	0.38	0.41	0.62
Tb		0.26	0.13	0.21	0.09	0.08	0.08	0.04	0.01	0.12	0.04	0.01	0.06	0.02	0.04	0.22	0.10	0.01	0.03	0.08	0.09	0.14
Dy		2.00	1.14	1.52	0.72	0.58	0.61	0.28	0.11	0.91	0.29	0.11	0.50	0.13	0.30	1.37	0.67	0.06	0.22	0.57	0.71	1.03
Ho		0.41	0.24	0.31	0.14	0.12	0.13	0.06	0.02	0.20	0.05	0.02	0.11	0.03	0.07	0.27	0.14	0.01	0.05	0.12	0.15	0.21
Er		1.32	0.69	0.91	0.44	0.35	0.36	0.17	0.06	0.53	0.15	0.08	0.31	0.11	0.22	0.78	0.41	0.05	0.18	0.36	0.46	0.67
Tm		0.23	0.10	0.13	0.06	0.05	0.06	0.03	0.01	0.07	0.02	0.01	0.04	0.02	0.03	0.12	0.06	0.01	0.03	0.06	0.08	0.11
Yb		1.51	0.69	0.86	0.45	0.33	0.38	0.17	0.06	0.51	0.15	0.09	0.30	0.13	0.22	0.71	0.36	0.07	0.21	0.32	0.45	0.68
Lu		0.23	0.11	0.13	0.07	0.05	0.06	0.03	0.02	0.08	0.04	0.02	0.05	0.02	0.04	0.12	0.07	0.01	0.04	0.06	0.08	0.09
Hf		0.70	0.12	0.13	0.07	0.08	0.06	0.03	-0.01	0.11	0.04	0.01	0.04	0.09	0.06	0.19	0.15	0.05	0.05	0.11	0.09	0.11
Ta		0.05				0.00								0.02							0.01	0.01
Pb		10.64				1.00															9.69	7.09
Th		0.09				0.01								0.02							0.01	0.00
U		0.10				0.00								0.04							0.00	0.01

Sample No.	UAE	4346	208	236	280	342	422	456	3048	3056	3080	3151	4821	4057
Rock type		Pyroxenite	Wehrlite	Wehrlite	Wehrlite	Wehrlite	Wehrlite	Wehrlite	Wehrlite	Wehrlite	Wehrlite	Wehrlite	Wehrlite	Impregnated dunite
Block		Aswad	Khor Fakkan	Khor Fakkan	Khor Fakkan	Khor Fakkan	Khor Fakkan	Aswad	Aswad	Aswad	Aswad	Aswad	Aswad	Aswad
SiO_2	wt %	48.71	40.73	41.64	40.96	55.62	41.04	38.99	47.36	43.02	43.91	42.35	44.52	38.74
TiO_2		0.06	0.02	0.02	0.02	0.02	0.04	0.04	0.38	0.23	0.22	0.41	0.18	0.01
Al_2O_3		1.04	1.76	3.23	0.97	1.38	3.43	1.51	24.20	4.81	6.44	7.82	6.21	1.11
Fe_2O_3		5.51	12.19	11.05	8.00	9.05	10.27	9.52	4.88	10.87	10.28	12.50	12.71	9.16
MnO		0.12	0.15	0.14	0.11	0.16	0.13	0.13	0.07	0.16	0.18	0.21	0.19	0.14
MgO		26.03	37.28	37.10	35.70	30.39	36.56	37.29	5.66	29.62	29.01	28.54	26.14	40.62
CaO		15.49	1.99	2.28	4.51	3.82	1.79	1.30	15.10	5.89	6.15	5.65	6.85	1.21
Na_2O		0.04	0.07	0.11	0.03	0.02	0.14	0.12	1.86	0.29	0.30	0.53	0.17	0.04
K_2O		0.01	0.04	0.03	0.00	0.01	0.02	0.01	0.06	0.07	0.08	0.09	0.05	0.02
P_2O_5		0.01	0.01	0.02	0.01	0.01	0.01	0.01	0.04	0.03	0.02	0.04	0.00	0.00
Loss On Ignition		2.13	7.12	5.75	10.99	0.15	7.82	10.46	0.92	4.99	4.76	3.28	4.44	8.28
Total		99.16	101.36	101.37	101.30	100.63	101.25	99.37	100.53	99.99	101.35	101.42	101.46	99.33
V	parts per million	94.90	36.00	53.00	41.00	89.00	46.00		102.74	102.94	110.60	86.10	118.37	15.04
^{52}Cr		3514.92	2475.00	6529.00	3496.00	2494.00	3064.00		546.20	3199.25	2746.50	207.06	2896.02	2597.90
^{53}Cr														
Mn		0.11							0.07	0.15	0.15	0.19	0.19	0.13
Co		64.32	133.00	108.00	104.00	72.00	103.00		25.43	107.34	95.84	108.19	99.68	119.49
^{60}Ni			1312.00	2029.00	1091.00	519.00	2152.00		132.14	1368.60	909.89	824.54	848.59	1322.44
^{62}Ni		2720.39							108.78	1112.31	754.17	707.96	750.28	1141.23
Zn		31.51							18.88	59.14	52.86	67.87	38.41	41.23
Ga		1.15	1.59	2.60	1.01	1.51	3.16		14.18	5.02	5.57	6.67	5.47	1.46
Rb		0.19	0.30	0.39	0.14	0.06	0.41		0.32	0.53	1.13	1.15	0.18	0.95
Sr		6.58	18.03	10.91	14.27	0.00	8.66		132.12	67.07	30.96	110.54	28.03	4.51
Y		1.16	0.28	0.43	0.53	0.26	0.40		11.47	8.79	6.23	9.03	2.91	0.35
Zr		0.57	0.17	0.32	1.18	0.33	0.00		24.40	20.42	18.02	15.24	1.93	1.68
Nb		0.08	0.02	0.02	0.05	0.01	0.00		0.99	0.66	1.43	0.60	0.09	0.00
Cs		0.07							0.05	0.02	0.02	0.09	0.03	0.14
Ba		6.53	3.59	6.32	4.90	7.37	6.58		39.85	0.75	6.66	6.17	15.19	9.93
La		0.00							0.88	0.35	0.34	0.87	0.03	0.00
Ce		0.01	0.05	0.04	0.03	0.03	0.04		2.96	1.27	1.15	2.72	0.21	0.01
Pr		0.01	0.01	0.01	0.01	0.00	0.01		0.53	0.25	0.22	0.48	0.05	0.00
Nd		0.09	0.05	0.07	0.08	0.03	0.05		2.81	1.43	1.21	2.45	0.32	0.02
Sm		0.09	0.03	0.03	0.04	0.01	0.02		1.08	0.64	0.48	0.82	0.15	0.01
Eu		0.03	0.01	0.02	0.02	0.00	0.02		0.46	0.19	0.18	0.32	0.08	0.01
Gd		0.14	0.05	0.06	0.07	0.02	0.03		1.40	0.91	0.69	1.11	0.28	0.02
Tb		0.03	0.01	0.01	0.01	0.01	0.01		0.26	0.18	0.13	0.20	0.06	0.00
Dy		0.27	0.06	0.09	0.11	0.05	0.06		1.77	1.32	0.95	1.41	0.42	0.03
Ho		0.05	0.02	0.02	0.02	0.02	0.02		0.36	0.28	0.20	0.28	0.09	0.01
Er		0.15	0.05	0.06	0.08	0.07	0.07		1.07	0.87	0.60	0.85	0.30	0.02
Tm		0.02	0.01	0.01	0.01	0.01	0.01		0.17	0.13	0.09	0.13	0.05	0.00
Yb		0.16	0.05	0.07	0.06	0.09	0.12		1.04	0.88	0.61	0.87	0.30	0.02
Lu		0.02	0.01	0.01	0.01	0.02	0.02		0.16	0.14	0.11	0.13	0.05	0.00
Hf		0.01							0.66	0.53	0.44	0.61	0.05	0.01
Ta		0.00							0.06	0.05	0.07	0.05	0.01	0.01
Pb		5.17							7.06	7.20	9.56	11.01	7.23	4.94
Th		0.00							0.05	0.02	0.04	0.05	0.00	0.00
U		0.00							0.03	0.02	0.03	0.04	0.01	0.01